PETROLOGIC AND GEOCHEMICAL TRACERS OF MAGMATIC MOVEMENT IN VOLCANIC ARC SYSTEMS: CASE STUDIES FROM THE ALEUTIAN ISLANDS AND KAMCHATKA, RUSSIA

By

Owen Kelly Neill

RECOMMENDED:

Advisory Committee Co-Chair

Advisory Committee Co-Chair

Chair, Department of Geology and Geophysics

APPROVED:

Dean, College of Natural Science and Mathematics

Dean of the Graduate School

29 April 2013

Date

PETROLOGIC AND GEOCHEMICAL TRACERS OF MAGMATIC MOVEMENT IN VOLCANIC ARC SYSTEMS: CASE STUDIES FROM THE ALEUTIAN ISLANDS AND KAMCHATKA, RUSSIA

A

THESIS

Presented to the Faculty

of the University of Alaska Fairbanks

in Partial Fulfillment of the Requirements

for the Degree of

DOCTOR OF PHILOSOPHY

By

Owen Kelly Neill

Fairbanks, Alaska

May 2013

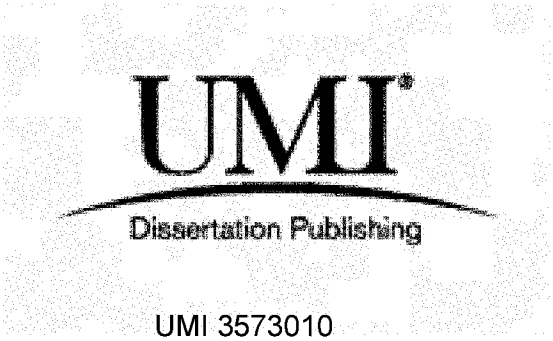

ProQuest LLC
789 East Eisenhower Parkway
P.O. Box 1346
Ann Arbor, MI 48106-1346

Abstract

Mixing, crystallization and degassing commonly affect magmas during storage, ascent and eruption from volcanoes. As these interactions cannot be observed directly, they must be characterized using chemical signatures of volcanic eruptive products. In this dissertation, geochemical tracers of magma mixing, crystallization and degassing were employed to investigate the magmatic systems of Kasatochi Island volcano, central Aleutian Islands, and Bezymianny Volcano, Kamchatka, Russia, in three studies.

The purpose of the first study was to characterize eruptive products from the 2008 eruption of Kasatochi Island volcano. This eruption produced pumiceous, medium-K andesite, as well as denser, medium-K basaltic andesite, with variable bulk compositions (~52-56 wt. % SiO_2 for the basaltic andesite, ~58-62 wt. % SiO_2 for the andesite). The basaltic andesite and andesite must have resided in separate storage areas until just prior to eruption, with mixing between these magmas limited to just prior to eruption.

The second study focused on basaltic andesite from the 2008 Kasatochi eruption, which contains two plagioclase phenocryst populations and anomalously calcic plagioclase microlites. Compositional heterogeneity in the basaltic andesite resulted from pre-eruptive mixing between mafic and silicic compositional end members. As the calcic plagioclase phenocrysts and microlites are out of equilibrium with groundmass glass, these phenocrysts and microlites likely crystallized mostly in the hotter (900-1000 °C) mafic mixing end member, while more sodic phenocrysts crystallized in the cooler (800-950 °C) felsic end member. Mixing between the silicic and mafic end members imposed

an undercooling on the mafic magma, triggering plagioclase microlite nucleation in these more calcic liquids.

The purpose of the final study was to investigate magmatic evolution of Bezymianny Volcano in Kamchatka, Russia through analyses of major, trace and volatile element compositions of melt inclusions. Inclusions dominantly record pressures of inclusion entrapment <50-100 MPa, indicating a zone of magmatic storage 2-4 km below the surface. Degassing and crystallization during ascent and shallow storage produces negative correlations between concentrations of incompatible lithophile (K_2O, Rb) and volatile (H_2O, CO_2) elements. Also, fluid ascent from depth leads to enrichment of shallowly-stored magma in lithium, on timescales of hours to days prior to eruption.

FOR SANTAKO

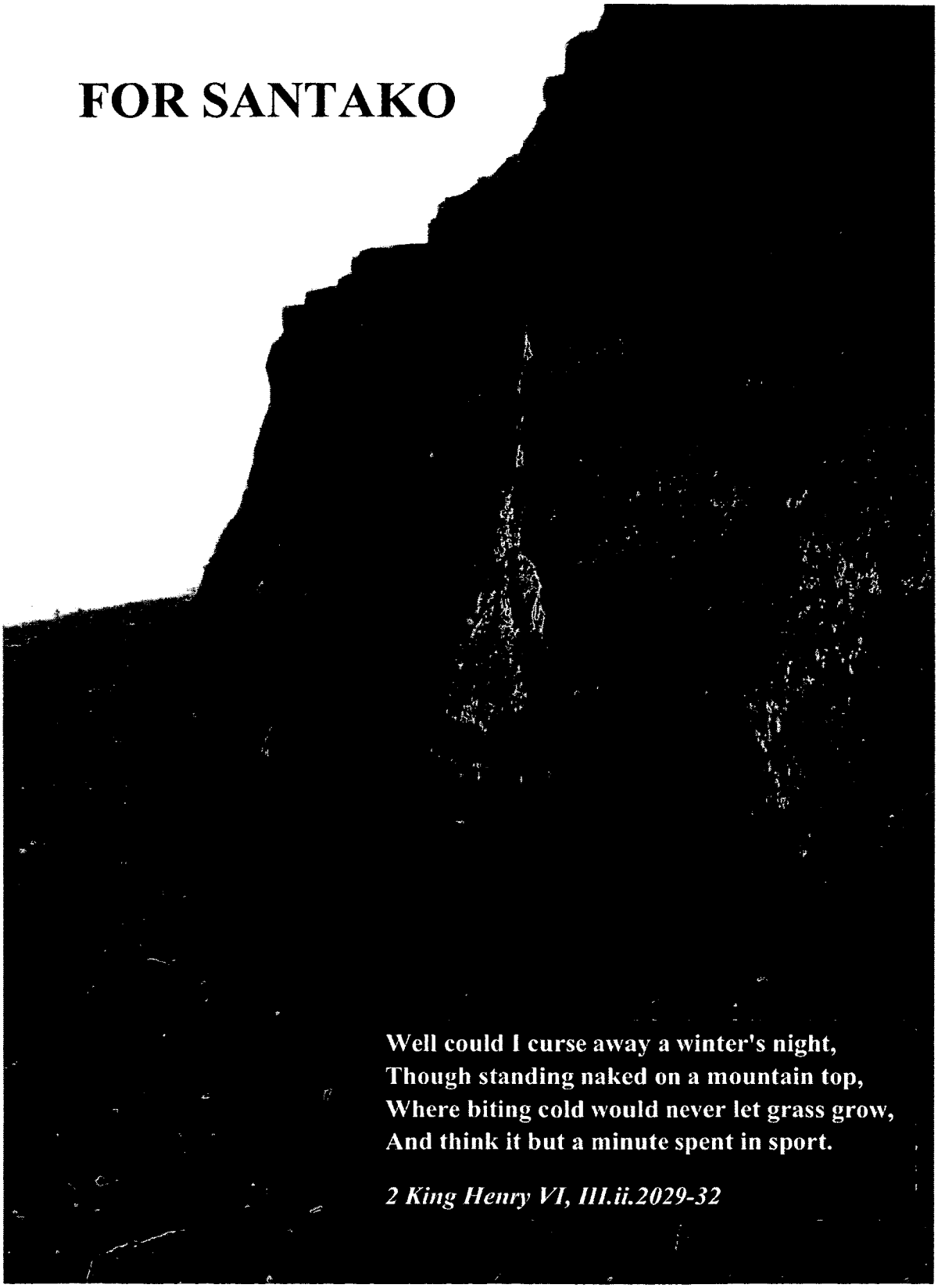

Well could I curse away a winter's night,
Though standing naked on a mountain top,
Where biting cold would never let grass grow,
And think it but a minute spent in sport.

2 King Henry VI, III.ii.2029-32

Table of Contents

Page

Signature Page i

Title Page ii

Abstract iii

Table of Contents vi

List of Figures xii

List of Appendices xv

Acknowledgments xvii

Chapter 1: Introduction 1

1.1: Dissertation Overview 1

1.2: First Geochemical Studies of Kasatochi 3

1.2.1: Petrological and Geochemical Characterization of the 2008 Kasatochi Eruption 3

1.2.2: Plagioclase Microlites at Kasatochi 5

1.3: Magmatic and Volatile Movement at Bezymianny Volcano 7

1.4: Summary 9

1.5: References 10

Chapter 2: Compositional Diversity in the Eruptive Products of the 2008 Kasatochi Eruption 15

2.1: Abstract 15

2.2: Introduction 16

2.2.1: Kasatochi Island Volcano 16

2.2.2: The 7-8 August, 2008 Eruption of Kasatochi 18

2.3: Methods 21

2.3.1: Sample Characterization 21

2.3.2: Bulk Chemistry 21

2.3.3: Mineral and Glass Compositions 22

2.3.4: Volatile Concentrations in Melt Inclusions 23

2.4: Results 25

2.4.1: Bulk Chemistry 25

2.4.2: Petrography 28

2.4.3: Pyroxene, Titanomagnetite, Amphibole and Olivine Compositions 29

2.4.4: Groundmass Glass 31

2.4.5: Plagioclase Textures and Compositions 32

2.4.6: H_2O and CO_2 Concentrations in Melt Inclusions 34

2.5: Discussion 34

2.5.1: Compositional Variations in the 2008 Kasatochi Eruptive Products 34

2.5.2: Basaltic Andesite..... 36

2.5.3: Andesite..... 38

2.5.4: Gabbroic Blocks..... 39

2.5.5: Implications for the 2008 Eruptive Sequence..... 40

2.6: Conclusions..... 43

2.7: Acknowledgments..... 44

2.8: Figures..... 46

2.9: References..... 62

Chapter 3: Pre-Eruptive Magma Mixing and Crystal Transfer Revealed by Phenocryst and Microlite Compositions in Basaltic Andesite from the 2008 Eruption of Kasatochi..... 75

3.1: Abstract..... 75

3.2: Introduction

3.2.1: Plagioclase Microlites in Volcanic Systems..... 76

3.2.2: Geologic Setting..... 78

3.3: Analytical Methods..... 81

3.4: Plagioclase in the 2008 Kasatochi Basaltic Andesite..... 82

3.4.1: Plagioclase Phenocrysts..... 82

3.4.2: Plagioclase Microlites..... 83

3.4.3: Plagioclase MgO and FeO Concentrations..... 84

3.5: Compositions of Groundmass Glass and Mafic Minerals 85

3.6: Pre-Eruptive Mixing Revealed by Phenocryst and Microlite Populations 86

3.6:1: Plagioclase Phenocrysts and Microlites Inherited from Mixing End Members 86

3.6:2: Mafic Phenocrysts Inherited from Mixing End Members 89

3.6:3: Temperature Constraints on Mixing End Members 91

3.7: Origins of High-An Plagioclase Microlites 94

3.7.1: Latent Heat Release Leads to More Calcic Microlites? 94

3.7.2: Mixing-Induced Microlite Crystallization 96

3.7:3: Minor and Trace Element Variations in Phenocryst Rims and Microlites 97

3.8: Summary 100

3.9: Acknowledgments 102

3.10: Figures 103

3.11: References 115

Chapter 4: Evolution of the Magmatic System of Bezymianny Volcano, Kamchatka, Russia: Insights from Compositional Analyses of Melt Inclusions....127

4.1: Abstract....127

4.2: Introduction....128

4.3: Methods....131

4.3.1: Sample Collection and Preparation....131

4.3.2: Secondary Ion Mass Spectrometry (SIMS)....132

4.3.3: Electron Probe Microanalysis (EPMA)....134

4.4: Compositions of Bezymianny Melt Inclusions....135

4.4.1: Major and Minor Oxides, Rb and Sr....135

4.4.2: H_2O, CO_2 and S....136

4.4.3: Li, Be and B....137

4.4.4: Halogens....139

4.5: Discussion....140

4.5.1: Melt Inclusion Entrapment Pressures and Depths....140

4.5.2: Shallow Magmatic Storage, Crystallization and Degassing at Bezymianny....142

4.5.3: Mechanisms for Low-Pressure Lithium Enrichment....145

4.5.4: Temporal Variations and Models for the Bezymianny Magma System....151

4.6: Conclusions....154

4.7: Acknowledgments....158

4.8: Figures..... 158

4.9: References..... 172

Chapter 5: Concluding Remarks..... 187

List of Figures

Page

Chapter 2: Compositional Diversity in the Eruptive Products of the 2008 Kasatochi Eruption

Figure 2-1: Location Maps of Kasatochi Island 46

Figure 2-2: Representative Photographs of Lithologies From the 2008 Kasatochi Eruption 47

Figure 2-3: Bulk-Rock Chemical Classification Diagrams 48

Figure 2-4: Trace Element Variation Diagrams 49

Figure 2-5: Major and Minor Element vs. SiO_2 Variation Diagrams 50

Figure 2-6: Trace Element vs. SiO_2 Variation Diagrams 51

Figure 2-7: Modal Phenocryst Proportions 52

Figure 2-8: Compositions of Pyroxene Phenocrysts 53

Figure 2-9: Compositions of Titanomagnetite Phenocrysts 54

Figure 2-10: Compositions of Amphibole Phenocrysts 55

Figure 2-11: Compositions of Groundmass Glass 56

Figure 2-12: Images of Representative Plagioclase Textures 57

Figure 2-13: Microprobe Transects of Plagioclase Phenocrysts 58

Figure 2-14: Compositions of Plagioclase Phenocryst Cores and Rims 59

Figure 2-15: H_2O and CO_2 Concentrations of Melt Inclusions 60

Figure 2-16: Schematic Mixing Relationships 61

Chapter 3: Pre-Eruptive Magma Mixing and Crystal Transfer Revealed by Phenocryst and Microlite Compositions in Basaltic Andesite from the 2008 Eruption of Kasatochi Volcano

Figure 3-1: Bulk Compositions..... 103

Figure 3-2: Representative Electron Microprobe Transects of Plagioclase Phenocrysts..... 104

Figure 3-3: Plagioclase Phenocryst and Microlite Compositions..... 105

Figure 3-4: Backscatter Electron Image of Zoned Plagioclase Microlites..... 106

Figure 3-5: Plagioclase Iron and Magnesium Concentrations..... 107

Figure 3-6: Groundmass Glass Compositions..... 108

Figure 3-7: Titanomagnetite Phenocryst Compositions..... 109

Figure 3-8: Amphibole Phenocryst Compositions..... 110

Figure 3-9: Plagioclase Ca/Na Ratios..... 111

Figure 3-10: Plagioclase FeO/MgO Ratios..... 112

Figure 3-11: Plagioclase-Liquid Hygrometry..... 113

Figure 3-12: Predicted Latent Heat Release from Microlite Crystallization..... 114

Chapter 4: Evolution of the Magmatic System of Bezymianny Volcano, Kamchatka, Russia: Insights from Compositional Analyses of Melt Inclusions

Figure 4-1: Location Map and Photo of Bezymianny 158

Figure 4-1: Representative Photomicrograph of Melt Inclusions 159

Figure 4-3: SIMS Calibration Curves 160

Figure 4-4: Major, Minor and Trace Element vs. SiO_2 Variation Diagrams 161

Figure 4-5: Variations in SiO_2 and H_2O with Eruption Date 162

Figure 4-6: Melt Inclusion H_2O and CO_2 Concentrations 163

Figure 4-7: Variations in H_2O, Cl and K_2O with S concentration 164

Figure 4-8: Variations in H_2O, CO_2 and S with Rb concentration 165

Figure 4-9: Variations in Light Trace Elements, Halogens, K_2O and Sr with H_2O concentration 166

Figure 4-10: Variations in Light Trace Elements, Halogens, K_2O and Sr with Rb concentration 167

Figure 4-11: Variations in K_2O and Rb with Entrapment Pressure 168

Figure 4-12: Variations in Li and Cl with Entrapment Pressure 169

Figure 4-13: Variations in CO_2, S and Na_2O with Li concentration 170

Figure 4-14: Timescales of Li Diffusion Through Plagioclase 171

List of Appendices

(Please note that all appendices are included electronically on the compact disc accompanying this dissertation)

Chapter 2: Compositional Diversity in the Eruptive Products of the 2008 Kasatochi Eruption

Appendix 2-1: Sample Descriptions

Appendix 2-2: Analytical Conditions for Electron Microprobe Analyses

Appendix 2-3: Bulk Chemical Analyses of 2008 Kasatochi Samples

Appendix 2-4: Modal Phenocryst Proportions of 2008 Kasatochi Samples

Appendix 2-5: Electron Microprobe Analyses of Clinopyroxene

Appendix 2-6: Electron Microprobe Analyses of Orthopyroxene

Appendix 2-7: Electron Microprobe Analyses of Titanomagnetite

Appendix 2-8: Electron Microprobe Analyses of Amphibole

Appendix 2-9: Electron Microprobe Analyses of Olivine

Appendix 2-10: Electron Microprobe Analyses of Groundmass Glass

Appendix 2-11: Electron Microprobe Analyses of Plagioclase Cores and Rims

Appendix 2-12: Analyses of H_2O and CO_2 in Melt Inclusions

Appendix 2-13: Core-Rim Transects of Plagioclase Phenocrysts

Chapter 3: Pre-Eruptive Magma Mixing and Crystal Transfer Revealed by Phenocryst and Microlite Compositions in Basaltic Andesite from the 2008 Eruption of Kasatochi Volcano

Appendix 3-1: Analytical Conditions for Electron Microprobe Analyses

Appendix 3-2: Electron Microprobe Analyses of Plagioclase Phenocryst Cores

Appendix 3-3: Electron Microprobe Analyses of Plagioclase Phenocryst Rims

Appendix 3-4: Electron Microprobe Analyses of Plagioclase Microlites

Appendix 3-5: Electron Microprobe Analyses of Groundmass Glass

Appendix 3-6: Electron Microprobe Analyses of Titanomagnetite

Appendix 3-7: Electron Microprobe Analyses of Amhibole

Appendix 3-8: Core-Rim Transects of Plagioclase Phenocrysts

Chapter 4: Evolution of the Magmatic System of Bezymianny Volcano, Kamchatka, Russia: Insights from Compositional Analyses of Melt Inclusions

Appendix 4-1: Sample Descriptions

Appendix 4-2: Compositions of Glass Standards used in SHRIMP Calibrations

Appendix 4-3: Compositions of Bezymianny Melt Inclusions

Appendix 4-4: Analytical Conditions for Electron Microprobe Analyses

Acknowledgments

I am deeply indebted to the members of my dissertation committee for their efforts in helping me complete this dissertation. I thank Pavel Izbekov for his boundless creative energy, and for constantly challenging me to deepen my thinking; Jessica Larsen for her patience, editorial prowess, and outstanding instruction on the chemistry and physics of magma; Christopher Nye (ADGGS) for sharing his astonishing wealth of knowledge on subjects such as trace element geochemistry, magmatic systems and Alaskan geology; and Kenneth Severin for his willingness to teach, which has expanded beyond measure my comprehension of electronics, data analysis and laboratory management. These exemplary scientists embody the highest standards of professional excellence, and it is against their standards that I will measure my future work.

I am very grateful to Heather Bleick (USGS), Cheryl Cameron (ADGGS), Pavel Plechov (Moscow State U.), Vasily Shcherbakov (Moscow State U.), and Jorge Vazquez (USGS) for their invaluable collaboration in the studies herein, and the members of the PIRE-Kamchatka project and of the ongoing interdisciplinary study of Kasatochi for their assistance in field work. I also thank the many fine scientists who have generously shared their expertise in a variety of subjects, including Michael Clynne (USGS), Michelle Coombs (USGS), Sarah de Angelis, Ronni Grapenthin, Alla Grikurova, Eric Hellebrand (U. Hawai'i), Ian F. Kilmister, Taryn Lopez, Trina Mamoon, William Scott (USGS), Karen Spaleta, Steven Turner (Harvard U.), Christopher Waythomas (USGS), Michael West, Heather Wright (USGS), Joseph Wooden (Stanford U.), and the faculty, staff and

students of the UAF Department of Geology and Geophysical Institute. I also am also grateful to the geology departments of Amherst College and the University of Hawai'i at Mānoa, especially my former advisors, Tekla Harms (Amherst Coll.) and Julia Hammer (U. Hawai'i), for providing me with excellent foundations on which to begin this work.

Funding for this work was provided by the National Science Foundation, the US Fish and Wildlife Service, the Jack Kleinman Fellowship Program, the American Recovery and Reinvestment Act, the Alaska Volcano Observatory, the North Pacific Research Board, and the UAF Advanced Instrumentation Laboratory. Special thanks to the USFWS, Jeff Williams in particular, who provided the opportunity to visit Kasatochi. Capt. Billy Pepper and the crew of the M/V *Tiĝlax̂* provided safe transport to and from Kasatochi; their professionalism, hospitality and fine seamanship were much appreciated.

Finally, I thank my parents, Theresa Kelly and Stephen Neill, for their unending support, love and encouragement, not only during my time at UAF, but everywhere I go and in everything I do.

These acknowledgments reflect the generous contributions of the people and organizations listed above to this dissertation, but do ***NOT*** necessarily indicate their acceptance or endorsement of the ideas and conclusions presented herein. Any mistakes, misconceptions or typographical errors are entirely my own.

Owen Kelly Neill
Fairbanks, Alaska, USA
18 May, 2013

Chapter 1: Introduction

To grant me a vision of nature's forces
That bind the world, all its seeds and sources
And innermost life -- all this I shall see,
And stop peddling in words that mean nothing to me.

Goethe, Faust, *354-385*

1.1: Dissertation Overview

In addition to being one of nature's most spectacular phenomena, the eruption of magma from a volcano involves highly complex, and not always well-understood, processes that move magma from storage regions within the earth's crust to the surface. Unfortunately, the paths that a magma may take on its journey upwards, and the ways in which different magmas can evolve and interact along these pathways, cannot be observed directly, and therefore many models for such processes are based on *ex post facto* measurements of the chemical compositions of the products of volcanic eruptions. The purpose of this dissertation is to use different geochemical tracers to evaluate how magmas move, mix, degas and crystallize, in order to better understand the subsurface magmatic systems of Kasatochi Island volcano in the central Aleutian Islands, and Bezymianny Volcano, located in Kamchatka, Russia. Such measurements can help elucidate how magmas ascend to the surface, degas, crystallize, mix with other magmas, and erupt, processes that are key to understanding how magmas move through the

subsurface plumbing systems beneath volcanoes. Improved understanding of how magmas move through the subsurface plumbing systems can, in turn, be of great benefit when estimating the causes and consequences of eruptions of any given volcano.

Both Kasatochi and Bezymianny have received increasing attention from volcanologists in recent years. Prior to its eruption in 2008, Kasatochi had been mostly ignored in studies of Aleutian volcanism. The work presented in Chapters 2 and 3 represents some of the first geochemical studies ever focused specifically on Kasatochi, shedding the first light on this under-studied but highly explosive island volcano. Bezymianny, meanwhile, is considered an excellent analogue for one of North America's most famous volcanoes, Mount St. Helens in southwestern Washington. As such, studies of Bezymianny can offer new insights into the dynamics of Mount St. Helens, a volcano that has been active as recently as 2008 and killed 57 people during its most famous eruption in 1980. In a similar vein, studies of these volcanoes can also be of broader benefit beyond strictly academic volcanology. These two volcanoes are both situated along trans-Pacific airline routes, and have the potential to cause serious disruption to commerce and potentially loss of life, should an airplane encounter ash from an eruption of one of these volcanoes. Understanding the magmatic systems of volcanoes such as these can help elucidate how, why and when they erupt, which can in turn help mitigate the threats they pose to air travel.

1.2: First Geochemical Studies of Kasatochi

1.2.1: Petrological and Geochemical Characterization of the 2008 Kasatochi Eruption

The 2008 eruption of Kasatochi, an island stratovolcano in the central Aleutian islands, was something of a surprise. With a largely unconstrained historical record of eruptions, Kasatochi was evaluated as only a moderate threat by the hazard assessment of Ewart et al. (2005). While the 2008 eruption generated considerable interest in Kasatochi due to its anomalously energetic seismicity (Ruppert et al., 2011), its considerable release of sulfur dioxide, an important greenhouse gas (e.g., Kristiansen et al., 2010), and its deleterious effects on the island's flora and fauna (e.g., Williams et al., 2010), studies of the geology of Kasatochi remain sparse. Prior geological studies focused on the island were devoted almost exclusively to the geomorphologic effects and volcanic sedimentology of the 2008 eruption (Scott et al., 2010; Waythomas et al., 2010a; Waythomas et al., 2010b). Published petrologic and geochemical data from Kasatochi is limited to the characterization of one basaltic specimen, first reported in Kay and Kay (1985), and referenced sporadically in more general studies of petrogenesis in the Aleutians (e.g., Yogodzinski et al., 1995; George et al., 2003). It is therefore impossible to consider problems of magma movement, mixing, degassing or crystallization, without first addressing the basic geology, petrology and geochemistry of the island.

Chapter 2 addresses this basic deficiency in the general geologic knowledge of Kasatochi, and provides the groundwork for future petrologic and geochemical studies of the island. Also, using the major, minor and trace element concentrations of bulk

samples, and the major and minor element concentrations of minerals, this chapter provides a preliminary model for the state of the Kasatochi magma system during the 2008 eruption. The 2008 eruption produced andesite and basaltic andesite clasts, which vary in bulk composition, with andesite clasts containing ~58-62 wt. % SiO_2 and basaltic andesite clasts falling between ~52-56 wt. % SiO_2. The presence of banded clasts indicates some degree of pre-eruptive interaction between the two magmas, but in the main, pre-eruption physical and chemical interactions between the andesite and basaltic andesite appear to have been very limited. Mechanisms to produce compositionally diverse magmas within a single eruption from a single magmatic storage region, such as pre-eruptive mixing or eruption from a zoned reservoir, are specifically contraindicated by the overall bulk-rock compositional trends, as the overall linear trends seen in element-element variation diagrams shown in Chapter 2 are not congruent throughout all components. The andesite and basaltic andesite must have resided in spatially and chemically distinct storage areas until just prior to eruption, with any mixing between the two magmas limited to a brief period prior to eruption, and affecting only a small portion total volume of erupted material. Magmatic ascent rates were likely high (>0.1-0.2 m/s), as both the andesite and basaltic andesite contain phenocrysts of amphibole with no evidence of disequilibrium or breakdown, which would have formed had the magma spent a prolonged period of time outside of the P-T conditions where amphibole is stable.

1.2.2: Plagioclase Microlites at Kasatochi

Plagioclase microlites are small (<150 μm) crystals of plagioclase found in the groundmasses of volcanic rocks, which are typically assumed to grow syn-eruptively due to the high effective undercooling induced by decompression and degassing during magmatic ascent (e.g., Geschwind and Rutherford, 1995; Hammer and Rutherford, 2002). If such a model were in operation, the microlites would grow from the final interstitial melts available in the system prior to eruption and quenching. Such melts should be some of the most evolved, sodic melts available throughout the magma's lifecycle, and therefore the plagioclase growing from them should also be the some of the most sodic in the system. Based on the assumption of syn-eruptive microlite crystallization, measurements of plagioclase microlite textures and compositions have proved a powerful tool for deciphering the magmatic histories of volcanic rocks, used to infer magmatic parameters such as lava effusion rates (e.g., Noguchi et al., 2008), magma ascent rates (e.g., McCanta et al., 2007), H_2O exsolution rates (e.g., Toramaru et al., 2008), and crystal growth rates (e.g., Armienti, 2008).

However, as outlined in Chapter 3, the microlites at Kasatochi do not conform to this standard model. Similar to Soufriere Hills and Mount Pelée Volcanoes in the Caribbean arc (Couch et al., 2003; Martel et al., 2006), microlites from the 2008 Kasatochi basaltic andesite are highly calcic, far more calcic than the rims of plagioclase phenocrysts, which should also have grown in those final, most sodic melts. Rather than being the products of decompression crystallization, these microlites are the result of pre-

eruptive magma mixing between mafic and felsic end members, which also contributed to heterogeneities in the bulk and phenocryst compositions of the basaltic andesite. The basaltic andesite contains two plagioclase phenocryst populations, which are derived from these two different sources. The more sodic, oscilliatory zoned Group 1 plagioclase phenocrysts likely crystallized in the silicic mixing end member at lower temperatures (~800-950 °C) in addition to high-Ti titanomagnetite and low-Al amphibole phenocrysts. The higher-An, texturally homogenous Group 2 plagioclase phenocrysts likely crystallized in the hotter (~900-1000 °C), more mafic end member with low-Ti titanomagnetite and high-Al amphibole phenocrysts.

The Group 2 plagioclase phenocrysts, along with the highly calcic plagioclase microlites, are out of equilibrium with measured groundmass glass compositions, unlike the Group 1 phenocrysts, and therefore the calcic microlites likely derive mostly from the mafic end member as well. Mixing between the cooler, silicic end member and the hotter, mafic end member imposed an undercooling on the mafic magma, which triggered a burst of plagioclase microlite nucleation in a more calcic liquid. The high undercooling created by the mixing was exacerbated by degassing due to syn-eruptive decompression, causing boundary layers rich in incompatible elements (e.g., Fe, Mg) and depleted in compatible elements (e.g., Ca) from around microlites and Group 2 phenocrysts, leading to the formation of more sodic rims on Group 2 phenocrysts and leading to higher Fe and Mg concentrations in more sodic microlites and Group 2 rims. Chapter 3 not only provides insight into magma mixing processes at Kasatochi based on bulk-rock, phenocryst and plagioclase microlite compositions, but also highlights the importance of

verifying standard assumptions behind petrological models. Inferring magmatic parameters such as those described above based on measurements of the textures and compositions of the microlites from the 2008 Kasatochi basaltic andesite would yield spurious and misleading results, as they were not formed under standard conditions.

1.3: Magmatic and Volatile Movement at Bezymianny Volcano

While the venue shifts for the third major project presented in this dissertation, the overriding theme of tracing magma movement with geochemistry remains the same. Chapter 4 presents an examination of the magmatic evolution, fluid movement and degassing processes at Bezymianny Volcano in Kamchatka, Russia. Bezymianny was chosen as a target for this due to its unique characteristic eruption on 30 March, 1956, which was triggered by the failure of the flank of the volcano which led to a directed lateral explosion, a sequence almost identical to the 1980 eruption of Mount St. Helens (Bogoyavlenskaya et al., 1985). Comparative studies of these two volcanoes (such as those listed above) have tended to focus on similarities in the styles of their climactic eruptions, particularly the flank failures and directed lateral explosions (e.g., Bogoyavlenskaya et al., 1985; Belousov, 1996; Belousov et al., 2007; Neill et al., 2010). However, comparisons of the volcanoes from a geochemical perspective and the responses of the magmatic systems to their unique progressions after their climactic eruptions are comparatively rare. In this regard, Bezymianny offers an opportunity to use

similar geochemical tracers to those employed at Kasatochi in Chapter's 2 and 3, but at a better-studied volcano with a much longer recorded history of eruptive activity.

In Chapter 4, measurements of major, minor and trace elements in melt inclusions by electron microprobe and secondary ion mass spectrometry are used to examine magmatic evolution, fluid movement and degassing processes at Bezymianny Volcano in Kamchatka, Russia. Melt inclusions are small volumes of melt entrapped within the structure of phenocrysts, which can provide snapshots of the magmatic system prior to syn-eruptive modifications, if the liquids contained within are isolated from the magmatic system by the host crystal (e.g., Kent, 2008; Metrich and Wallace, 2008). Thus, analyses of the compositions of melt inclusions provide a probe into different regions of a volcano's magmatic plumbing system. Analyses of lithium and volatile element concentrations in melt inclusions have revealed that magma at Mount St. Helens is stored at shallow levels beneath the volcano, where it experiences significant enrichment in lithium due to "gas streaming," or the upward flow of volatile- and lithium-rich magmatic fluids from deep in the magma system (e.g., Berlo et al., 2004; Blundy et al., 2008). As described in Chapter 4, analyses of melt inclusions have revealed that magma at Bezymianny undergoes similar shallow storage and Li-enrichment due to gas streaming, but unlike at Mount St. Helens, such gas streaming is a much more transient feature, occurring on timescales of only days or weeks prior to eruption, and ceasing almost entirely in more recent eruptions, as the edifice at Bezymianny has rebuilt itself. This indicates that while processes occurring within the magmatic systems at Bezymianny and

Mount St. Helens may mirror one another superficially, local variations in volcanic character may generate distinct differences between otherwise-similar systems.

1.4: Summary

Application of different geochemical tracers to the magmatic plumbing systems of Kasatochi and Bezymianny reveal two very different magmatic environments, despite both volcanoes producing eruptive products that are superficially similar in composition. The geochemical tracers applied to the 2008 eruption of Kasatochi reveal it to have been a violent, short-duration event, marked by high magmatic ascent rates and rapid movements of magma through the crust that did not allow for complete mixing and chemical homogenization of the eruptive products or amphibole breakdown, or for the signatures of pre-eruptive mixing with the basaltic andesite to be completely erased. By contrast, geochemical tracers applied to Bezymianny reveal its long-term evolution, with patterns of volatile movement and shallow magmatic storage changing as the volcano has erupted and effused since the climactic eruption in 1956. Further work directed at Kasatochi may reveal whether such short, highly explosive events that produce such heterogeneous eruptive products are the norm at Kasatochi, as well as building on the studies presented here to paint a more complete picture of the island's magmatic system and history. By contrast, further work at Bezymianny will help continue to document the

volcano's longer-term evolution, and how processes of volatile and magma movement continue to evolve as the volcano rebuilds itself.

Chapters 2, 3 and 4 are all currently being prepared for peer review and possible publication in the *Journal of Volcanology and Geothermal Research*. Citations and reference lists in all chapters are formatted according to the requirements of this journal.

1.5: References

Armienti, P., 2008. Decryption of igneous rock textures: crystal size distribution tools. Rev Mineral Geochem, 69: 623-649. doi: 10.2138/Rmg.2008.69.16

Belousov, A., 1996. Deposits of the 30 March 1956 directed blast at Bezymianny volcano, Kamchatka, Russia. B Volcanol, 57(8): 649-662.

Belousov, A., Voight, B. and Belousova, M., 2007. Directed blasts and blast-generated pyroclastic density currents: a comparison of the Bezymianny 1956, Mount St Helens 1980, and Soufriere Hills, Montserrat 1997 eruptions and deposits. B Volcanol, 69(7): 701-740. doi: 10.1007/s00445-006-0109-y

Berlo, K., Blundy, J., Turner, S., Cashman, K., Hawkesworth, C. and Black, S., 2004. Geochemical precursors to volcanic activity at Mount St. Helens, USA. Science, 306(5699): 1167-1169. doi: 10.1126/science.1103869

Blundy, J., Cashman, K.V. and Berlo, K., 2008. Evolving magma storage conditions beneath Mount St. Helens inferred from chemical variations in melt inclusions from the 1980–1986 and current (2004–2006) eruptions. In: D.R. Sherrod, W.E. Scott and P.H. Stauffer (Editors), A Volcano Rekindled: The Renewed Eruption of Mount St. Helens, 2004-2006. US Geol Surv Prof Pap 1750, pp. 775-790.

Bogoyavlenskaya, G.E., Braitseva, O.A., Melekestsev, I.V., Kiriyanov, V.Y. and Miller, C.D., 1985. Catastrophic Eruptions of the Directed-Blast Type at Mount St-Helens, Bezymianny and Shiveluch Volcanos. J Geodyn, 3(3-4): 189-218.

Couch, S., Harford, C.L., Sparks, R.S.J. and Carroll, M.R., 2003. Experimental Constraints on the Conditions of Formation of Highly Calcic Plagioclase Microlites at the Soufrire Hills Volcano, Montserrat. J Petrol, 44(8): 1455-1475. doi: 10.1093/petrology/44.8.1455

Ewart, J.W., Guffanti, M. and Murray, T.L., 2005. An Assessment of Volcanic Threat and Monitoring Capabilities in the United States: Framework for a National Volcano Early Warning System. In: U.S.G. Survey (Editor). Open-File Report OF 2005-1164, pp. 62.

George, R., Turner, S., Hawkesworth, C., Morris, J., Nye, C., Ryan, J. and Zheng, S.-H., 2003. Melting processes and fluid and sediment transport rates along the Alaska-Aleutian arc from an integrated U-Th-Ra-Be isotope study. J Geophys Res, 108(B5): 2252. doi: 10.1029/2002jb001916

Geschwind, C.H. and Rutherford, M.J., 1995. crystallization of microlites during magma ascent - the fluid-mechanics of 1980-1986 eruptions at Mount St. Helens. B Volcanol, 57(5): 356-370.

Hammer, J.E. and Rutherford, M.J., 2002. An experimental study of the kinetics of decompression-induced crystallization in silicic melt. J Geophys Res-Sol Ea, 107(B1). doi: 10.1029/2001jb000281

Kay, S. and Kay, R., 1985. Aleutian tholeiitic and calc-alkaline magma series I: The mafic phenocrysts. Contrib Mineral Petr, 90(2): 276-290. doi: 10.1007/bf00378268

Kent, A.J.R., 2008. Melt inclusions in basaltic and related volcanic rocks. Rev Mineral Geochem, 69: 273-331. doi: 10.2138/rmg.2008.69.8

Kristiansen, N.I., Stohl, A., Prata, A.J., Richter, A., Eckhardt, S., Seibert, P., Hoffmann, A., Ritter, C., Bitar, L., Duck, T.J. and Stebel, K., 2010. Remote sensing and inverse transport modeling of the Kasatochi eruption sulfur dioxide cloud. J Geophys Res-Atmos, 115: D00L16. doi: 10.1029/2009jd013286

Martel, C., Radadi Ali, A., Poussineau, S., Gourgaud, A. and Pichavant, M., 2006. Basalt-inherited microlites in silicic magmas: Evidence from Mount Pelée (Martinique, French West Indies). Geology, 34(11): 905-908. doi: 10.1130/g22672a.1

McCanta, M.C., Rutherford, M.J. and Hammer, J.E., 2007. Pre-eruptive and syn-eruptive conditions in the Black Butte, California dacite: Insight into crystallization kinetics in a silicic magma system. J Volcanol Geoth Res, 160(3-4): 263-284. doi: 10.1016/J.Jvolgeores.2006.10.004

Metrich, N. and Wallace, P.J., 2008. Volatile Abundances in Basaltic Magmas and Their Degassing Paths Tracked by Melt Inclusions. Rev Mineral Geochem, 69: 363-402. doi: 10.2138/Rmg.2008.69.10

Neill, O.K., Hammer, J.E., Izbekov, P.E., Belousova, M.G., Belousov, A.B., Clarke, A.B. and Voight, B., 2010. Influence of pre-eruptive degassing and crystallization on the juvenile products of laterally directed volcanic explosions. J Volcanol Geoth Res, 198(1-2): 264-274. doi: 10.1016/j.jvolgeores.2010.09.011

Noguchi, S., Toramaru, A. and Nakada, S., 2008. Relation between microlite textures and discharge rate during the 1991-1995 eruptions at Unzen, Japan. J Volcanol Geoth Res, 175(1-2): 141-155. doi: 10.1016/J.Jvolgeores.2008.03.025

Ruppert, N.A., Prejean, S. and Hansen, R.A., 2011. Seismic swarm associated with the 2008 eruption of Kasatochi Volcano, Alaska: Earthquake locations and source parameters. J Geophys Res, 116: B00B07. doi: 10.1029/2010jb007435

Scott, W.E., Nye, C.J., Waythomas, C.F. and Neal, C.A., 2010. August 2008 Eruption of Kasatochi Volcano, Aleutian Islands, Alaska-Resetting an Island Landscape. Arct Antarct Alp Res, 42(3): 250-259. doi: 10.1657/1938-4246-42.3.250

Toramaru, A., Noguchi, S., Oyoshihara, S. and Tsune, A., 2008. MND (microlite number density) water exsolution rate meter. J Volcanol Geoth Res, 175(1-2): 156-167. doi: 10.1016/J.Jvolgeores.2008.03.035

Waythomas, C.F., Scott, W.E., Prejean, S.G., Schneider, D.J., Izbekov, P. and Nye, C.J., 2010a. The 7-8 August 2008 eruption of Kasatochi Volcano, central Aleutian Islands, Alaska. J Geophys Res, 115: B00B06. doi: 10.1029/2010jb007437

Waythomas, C.F., Scott, W.E. and Nye, C.J., 2010b. The geomorphology of an Aleutian Volcano following a major eruption: the 7-8 August 2008 eruption of Kasatochi Volcano, Alaska, and its aftermath. Arct Antarct Alp Res, 42(3): 260-275. doi: Doi 10.1657/1938-4246-42.3.260

Williams, J.C., Drummond, B.A. and Buxton, R.T., 2010. Initial Effects of the August 2008 Volcanic Eruption on Breeding Birds and Marine Mammals at Kasatochi Island, Alaska. Arct Antarct Alp Res, 42(3): 306-314. doi: 10.1657/1938-4246-42.3.306

Yogodzinski, G.M., Kay, R.W., Volynets, O.N., Koloskov, A.V. and Kay, S.M., 1995. Magnesian andesite in the western Aleutian Komandorsky region: Implications for slab melting and processes in the mantle wedge. Geol Soc Am Bull, 107(5): 505-519. doi: 10.1130/0016-7606(1995)107

Chapter 2: Compositional Diversity in the Eruptive Products of the 2008 Kasatochi Eruption[1]

For you, the city, thus I turn my back
There is a world elsewhere

Coriolanus, III.iii.,166-67

2.1: Abstract

The 7-8 August 2008 eruption of the Kasatochi Island volcano, located in the central Aleutians Islands, Alaska, produced lithic-rich pyroclastic falls and flows containing a juvenile magmatic component dominated by two lithologies, an andesite with 58-62 wt. % SiO_2 and a basaltic andesite with 52-55 wt. % SiO_2. Banded pumice, intermediate in composition, was also erupted but is subordinate in volume. Both lithologies contain a phase assemblage of plagioclase, amphibole, ortho- and clinopyroxene and Fe-Ti oxides. SIMS measurements of H_2O and CO_2 concentrations in melt inclusions indicate pre-eruptive volatile contents of ~5-7 wt. % H_2O and <1000 ppm CO_2 in both lithologies. Whole rock major and trace element compositions indicate that the andesite and basaltic andesite had only minor interaction prior to eruption and were

[1] Neill, O.K., Izbekov, P.E., Nye, C.J., Bleick, H.B., Cameron, C.E., and Larsen, J.F. (*in prep*) Compositional diversity in the eruptive products of the 2008 eruption of Kasatochi volcano, Central Aleutian Islands, Alaska. To be submitted to *Journal of Volcanology and Geothermal Research.*

likely stored in separate regions. Storage conditions, however, were likely similar (8-12 km depth at ~850-950°C for the andesite and 900-1000 °C for the basaltic andesite). Resorption textures and zoning patterns of plagioclase phenocrysts, combined with bulk chemical trends, indicate that the basaltic andesite had been affected prior to eruption by episodes of mafic recharge, which did not affect the andesite. Ascent rates were likely high (>0.2 m s^{-1}), exceeding the onset of amphibole breakdown. Gabbroic xenoliths, consisting of amphibole-plagioclase-pyroxene gabbro, were also included in the eruptive products and were most likely carried with the basaltic andesite during ascent.

2.2: Introduction

2.2.1: Kasatochi Island Volcano

Kasatochi is a volcanic island in the central Aleutian Islands, consisting of a 3-km-wide volcanic cone rising ~300 m above sea level (Fig. 2-1), with the summit truncated by a 1.2-km-wide crater containing a brackish (Bailey and Trapp, 1986) crater lake. Exposed pre-2008 deposits consist of an interbedded basal package of hyaloclastites, lahars, pyroclastic units and lava flows, labeled here as the Peregrine volcaniclastic unit (VCU); a next-younger series of basalt, basaltic andesite and andesite lava flows; and an uppermost unit of pyroclastic flow (PF) and surge deposits, best exposed on the southwest side of the island, representing the most recent explosive

activity at Kasatochi prior to 2008 and referred to herein as the penultimate PFs (Waythomas et al., 2010a). Beyond a few early reports (Grewingk, 1850; Jaggar, 1927; Coats, 1950), little was known about the pre-2008 eruptive history of Kasatochi, although Waythomas et al. (2010a) suggest that the most recent significant explosive event could not have occurred more recently than several hundred years, predating the historical record of the area.

Because of its remote location and lack of recorded eruptive history, studies of Kasatochi are rare; in fact, no geologic studies focused specifically on Kasatochi are published prior to 2008, although the location and general geologic setting are described in preliminary surveys of the area (e.g., Coats, 1956) and the island is mentioned in a few studies of magma petrogenesis in the Aleutian Island arc system (Kay and Kay, 1985; Myers et al., 1985; Romick et al., 1992; Yogodzinski et al., 1995; Yogodzinski and Kelemen, 1998; George et al., 2003; Yogodzinski et al., 2010). The only pre-2008 published chemical analyses of Kasatochi eruptive products come from the sample KAS-7, a calc-alkaline, high-Al basalt, containing plagioclase, olivine and clinopyroxene, analyses of which were first reported in Kay and Kay (1985) and later used in subsequent studies of the area (e.g., Yogodzinski et al., 1995; George et al., 2003). Prior to the 2008 eruption, Kasatochi had been classified as a moderate threat volcano due to its remoteness and lack of recorded eruptions (Ewert et al., 2005). The Alaska Volcano Observatory (AVO), the agency responsible for monitoring Alaska volcanoes, has no permanent monitoring stations on the island.

The purpose of this study is to characterize the petrology and geochemistry of the 2008 Kasatochi eruptive products and to develop an initial model for the Kasatochi magmatic system prior to and during the eruption. More specifically, this study compares the bulk and constituent mineral compositions of andesite, basaltic andesite and gabbroic material in order to determine the mechanisms by which the andesite and basaltic andesite came to coexist and ascend together to the surface.

2.2.2: The 7-8 August, 2008 Eruption of Kasatochi

Retrospective analysis showed that pre-eruptive seismicity at Kasatochi began approximately one month prior to eruption. At the time, however, unrest indicative of potential eruption was only recognized due to the marked increase in seismic activity on 6 August, 2008, ~36 hours prior to the eruption (Ruppert et al., 2011). The first ash plume was detected on the afternoon of 7 August, and continuous ash emission continued for approximately 21 hours, punctuated by five major explosive events during this period (Arnoult et al., 2010; Fee et al., 2010; Ruppert et al., 2011). The pre-eruptive and syn-eruptive seismicity was exceptionally strong and included one earthquake of magnitude 5.9 and ~12 earthquakes with a magnitude of 4 or greater (Ruppert et al., 2011). The total seismic energy released was the largest recorded during any volcanic eruption in Alaska since the AVO began monitoring Alaskan volcanoes in 1988 (Waythomas et al., 2010a). The explosions at Kasatochi produced ash-gas plumes that rose to heights up to 18km above sea level (ASL) and emitted 0.3 Tg of fine (1-10 μm) ash and ~1.7 Tg of sulphur

dioxide, making Kasatochi the single largest point source emission of SO_2 since the 1991 eruptions of Cerro Hudson and Pinatubo volcanoes (Bluth et al., 1992; Karagulian et al., 2010; Kristiansen et al., 2010; Prata et al., 2010). According to Waythomas et al. (2010a), the total volume of erupted material exceeds 0.2 km^3 bulk volume, placing the 2008 eruption of Kasatochi at 3-4 on the Volcanic Explosivity Index (Newhall and Self, 1982).

Scott et al. (2010) and Waythomas et al. (2010a; 2010b) provide full descriptions of the pyroclastic deposits from the 2008 Kasatochi eruption; a brief summary is included here. In addition to ash and SO_2, the explosions at Kasatochi produced voluminous pyroclastic flows, which increased the area of the island by ~30% and covered the island with pyroclastic deposits that vary in thickness between ~2 and 30 m. The sequence is divided into four main layers. Layer 1, which is stratigraphically lowest, consists of thinly bedded mud and ash fall, likely from early phreatomagmatic explosions caused by the interaction of ascending magma with the water of the crater lake, clearing water and lake sediments from the crater. Layer 2 is a massive, yellowish-grey, friable pyroclastic-flow deposit that, in places, exceeds 15 m in thickness, the result of a voluminous pyroclastic flow following the opening explosions. Layer 3 contains a sequence of massive pyroclastic-flow deposits interspersed with thinly bedded surge deposits and coarse lapilli fall beds with a maximum thickness of ~20 m. Layer 4, the uppermost layer, consists of ash and accretionary-lapilli deposits, alternating between finely bedded, and in places, cross-bedded, surge deposits and ash/lapilli fall beds. These deposits are likely the result of magmatic/phreatomagmatic explosions at the end of the eruption, as magma output waned and water was able flow into the vent from remaining lake water and from

groundwater outflow into the enlarged crater. All four layers are lithic-rich (50-90% of clasts, Waythomas et al., 2010a), with lithics acquired mostly from the crater walls. The small size of the island means that distal deposits (>0.5 km from vent) that would likely be less lithic-rich are unavailable, though ash and floating pumice from the eruption were found on nearby islands (Scott et al., 2010; Waythomas et al., 2010a).

Juvenile pyroclasts produced by the 2008 Kasatochi eruption are heterogeneous in hand-specimen appearance (Fig. 2-2). White, pumiceous clasts (Fig. 2-2a) contain vesicles up to 5-10 mm in diameter, with plagioclase, amphibole, pyroxene and titanomagnetite phenocrysts surrounded by glassy groundmass. Grey-brown clasts (Fig. 2-2b) are typically denser, with surface vesicles <1 mm. Phenocrysts appear similar to those in whiter clasts, though macroscopic glass is rare. Banded clasts (Fig. 2-2c) are common, with sharp boundaries between darker, denser domains and lighter-colored, more vesicular regions. In these banded clasts, the volume of darker material can be much greater, much less or approximately equal to the volume of lighter material in banded clasts; proportions of the two components do not appear to vary systematically with either clast size or stratigraphic position. Blocks of amphibole-plagioclase-pyroxene gabbro are also present in the upper parts of Layer 3 (Fig. 2-2d). Textures of these blocks vary, but all contain tabular or lathlike amphibole and plagioclase crystals, which can exceed 5 cm in length, along with minor amounts of clinopyroxene and titanomagnetite. Some samples also contain fine, black interstitial matrix, which is finely vesicular and composed of brown glass and abundant quench microlites. Holocrystalline blocks are often highly friable.

2.3: Methods

2.3.1: Sample Characterization

A representative suite of juvenile pyroclasts and gabbro blocks was collected from the 2008 Kasatochi deposits during trips to the island in the summers of 2008, 2009, 2010 and 2011 and has been partially characterized by previous authors (Izbekov, 2008; Izbekov et al., 2009; Waythomas et al., 2010a). As Layers 1 and 4 are nearly devoid of juvenile pyroclasts >2 mm in diameter, both gabbro blocks and juvenile clasts were taken exclusively from Layers 2 and 3, the main 2008 pyroclastic-flow units. Individual mineral phases were identified visually in hand sample and thin section and by energy dispersive spectrometry (EDS) using a CAMECA SX-50 electron microprobe, equipped with an EDAX EDS detector, at the Advanced Instrumentation Laboratory (AIL) of the University of Alaska Fairbanks. Phenocryst proportions were determined by point counting (1000 points) of thin sections, using a standard petrographic microscope and automated stage. Descriptions of samples used in this study are provided in Appendix 2-1. Readers should note that all appendices are included electronically on the compact disc accompanying this dissertation.

2.3.2: Bulk Chemistry

Whole-rock concentrations of Ni, Cr, Sc, V, Ba, Sr, Zr, Ga, Cu and Zn, as well as major and minor element concentrations, were determined by X-ray fluorescence

spectrometry (XRF) at the GeoAnalytical Laboratory, Washington State University, using procedures outlined in Johnson et al. (1999). To summarize, samples were cleaned in an ultrasonic bath, then lightly crushed and picked by hand to remove any altered or organic material. The resulting chips were washed again in deionized water in an ultrasonic bath and then powdered in a tungsten carbide shatterbox for ~2 minutes. Approximately 3g of sample material, mixed with ~7g of $Li_2B_4O_7$ flux, was fused into a glass disc and analyzed using a ThermoARL XRF Spectrometer. Whole-rock concentrations of U, Th, Pb, Nb, Hf, Ta, Rb, Cs, Y and the lanthanide series elements were measured by inductively coupled plasma mass spectrometry (ICP-MS) at the WSU GeoAnalytical Laboratory, using procedures outlined in Knaack et al. (1994) and Johnson et al. (1999). Powders were fused at 1000°C in a muffle furnace, distilled via open-vial acid digestion using mixtures of HNO_3 and $HClO_4$, and analyzed using a Finnegan Element2 ICP-MS. Also analyzed by XRF and ICP-MS were two separates of the finely crystalline interstitial matrix material, picked by hand from different gabbroic blocks. Major and minor element concentrations are reported as oxides, although they are referred to as "elements" to avoid terminological confusion with Fe-Ti oxide minerals.

2.3.3: Mineral and Glass Compositions

Minerals, groundmass glass and melt inclusions were analyzed for major and some minor element concentrations by wavelength-dispersive X-ray spectrometry using the 4-spectrometer CAMECA SX-50 electron microprobe at AIL and a 5-spectrometer

JEOL JXA-8900 electron microprobe at the U.S. Geological Survey in Menlo Park, CA (see Appendix 2-2 for operating conditions and analytical uncertainties). Concentrations were obtained from raw intensities using a ZAF intensity correction. During analyses of groundmass glass and melt inclusions, the beam was defocused to a diameter of ~10 μm, and Si, Na and K were counted first to minimize elemental migration during analyses. Na intensities were also corrected in glass and melt inclusion analyses using Time-Dependent Intensity corrections through ProbeForEPMA software (Nielsen and Sigurdsson, 1981; Donovan et al., 2007). Mineral structural formulae and end-members were calculated from oxide analyses using ILMAT (Lepage, 2003) for titanomagnetite, Probe-Amph (Tindle and Webb, 1994) for amphibole and CALCMIN (Brandelik, 2009) for all other mineral phases. Similar to bulk compositions, elemental concentrations determined by electron microprobe are reported as oxides in all appendices but referred to as "elements" in text.

2.3.4: Volatile Concentrations in Melt Inclusions

Melt inclusions from the 2008 Kasatochi andesite were previously analyzed by Izbekov et al. (2009). To complement that study, melt inclusions in plagioclase and pyroxene crystals from the 2008 Kasatochi basaltic andesite were prepared for analyses of H_2O and CO_2 by SIMS using procedures outlined by Blundy et al. (2005), Humphreys et al. (2008) and Wright et al. (2012). To summarize, inclusions were exposed, polished, and soaked in acetone to removing polishing and mounting compounds, then mounted in

indium and coated with gold. These melt inclusions were then analyzed for H_2O and CO_2 concentrations using a primary beam of $^{16}O_2^-$ ions with an accelerating voltage of 10.5 kV, a beam current of ~2 nA, and a beam diameter of ~20 μm, using the SHRIMP-RG ion microprobe at the Stanford University/USGS SUMAC facility. The beam was rastered over a 100 x 100 μm area around the analytical spot to remove the gold coat and surface contaminants. Four counting cycles were used in each analysis to measure on-peak counts for $^{28}Si^1H$, ^{12}C, and ^{30}Si and off-peak background counts on both sides of the $^{28}Si^1H$ peak with a mass resolution of 7000 at 10% peak height. Concentrations of the analyzed elements in unknowns were derived from calibration curves of known concentrations of standards synthesized by Mangan and Sisson (2000) normalized to wt. % SiO_2, versus measured count rates of analyzed standards normalized to ^{30}Si. Analytical uncertainties were calculated based on counting statistics using the SQUID2 data reduction software (Ludwig, 2009).

Some analytical spots intersected with the host mineral. These were identified visually and by EDS analyses of the ablation pits using the AIL CAMECA SX-50 electron microprobe. Concentrations based on these contaminated spots are not reported here. Also, in a finding that mirrors that of Wright et al. (2012), some spots produced anomalously high CO_2 concentrations, accompanied by large fluctuations in count rates across the four counting cycles. Wright et al. (2012) suggest that this is the result of surface contamination not fully removed by the pre-ablation and suggest reporting only CO_2 measurements where the variability in ^{12}C count rates is low. As such, only CO_2 measurements where the analytical uncertainty is <10% of calculated concentration, or

where calculated CO_2 concentrations are <150 ppm, are reported here. Analyses from Izbekov et al. (2009) referred to in this study are similarly filtered to remove potentially spurious CO_2 data.

2.4: Results

2.4.1: Bulk Chemistry

Bulk compositions are reported in Appendix 2-3. The white, pumiceous pyroclasts are medium-K andesite, extending the compositional range determined by Izbekov (2008) to higher SiO_2, while the denser, grey-brown clasts are medium-K basaltic andesite (Fig. 2-3). Andesite and basaltic andesite samples are collinear in FeO^T/MgO vs. SiO_2 and roughly follow the tholeiitic/calc-alkaline dividing line of Miyashiro (1974), with andesite being slightly calc-alkaline and basaltic andesite being slightly tholeiitic. Both the andesite and basaltic andesite vary in bulk composition, with andesite clasts containing ~58-62 wt. % SiO_2 and basaltic andesite clasts containing ~52-56 wt. % SiO_2 (Fig. 2-3). There is an apparent compositional gap between 56 and 58 wt % SiO_2 that separates the andesite and basaltic andesite, although some banded samples have compositions in this range. Andesites are significantly enriched relative to basaltic andesites in large-ion lithophile elements (LILE) elements (excluding Sr), light rare-earth elements (LREE), high field-strength elements (HFSE) and U-series (U, Th, Pb) elements

(Fig. 2-4A) but are only slightly enriched in heavy rare-earth elements (HREE). Chondrite-normalized rare-earth element patterns from both the andesite and the basaltic andesite show no significant europium anomaly (Fig. 2-4B); Eu/Eu* values, calculated using chondritic values of Sun and McDonough (1989), range from 0.95-1.05 in the andesite and 0.99-1.08 in the basaltic andesite. Major and minor element versus silica variation diagrams (Fig. 2-5) indicate that the basaltic andesite compositions fall along generally linear trends for most major and minor elements except MnO. Trace element variations in the basaltic andesite are also generally linear, though there the trends are not quite as coherent, especially in Sr and Pb (Fig. 2-6).

Andesite samples display more heterogeneity than the basaltic andesite (Figs. 2-5, 2-6), although they vary over a similar range of SiO_2 content. For some elements (e.g., TiO_2, MgO, CaO, Cs, Pb), andesite samples define linear arrays; others (e.g., Al_2O_3, MnO, P_2O_5, Sr, Y, HREE) show more scatter. While scatter may be an artifact of analytical uncertainty in some cases (Ta and HREE), trends in the andesite compositions are not nearly as coherent as those defined by the basaltic andesite. Furthermore, while the andesite and basaltic andesite fall along a single linear trend in some elements (e.g., TiO_2, MgO, CaO, Cs), they also define trends that are not co-linear in other elements (e.g., Al_2O_3, P_2O_5, Pb, Y, HREE).

A comparison of the compositions of the 2008 eruption with analyses of samples from pre-2008 lavas and pyroclastic deposits (C.J. Nye, unpublished data) shows that while 2008 and pre-2008 material are similar in composition for most major, minor, and

some trace elements, most pre-2008 material is easily distinguishable from 2008 material on the basis of Y, HREE, Sr and, especially, Cs and Pb concentrations. Cs and Pb tend to be especially depleted in pre-2008 samples, Y and HREE tend to be moderately depleted, while Sr is highly variable (Fig. 2-6). The only exceptions are clasts from the penultimate PF's, which represent the most recent explosive products of Kasatochi prior to 2008 (Waythomas et al., 2010a). While they have not been studied and sampled exhaustively, samples from this unit contain the same mineral assemblage of plagioclase, clino- and orthopyroxene, amphibole and titanomagnetite and closely mirror 2008 bulk compositions. Basaltic andesite samples from the penultimate PF's are similar to the most evolved 2008 basaltic andesite (though the agreements in MnO, Pb and Sr are weak, especially with the lowest-SiO_2 penultimate PF samples). However, the four most silicic penultimate PF samples are chemically indistinguishable from the more mafic 2008 andesite in all components (Figs. 2-5, 2-6).

Bulk compositions of the gabbroic blocks (Figs. 2-3, 2-5, 2-6) are highly variable, likely reflecting differing modal proportions of the component minerals. They are highly depleted in incompatible elements and appear to lie somewhat along trends defined by the basaltic andesite in certain components (e.g., CaO, Cs, Pb), though given their scatter, they cannot be truly characterized as co-linear with either of the more silicic lithologies. The black interstitial groundmass found in some blocks, analyzed in two hand-picked separates, is a basaltic magma (~50 wt. % SiO_2, Fig. 3), which lies on compositional trends defined by the basaltic andesite in some components, though the agreement in elements such as Al_2O_3, MgO and Sr is poor.

2.4.2: Petrography

Whereas the andesite and basaltic andesite differ compositionally, they both contain phenocryst assemblages of, in descending order of abundance, plagioclase, clinopyroxene, orthopyroxene, amphibole and titanomagnetite (Fig. 2-7, Appendix 2-4). Olivine and apatite are also present in trace amounts in both the basaltic andesite and andesite, along with some FeS inclusions in titanomagnetite. Mafic minerals from all lithologies are generally unzoned and unreacted. Most notably, despite the overall compositional heterogeneity of the Kasatochi eruptive products, amphibole phenocrysts from all lithologies lack the opacitization or breakdown rims indicative of significant time spent outside of stable P-T-X conditions (e.g., Garcia and Jacobson, 1979; Rutherford and Hill, 1993; Browne and Gardner, 2006). Polymineralic clots, generally of plagioclase, clino- and orthopyroxene (±titanomagnetite and amphibole), appear in both the andesite and basaltic andesite, though they are more common in the latter. Groundmasses in the basaltic andesite are qualitatively more microlite-rich than in the andesite. Groundmasses in both lithologies are dominated by quenched glass and elongate/lathlike plagioclase microlites, as well as rarer, more tabular clinopyroxene and titanomagnetite. Phenocryst abundances are generally higher in the basaltic andesite (~30-55 vol. %) than in the andesite (~15-30 vol. %, Fig. 2-7). This raises the possibility that the compositional diversity of the 2008 Kasatochi eruptive products may simply be the result of the accumulation of phenocrysts in the basaltic andesite relative to the andesite, though as will be explained later, such accumulation cannot account for the full range of compositional diversity or in the compositional trends.

Gabbroic blocks are nearly holocrystalline and are dominated by amphibole and plagioclase, with lesser amounts of clinopyroxene and titanomagnetite and trace amounts of orthopyroxene and olivine (Appendix 2-4). Gabbroic samples display a wide variety of textures and grain sizes. Blocks with all crystals <5 mm are not uncommon, but plagioclase crystals may exceed 2 cm in length, while a few samples contain 12-cm long amphibole in a medium-grained matrix. Plagioclase is generally equigranular and can be nearly transparent. Amphibole crystals vary from nearly equigranular to lathlike morphologies and in some samples display a strong preferred orientation. Some blocks are mineralogically layered (Fig. 2-2), with plagioclase-dominant layers up to several centimeters thick alternating with amphibole-dominant layers, whereas other blocks have centimeters-thick layers with equigranular, fine-grained gabbro alternating with medium- or coarse-grained gabbro at sharp interlayer boundaries. The interstitial basaltic magma found in some blocks is dominated by brown glass and lathlike plagioclase microlites <50 μm in length.

2.4.3: Pyroxene, Titanomagnetite, Amphibole and Olivine Compositions

Pyroxene, amphibole and titanomagnetite phenocrysts in basaltic andesite samples show minimal compositional variations within individual crystals, but compositions vary somewhat between individual crystals. Clinopyroxene compositions show little variation, with all but one phenocryst having compositions of $En_{40-44}Wo_{41-43}$ (Fig. 2-8, Appendix 2-5); one measured crystal had slightly elevated Ca (Wo_{46}).

Orthopyroxene compositions range from En_{63} – En_{69}, with slight variations in Ca content (Fig. 2-8, Appendix 2-6). Titanomagnetite compositions in the basaltic andesite show much greater compositional variability than titanomagnetite from the andesite or gabbro; low-Ti titanomagnetite phenocrysts do not vary significantly in Ti content but vary widely in Fe, while the high-Ti titanomagnetite shows an approximately negative correlation between Fe and Ti (Fig. 2-9, Appendix 2-7). Amphibole phenocrysts from the basaltic andesite show no systematic intragranular compositional variations but vary overall along a continuous spectrum from relatively high-Fe, low-alkali, low-Al phenocryst compositions to relatively low-Fe, high-alkali, high-Al compositions (Fig. 2-10, Appendix 2-8).

As in the basaltic andesite, mafic minerals in andesite samples show minimal compositional zonation. Clinopyroxene phenocrysts show a similar range of compositions to the basaltic andesite ($En_{42-44}Wo_{41-44}$), though no higher-Ca phenocrysts were found (Fig. 2-8). Orthopyroxene phenocrysts are often anhedral and sometimes surrounded by clinopyroxene rims. Orthopyroxene in andesite samples are similarly homogeneous in composition (En_{64-67}) and also overlap basaltic andesite compositions (Fig. 2-8). Titanomagnetite phenocrysts have compositions similar to the high-Ti titanomagnetite phenocrysts in the basaltic andesite, with an approximately negative correlation between Fe and Ti, though andesite titanomagnetite phenocrysts vary less in both Ti- and Fe-content (Fig. 2-9). In contrast to the wide range in amphibole compositions observed in basaltic andesite samples (Fig. 2-10), andesitic amphibole compositions cluster near the low-Al/low alkali, high-Fe/high-Si end of the range of

basaltic andesite amphiboles, though they have lower Fe contents than the most Al-poor amphiboles from the basaltic andesite.

Like the more silicic lithologies, mafic phenocrysts in gabbro lack notable compositional zonation. Clinopyroxenes are compositionally similar to the highest-Ca basaltic andesite clinopyroxene (En_{40-43}, Wo_{46-48}), though they do not overlap compositionally with any andesite clinopyroxene compositions (Fig. 2-8). Similarly, gabbroic titanomagnetite compositions (Fig. 2-9) are similar in Ti content to titanomagnetite from the basaltic andesite (though lower Fe) but have lower Ti and lower Fe than titanomagnetite in andesite. Amphibole compositions (Fig. 2-10) in the gabbro are relatively similar in composition to the more Al- and alkali-rich amphiboles, Fe- and Si-poor amphiboles from the basaltic andesite. Unlike the silicic lithologies, olivine is present in trace quantities in the gabbro. Olivine occurs as resorbed cores in amphibole phenocrysts with clinopyroxene often growing between an olivine core and amphibole host. These olivines are also unzoned, with compositions ~Fo_{74} (Appendix 2-9).

2.4.4: Groundmass Glass

Basaltic andesite groundmass glass compositions fall along linear trends in major-element compositions (Fig. 2-11, Appendix 2-10), extending to compositions both more and less evolved than glass in andesite samples. Andesite groundmass glass compositions have a more limited range in SiO_2 and CaO than the basaltic andesite, though the range in Al_2O_3 and K_2O is approximately the same. Trends in glass compositions from both

lithologies generally overlap, though at a given SiO_2 content, basaltic andesite glasses are slightly more K_2O-rich.

2.4.5: Plagioclase Textures and Compositions

Plagioclase phenocrysts in the andesite and basaltic andesite contain a similar set of textures (Fig. 2-12) and zoning patterns (Fig. 2-13). About 60% of plagioclase phenocrysts in the basaltic andesite and ~20% of plagioclase in the andesite have high-An (>An_{80}) cores (Figs. 2-12A and B, 2-13A, 2-14, Appendix 2-11). Resorbed cores (Fig. 2-12A) are also common and can be found in phenocrysts of all core compositions and in ~50% of phenocrysts in both the andesite and basaltic andesite (Fig. 2-14). In the basaltic andesite, resorbed cores are actually more common in phenocrysts with core compositions of <An_{80} (Fig. 2-13).

Plagioclase phenocrysts in both the andesite and basaltic andesite, regardless of core compositions, usually contain oscillatory zoning with an overall normal compositional zoning trend (Fig. 2-12A and B, 2-13A, B and C), converging to a fairly narrow range of An contents, though andesite rims are slightly more sodic. Approximately 85% of phenocrysts in andesite samples have rim compositions of An_{50-60}, while ~60% of basaltic andesite plagioclase rims fall within An_{55-65}. The concentric, oscillatory zonation may be interrupted by rings of melt inclusions parallel to the zonation patterns, associated with abrupt spikes in An-content up to An_{70-80}, though the zonation patterns quickly return to the overall normal trend (Fig. 2-12B, 2-13A and B).

These rimward resorption features are found in ~45% of plagioclase phenocrysts in both the basaltic andesite and andesite (Fig. 2-14). There is no apparent correlation between resorption rings and relict cores; phenocrysts with resorbed cores do not always have resorption rings, while phenocrysts with resorption rings do not always have resorbed cores, or even high-An cores. Plagioclase phenocrysts that lack high-An cores and contain no dissolution features, either in the core or rimward, are equally common in the andesite and the basaltic andesite (~30%). Plagioclase microlites in both the andesite and basaltic andesite display a wide range of compositions, though they vary more widely in the basaltic andesite (Fig. 2-14)

A portion of plagioclase phenocrysts with unresorbed cores containing $>An_{80}$ have similar core and rim compositions (within ~5 mol. % An) and lack systematic oscillatory or concentric core-to-rim zoning (Fig. 2-12C, 2-13D). These are found exclusively in the basaltic andesite (Fig. 2-14), accounting for ~10% of the measured phenocrysts. These phenocrysts are euhedral, contain no dissolution features beyond a few small (<5 μm) melt inclusions, and can be very large (up to ~1 mm in diameter).

Gabbroic plagioclase crystals can reach up to 2 cm in size, are dominantly euhedral and have nearly uniformly high An contents ($>An_{90}$). Individual crystals are generally unzoned, though some crystals do show a precipitous drop in An content at the interface with the matrix melt, reaching compositions as low as $\sim An_{55}$ (Figs. 2-13D, 2-14). Gabbroic plagioclase crystals contain no resorption features beyond small, scattered melt inclusions and are texturally similar to the high-An, unresorbed plagioclase found in

the basaltic andesite. However, gabbroic plagioclase generally has >An_{90}, while the high-An, un-reacted plagioclase in the basaltic andesite generally are An_{80-85}.

2.4.6: H_2O and CO_2 Concentrations in Melt Inclusions

H_2O concentrations are comparable between the andesite and the basaltic andesite, with melt inclusions from both lithologies containing dominantly ~5-7 wt. % H_2O (Fig. 2-15, Appendix 2-12). CO_2-poor (<100 ppm) inclusions are more common in the andesite than the basaltic andesite, although inclusions from both lithologies are dominantly <400 ppm CO_2. Entrapment pressures, calculated based on H_2O-CO_2 solubility (Papale et al., 2006), are generally between 200 and 300 MPa for both the andesite and basaltic andesite, with maxima of ~390 MPa for the basaltic andesite and ~310 MPa for the andesite.

2.5: Discussion

2.5.1: Compositional Variations in the 2008 Kasatochi Eruptive Products

Banded clasts abound throughout the 2008 deposits, and clasts of disparate compositions can be found within individual deposits. Banded samples fall along mixing trends between andesite and basaltic andesite end-member compositions (Fig. 2-16) and

presumably represent mingling between the two magmas. Some unbanded higher-SiO_2 basaltic andesite and lower-SiO_2 andesite samples also lie along these trends, presumably representing homogenization after mingling. Some pre-eruptive interaction must have taken place between the andesite and basaltic andesite, including a degree of pre-eruptive homogenization.

The low (<25 ppm) Ni and Cr contents of the 2008 Kasatochi magmas (Appendix 2-3) relative to presumed parental compositions suggest that they are likely derived from evolved magmas that had previously experienced fractional crystallization. However, neither fractional crystallization nor mixing between the basaltic andesite and the andesite can explain the full spectrum of compositional heterogeneities observed in the 2008 samples. In fact, overall pre-eruption physical and chemical interactions between the andesite and basaltic andesite appear to have been limited. Europium anomalies are absent (Fig. 2-4), and compositional trends in the andesite and basaltic andesite are incongruent in some elements (e.g., Al_2O_3, MnO, P_2O_5, Pb, Y, HREE; Figs. 2-5, 2-6, 2-16), despite strong linear trends in others (e.g., MgO, CaO, Cs, Nb; Figs. 2-5, 2-6). This would contradict any kind of genetic link between the two lithologies, either through fractional crystallization, crystal accumulation or mixing between andesite and basaltic andesite end members, as no satisfactory linear or curvilinear trend can link the compositional distributions of the two lithologies. While a few unbanded, higher-SiO_2 basaltic andesite samples do fall along lines of mixing with the basaltic andesite, most andesite samples plot well away from the primary basaltic andesite mixing trends (Fig. 2-16). The andesite and basaltic andesite must have resided in spatially and chemically

distinct storage areas until just prior to eruption, with any mixing between the two magmas limited to a brief period prior to eruption, resulting in mingling and homogenization (as previously described) in only a small portion of the total volume of erupted material. The origins of the andesite and basaltic andesite will therefore be considered separately.

2.5.2: Basaltic Andesite

Basaltic andesite compositions form nearly linear arrays in all elements (Figs. 2-5, 2-6, 2-16). Plagioclase phenocrysts further indicate that mixing due to mafic recharge was an important process in the evolution of the basaltic andesite prior to eruption. About 50% of the analyzed plagioclase phenocrysts contain dissolution rings associated with spikes in An content (Fig. 2-13A and B). This feature is commonly associated with injection of mafic magmas, which can make the composition of the crystallizing liquid both hotter and more calcic, as well as increasing the melt H_2O content, any or all of which will promote higher-An plagioclase growth (e.g., Housh and Luhr, 1991; Putirka, 2005; Lange et al., 2009). Introduction of mafic magma has been frequently been invoked as an explanation for transient changes in conditions controlling plagioclase crystallization, causing dissolution of the outer edges of plagioclase phenocrysts with lower-An rims, followed by growth of higher-An plagioclase on top of the resorption features (Davidson and Tepley, 1997; Clynne, 1999; Murphy et al., 2000; Tepley et al., 2000; Couch et al., 2001; Izbekov et al., 2002; Browne et al., 2006; Ruprecht and

Wörner, 2007; Shcherbakov et al., 2011). 2008 Kasatochi basaltic andesite phenocrysts may contain from one to four dissoluton rings, indicating multiple discrete recharge events. In addition, ~50% of the plagioclase phenocrysts contain resorbed cores, with ~60% of all analyzed cores containing >An_{80}. Recharge magmas may also have contained crystals, leading to the high proportion of basaltic andesite plagioclase phenocrysts that have high-An cores. Furthermore, in cases of mixing driven by mafic replenishment, the difference in T-X conditions between the host magma and intruding magma, especially the added heat and increase in Ca, may cause a large portion of the cores to resorb (e.g., Tepley et al., 1999; Izbekov et al., 2002; 2004), which would lead to the high proportion of cores that show disequilibrium textures (Fig. 2-14). The linear compositional trends seen in the basaltic andesite are probably the result of mixing due to a recent injection of mafic magma into the basaltic andesite system. Deviations of high-SiO_2 basaltic andesite samples from the main basaltic andesite trend likely resulted from a brief period of mixing followed by homogenization with the andesite directly prior to eruption (Fig. 2-16).

The system that produced the basaltic andesite must have been well buffered, as seen in the return to pre-dissolution compositions and normal zonation outboard of the dissolution rings (Fig. 2-13). Disequilibrium textures or zoning in amphibole are also nearly absent, though the generally linear tend in amphibole phenocryst compositions may reflect the variability in bulk chemistry and may indicate their crystallization from a heterogeneous, mixed source. Mafic input must have been sufficient in volume, and/or sufficiently different in composition to alter plagioclase compositions but not enough to

cause more than short-term deviations in the overall plagioclase zoning behavior, and certainly not enough to promote the formation of wider "dusty" zoned plagioclase indicative of longer-term dissolution and re-crystallization of plagioclase under different T-X conditions (e.g., Clynne, 1999; Murphy et al., 2000; Izbekov et al., 2002; Browne et al., 2006; Shcherbakov et al., 2011). The final mafic injection that created the observed mixing array may also have led to the formation of high-An microlites in the basaltic andesite. Mafic recharge has produced high-An microlites in similar silicic systems (c.f. Couch et al., 2003; Martel et al., 2006), although this topic needs further exploration and will be discussed elsewhere (Neill et al., *in prep*).

2.5.3: Andesite

Andesite bulk compositions do not vary as uniformly as do the basaltic andesite, although they span a similar range of SiO_2 contents. Approximately 50% of andesite plagioclase phenocrysts contain resorption features, while 20% contain of cores >An_{80}, which, as in the basaltic andesite, suggests some history of mafic input as well as a magmatic system that is similarly well buffered. However, the simple two component mixing relationship seen in the compositions of basaltic andesite samples is absent from the andesite. Variations in andesite Y and LREE concentrations follow far less coherent linear trends than in the basaltic andesite (Fig. 2-6), while concentrations of components such as Al_2O_3, P_2O_5, Sr and HREE show minimal systematic variation of any kind (Figs.

2-5, 2-6). Any bulk chemical signature of any single mafic injection into the andesite storage region had been erased prior to the 2008.

2.5.4: Gabbroic Blocks

While bulk compositions of the gabbroic blocks do appear to reasonably extend the bulk chemical trends defined by both the andesite and basaltic andesite (Fig. 2-5, 2-6), given how much the gabbroic compositions vary, any direct petrogenetic connection to the andesite or basaltic andesite based on bulk chemistry would be tenuous at best. The range of gabbro bulk compositions may merely reflect modal mineral proportions, which are not necessarily those of the associated magmas from which they originated. Xenoliths and obvious large (>1 cm) amphibole and plagioclase antecrysts are commonly found embedded in basaltic andesite hand specimens but are very rare (though not entirely absent) in andesite samples. Also, plagioclase phenocrysts in the gabbro are unzoned, euhedral, with no dissolution features and compositions >An_{90}. Phenocrysts with such textures and compositions are found only in basaltic andesite samples. This suggests that significant assimilation and phenocryst transfer took place between the gabbro and the basaltic andesite but not to any great extent between the gabbro and andesite. This, in turn, suggests that the gabbroic blocks were dominantly carried by the basaltic andesite and had only limited contact with the andesite.

2.5.5: Implications for the 2008 Eruptive Sequence

The phase assemblage at Kasatochi does not lend itself to geothermobarometric techniques based on mineral or mineral-liquid equilibria. However, amphibole phenocrysts in both the andesite and basaltic andesite show no zonation or disequilibrium textures, and therefore both the andesite and basaltic andesite must have been stored under P-T conditions where amphibole is stable. If the calculated melt inclusion entrapment pressures (~200-300 MPa, Fig. 2-15) are taken as being approximately equivalent to pressure conditions of the pre-eruptive andesite and basaltic andesite magmatic storage regions, these pressures would correspond to depths of magmatic storage of ~8-11 km, assuming an average crustal density of 2700 kg m^{-3}. Previous experimental studies (Barclay et al., 1998; Moore and Carmichael, 1998; Cottrell et al., 1999; Blatter and Carmichael, 2001; Hammer et al., 2002; Pichavant et al., 2002) have constrained P-T regions of amphibole stability in andesite and basaltic andesite systems that are similar to Kasatochi in bulk composition and phase assemblage. These studies indicate that, at 200-300 MPa, amphibole would be stable in the andesite at ~850-950 °C and in the basaltic andesite at 900-1000 °C. These systems are not perfect analogues for Kasatochi, and the uncertainties in the experimentally determined amphibole stability regions can be large, but these temperatures and pressures are reasonable estimates for pre-eruptive storage conditions for the 2008 Kasatochi magmas.

Ruppert et al. (2011) suggest that faulting related to the pre-eruptive swarm of tectonic earthquakes, including the magnitude 5.8 event ~3.5 hours prior to the first

explosions, provided pathways for magma ascent. The earthquakes could have opened separate pathways for the andesite and basaltic andesite, which then traveled coincidently but independently until meeting in the upper reaches of the Kasatochi plumbing system. Roman et al. (2006) suggest that a similar system was active during the 1986 eruption of Augustine Volcano, Alaska, where a suite of low- to high-silica andesite magmas traveled separately through a network of dikes, coalescing only near the surface.

However, while the andesite and basaltic andesite are predominantly chemically distinct, they did coexist prior to eruption long enough for some homogenization to occur (Fig. 2-16). Given that the gabbroic blocks seem to have traveled mainly with the basaltic andesite, they must have been incorporated before the andesite and basaltic andesite began to interact. Had the gabbroic blocks been incorporated after the andesite and basaltic andesite had begun to move together, there would have presumably been sub-equal amounts of disaggregation and phenocryst transfer from gabbro to the two more silicic magmas. This implies that the earthquakes allowed for movement of the basaltic andesite upward, whereby it scavenged the gabbro and subsequently intersected the andesite body. The earthquake sequence directly prior to the eruption must have then opened pathways for the simultaneous eruption of the andesite and basaltic andesite, which had already begun to mingle. This sequence is similar to those seen at volcanoes such as Unzen in Japan (Nakamura, 1995), Pinatubo in the Philippines (Pallister et al., 1996), Soufriere Hills on Montserrat (Murphy et al., 2000) and Trident in Alaska (Coombs et al., 2000), where the interaction of an ascending mafic magma with a more silicic body was followed by an eruption.

Ascent of both the andesite and basaltic andesite must also have been sufficiently rapid to exceed the onset of amphibole breakdown, as no amphibole phenocrysts from either lithology display breakdown rims that form when magma ascends more slowly. Experimental studies of amphibole breakdown reactions in dacitic systems (Rutherford and Hill, 1993; Browne and Gardner, 2006) can be applied to Kasatochi to roughly estimate minimum ascent times based on the lack of reacted amphiboles. Although the experiments are not directly applicable to Kasatochi andesite and basaltic andesite compositions, the reaction rates can provide a general estimate at similar temperatures. Those experimental calibrations indicate that the Kasatochi amphiboles probably did not spend more than 18-24 hours outside of amphibole stability in transit from the magma storage region to shallow conduit depths or the surface. Based on starting depths of 8-11 km derived from melt inclusions, magmatic ascent rates would need to be at least ~0.1-0.2 m s^{-1} in order to reach the surface without causing amphibole breakdown.

The rapid magmatic ascent rates at Kasatochi are an important distinction between the Kasatochi case and the other similar studies mentioned previously. In cases such as Trident and Soufriere Hills, magmas spent sufficient time outside of equilibrium during mingling and ascent for significant disequilibrium phenocryst textures, such as dusty zoned plagioclase or amphibole reaction rims, to form. In the Trident case, there was even sufficient time for homogenization to occur. At Kasatochi, where pre-eruption interaction was limited, such disequilibrium textures are conspicuous by their absence. The tectonic faulting associated with the 2008 Kasatochi eruption as interpreted from the pre-eruptive seismic record (Ruppert et al., 2011) may have accelerated the opening of

pathways for magma movement, allowing magma transport through complex pathways (e.g., Roman et al., 2006) to occur rapidly. In addition, pre-eruptive H_2O contents were lower at both Trident (~3.5 wt. % H_2O, Coombs et al., 2000) and Soufriere Hills (4-5 wt. % H_2O, Barclay et al., 1998; Devine et al., 1998) than at Kasatochi. The energy provided by the expansion of these extra volatiles may have also sped up magmatic ascent rates at Kasatochi relative to those similar eruptions.

2.6: Conclusions

The 2008 eruption of Kasatochi produced juvenile clasts of basaltic andesite and andesite, which contain a similar assemblage of constituent minerals but are distinct from each other in several geochemical aspects. Together, they vary in composition from 52-62 wt. % SiO_2 and contain plagioclase, amphibole, clinopyroxene, orthopyroxene and titanomagnetite. The eruption also produced blocks of xenolithic amphibole-plagioclase-clinopyroxene gabbro, which were carried dominantly with the basaltic andesite.

Both the andesite and basaltic andesite display significant compositional heterogeneity. In the basaltic andesite, the abundance of plagioclase phenocrysts containing resorbed interiors, high-An cores and rimward spikes in An content associated with dissolution features indicate that the basaltic andesite evolved through a process of repeated mafic recharge, a finding supported by the trends in basaltic andesite bulk

chemical compositions. The lack of such trends in the andesite indicates that it was largely unaffected by this recharge and by the basaltic andesite until immediately prior to eruption, though resorption textures in plagioclase in the andesite indicate that experienced some limited effects of mafic recharge events at some point during its compositional evolution.

Banded clasts throughout the deposits indicate that the andesite and basaltic andesite were able to mechanically mingle prior to reaching the surface. However, the major and trace element compositions of both indicate that very little chemical mixing and homogenization occurred between the two magmas, meaning that the two lithologies were stored separately until shortly prior to the eruption. While prior studies have constrained pressures of magma storage to 200-300 MPa (equivalent to depths of ~8-11 km) for both lithologies, the basaltic andesites were likely stored at slightly hotter temperatures (900-1000°C) than the andesite (850-950°C). Ascent rates must have been high (>0.1 m s^{-1}), as neither the andesite nor basaltic andesite contains amphibole phenocrysts with reaction rims.

2.7: Acknowledgments

Insightful discussions with C. Bacon, M. Coombs, S. de Angelis, K. Putirka, K. Severin, T. Sisson, J. Vazquez, M. West, J. Wooden and H. Wright improved this

manuscript, while the UAF Advanced Instrumentation Laboratory, the USGS/SUMAC SHRIMP facility, and the Washington State University GeoAnalytical Laboratory are gratefully acknowledged for the use of their analytical capabilities. Special thanks are due to J. Williams for coordinating the Kasatochi field expeditions, and to the crew of the M/V *Tiĝlax̂* (Captain W. Pepper, D. Erickson, E. Nelson, J. Faris, A. Velsko, J. Masui, and R. Lee) for providing safe passage to and from the island. The authors also thank the members of the interdisciplinary team studying ecosystem response to the eruption of Kasatochi (including N. Bargmann, B. Drummond, F. Daniels, T. DeGange, G. Drew, S. Jewitt, G. Michaelson, D. Sikes, S.L. Talbot, S.S. Talbot, L. Walker, B. Wang and J. Williams) for their collaborations in both field and analytical work. Fieldwork for this study was supported by the U.S. Fish and Wildlife Service and by the North Pacific Research Board Project #923. Analytical work was supported by the American Recovery and Reinvestment Act, by the UAF Advanced Instrumentation Laboratory, by a Jack Kleinman Grant for Volcano Research from the Community Foundation of Southwest Washington, and by the United States Geological Survey Volcano Hazards Program through the Alaska Volcano Observatory, a cooperative program of the University of Alaska Fairbanks, the Alaska Department of Geological and Geophysical Surveys, and the USGS.

2.8: Figures

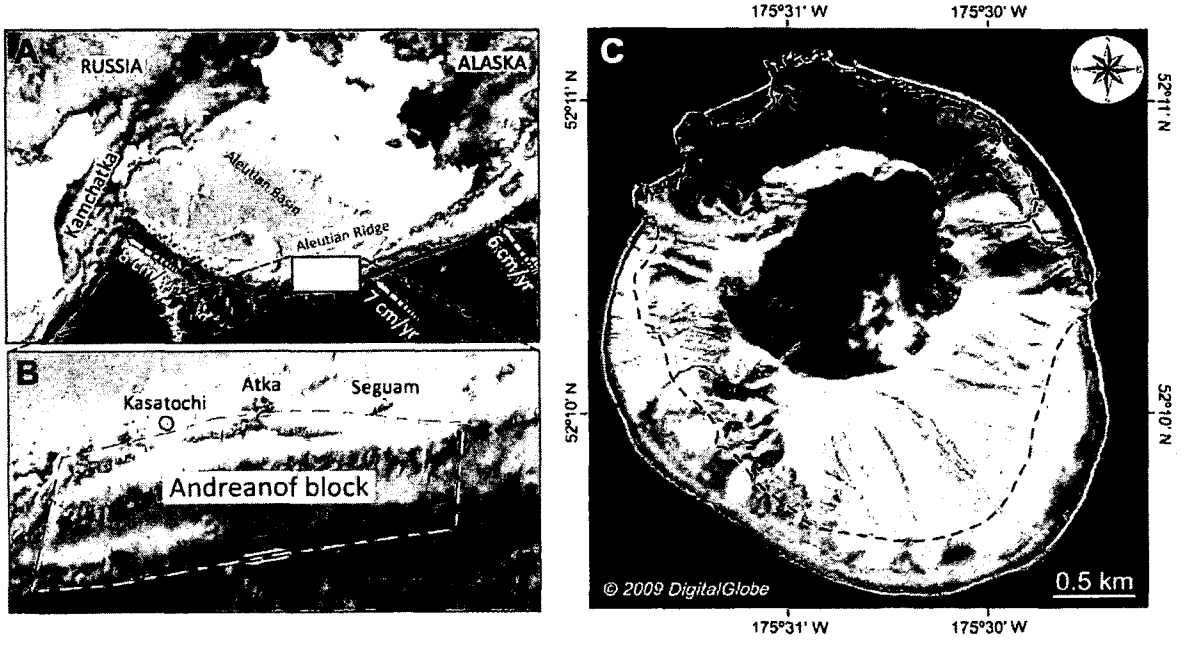

Figure 2-1: Location Maps of Kasatochi Island. A. and B. Location maps of Kasatochi volcano within the Aleutian arc based on SRTM and bathymetric data compilations of Ryan et al. (2009). Boundaries of the Andreanof block after Geist et al. (1988). C. QuickBird satellite image (© DigitalGlobe) of Kasatochi volcano acquired on 18 April 2009, 9 months after the eruption. The eruption extended the previous coastline (shown by dashed line) by as much as 400 meters and increased the area of the island by ~ 0.84 km^2 (Waythomas et al., 2010).

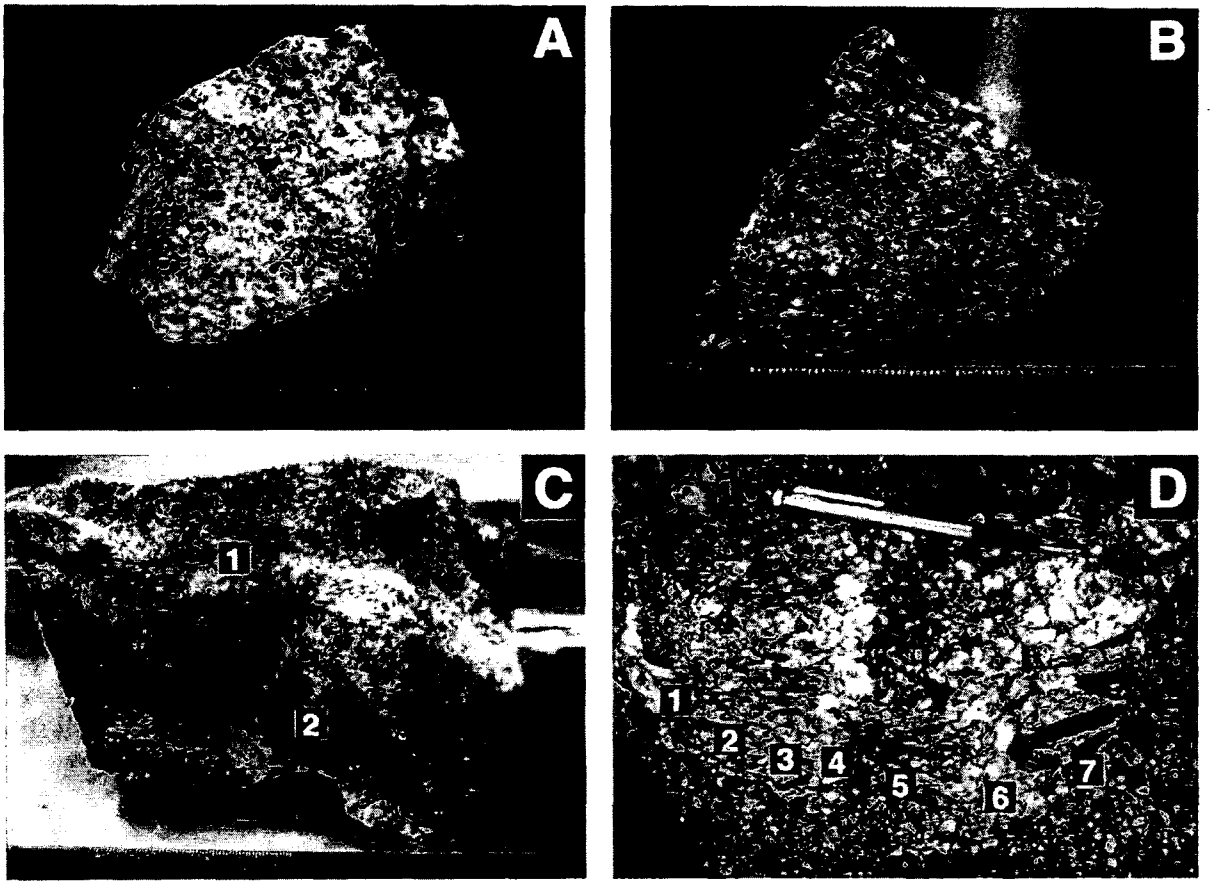

Figure 2-2: Representative Photographs of Lithologies from the 2008 Kasatochi Eruption. (A) Andesite pyroclast (58.0 wt. % SiO_2) collected from near the base of Layer 2. (B) Basaltic andesite pyroclast (52.9 wt. % SiO_2) collected from Layer 3. (C) Banded clast containing zones (1) vesicular, white (2) grey-brown, denser zones. (D) Amphibole-plagioclase gabbro block collected from Layer 3, containing layers of zonation in both grain size and mineral abundance. Different horizons include: (1) fine-grained (<2 mm) plagioclase and amphibole in sub-equal proportions; (2) medium-grained (~2-6 mm) plagioclase and amphibole in sub-equal proportions; (3, 5) amphibole and plagioclase, with amphibole slightly more abundant, amphibole up to 4 cm, plagioclase up to 2 cm; (4,6) coarse-grained (up to 1 cm) plagioclase with no mafic minerals; (7) coarse-grained amphibole and plagioclase with plagioclase slightly more abundant, amphibole up to 5 cm, plagioclase up to 2 cm. Mineral proportions estimated visually. Pen in Panel D is ~15 cm long.

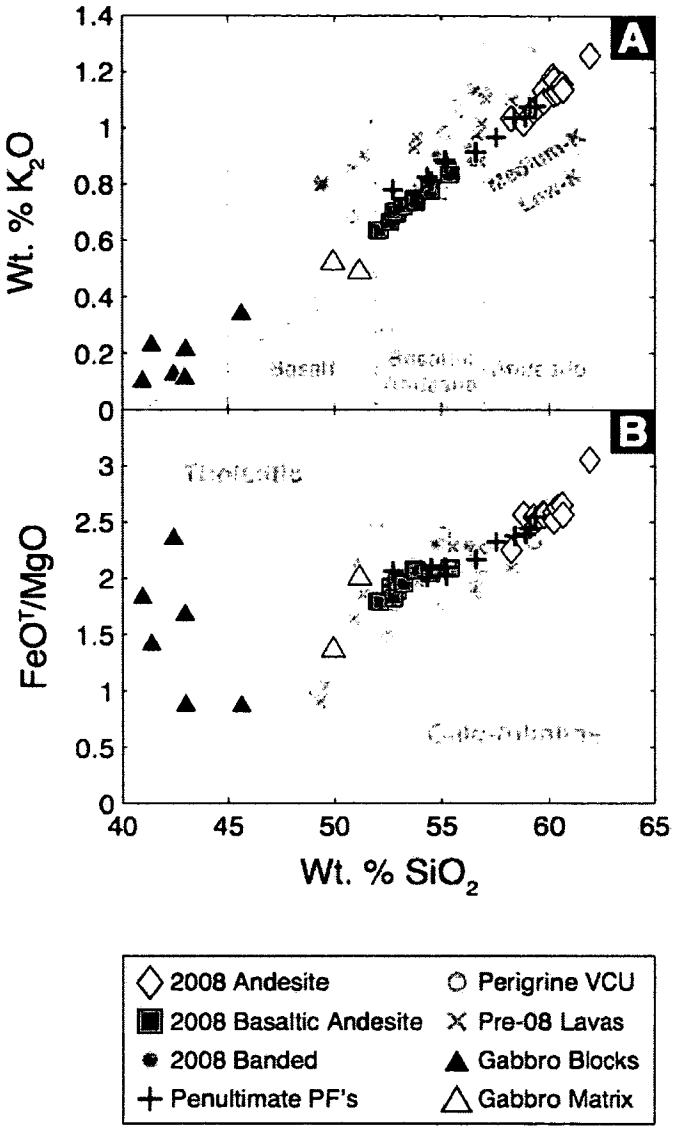

Figure 2-3: Bulk-Rock Chemical Classification Diagrams. Classification diagrams of all Kasatochi juvenile clasts, gabbro blocks and gabbro matrix separates. Analytical uncertainty is smaller than the size of the symbols. Individual analyses are listed in Appendix 2-3. Analyses of the penultimate pre-2008 pyroclastic unit (penultimate PF's – see text) and other pre-2008 eruptive material are included for comparison (C.J. Nye, unpub. data). (A) Bulk SiO_2 vs. K_2O classification, with compositional classifications after Le Bas et al. (1986) and low-K/medium-K boundary after Gill (1981). (B) Bulk SiO_2 vs. MgO/FeO^T classification diagram, after Miyashiro (1974). All Fe is given as FeO.

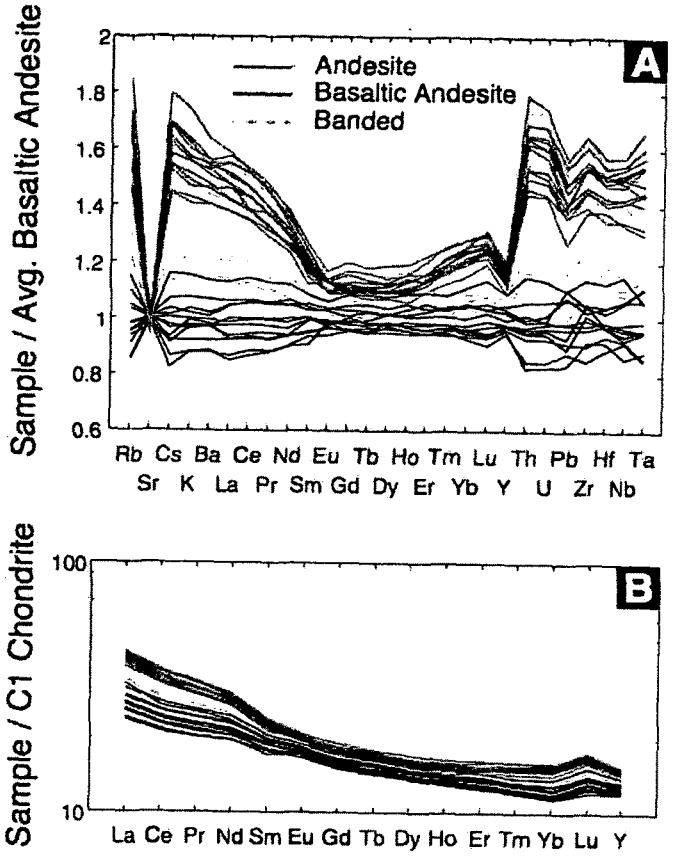

Figure 2-4: Trace Element Variation Diagrams. Concentrations are normalized to an average basaltic andesite composition (A) to emphasize differences between the andesite and basaltic andesite (c.f. Larsen et al., 2010) and to C1 chondritic values (B). Chondrite values after Sun and McDonough (1989). Individual analyses are listed in Appendix 2-3.

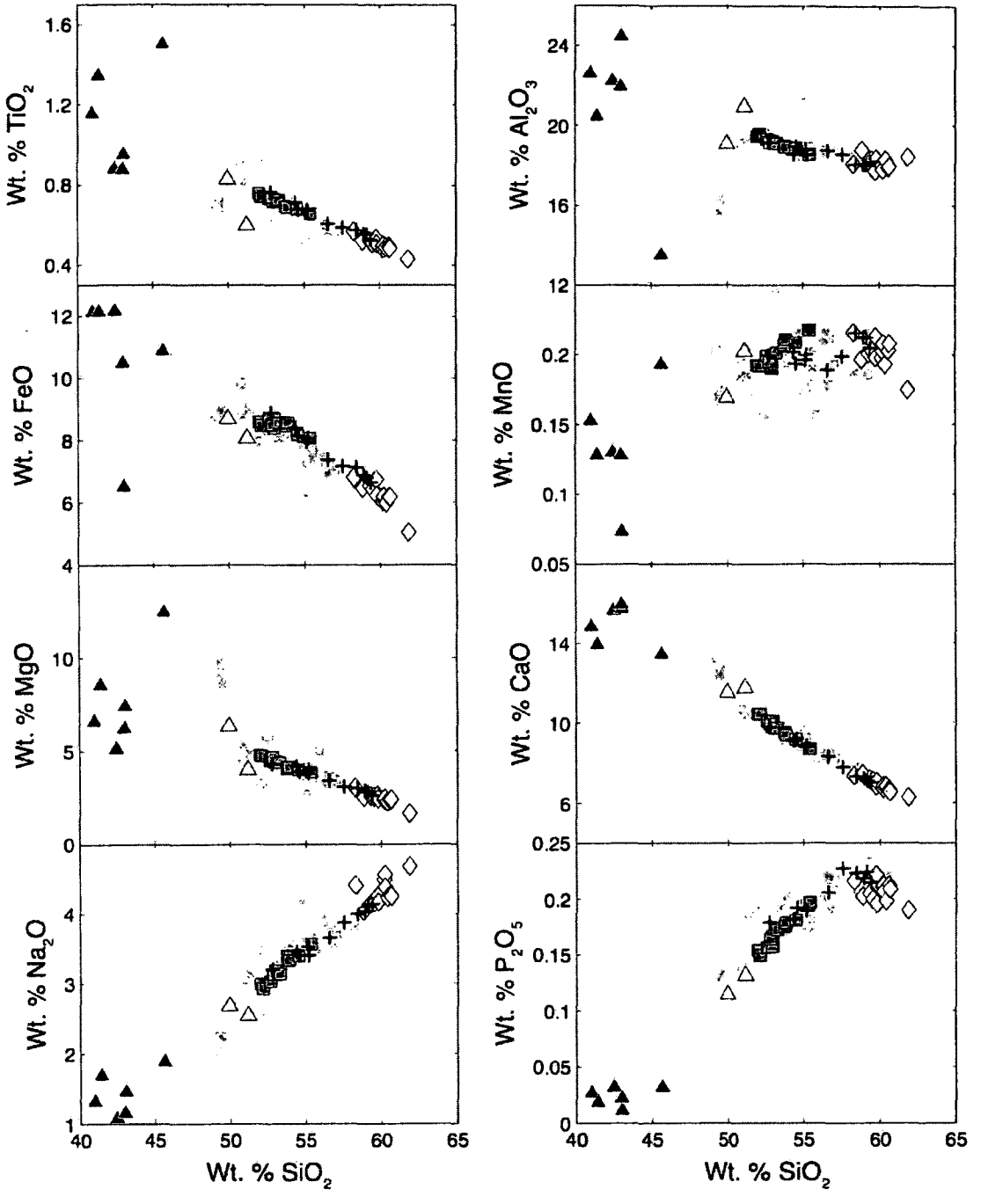

Figure 2-5: Major and Minor Element vs. SiO_2 Variation Diagrams. Symbols as in Fig. 2-3. Analytical uncertainty is smaller than the size of the symbols. Individual analyses are listed in Appendix 2-3. Analyses of pre-2008 eruptive material are included for comparison (C.J. Nye, unpub. data).

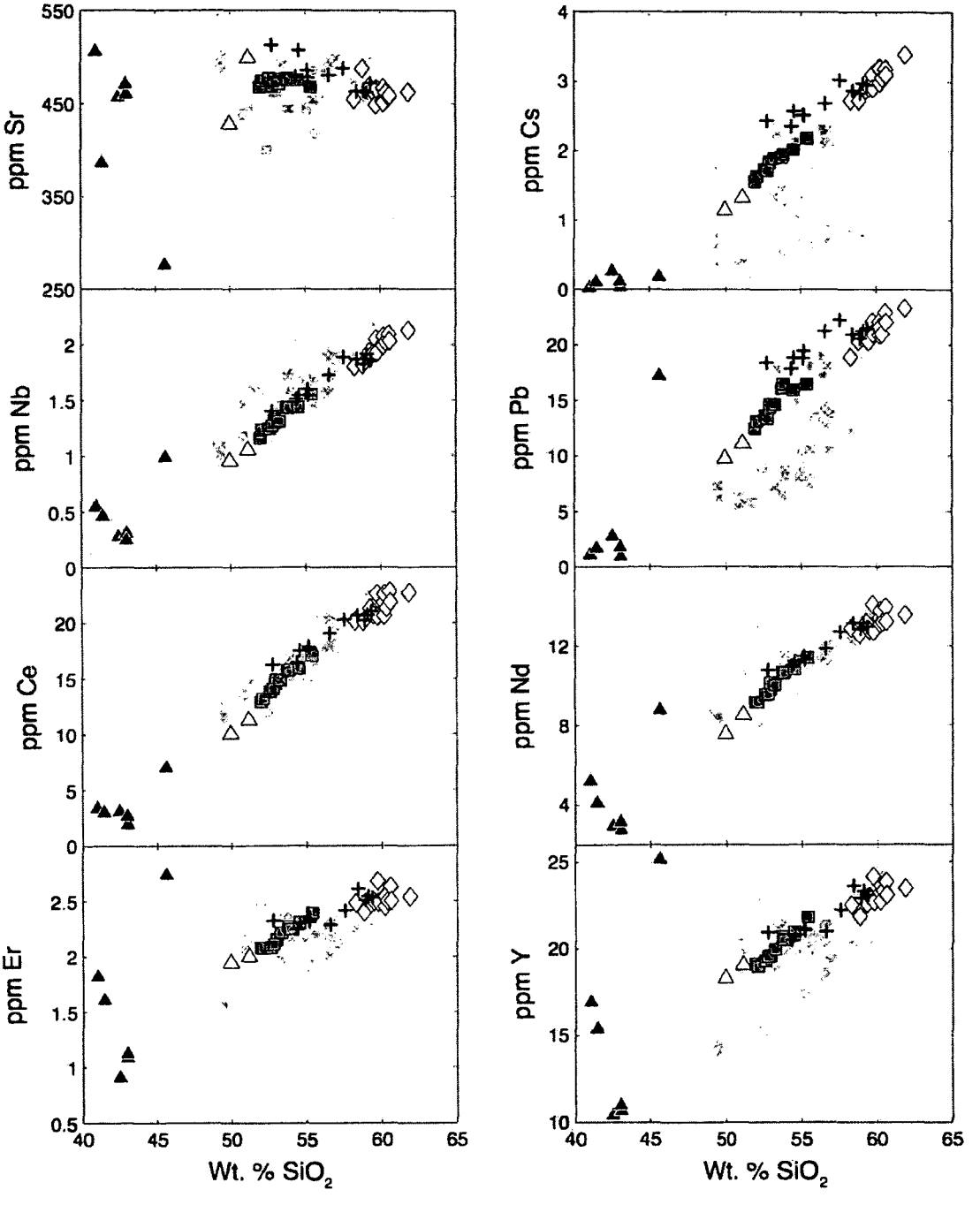

Figure 2-6: Trace Element vs. SiO_2 Variation Diagrams. Symbols as in Fig. 2-3. Analytical uncertainty is smaller than the size of the symbols. Individual analyses are listed in Appendix 2-3. Analyses of pre-2008 eruptive material are included for comparison (C.J. Nye, unpub. data).

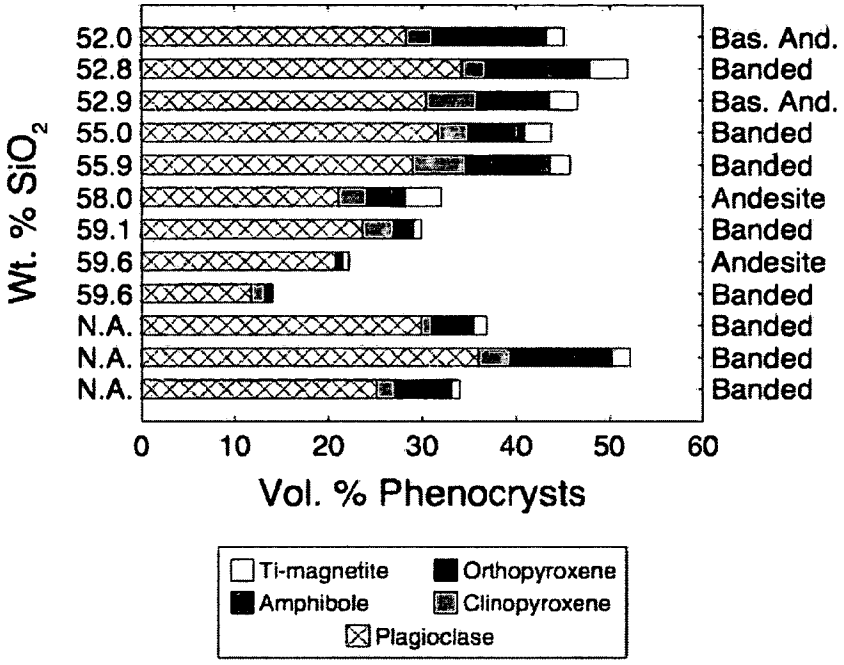

Figure 2-7: Modal Phenocryst Proportions. Phenocryst proportions are calculated on a vesicle-free basis. Individual mineral modes are given in Appendix 2-4. The lithology of each clast is listed at right.

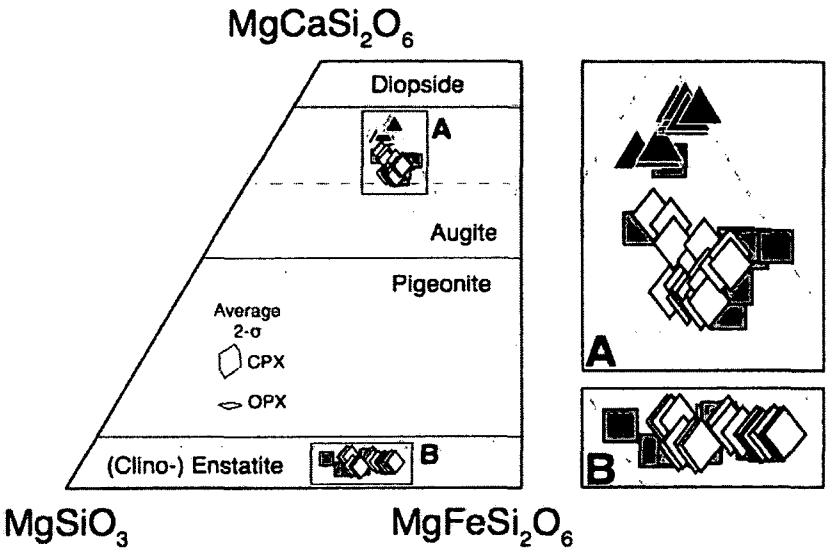

Figure 2-8: Compositions of Pyroxene Phenocrysts. Mineral classifications after Morimoto *et al.* (1988), with structural formulae calculated using CALCMIN (Brandelik, 2009). Portions of the classification diagram containing clinopyroxene (A) and orthopyroxene (B) compositions are expanded for clarity. Points represent the average composition of several analyses of an individual phenocryst (Appendices 2-5, 2-6). Error ellipses represent the average variation (2 standard deviations) of each averaged analysis. Orthopyroxene is present only in trace amounts in gabbro samples. Symbols as in Fig. 2-3.

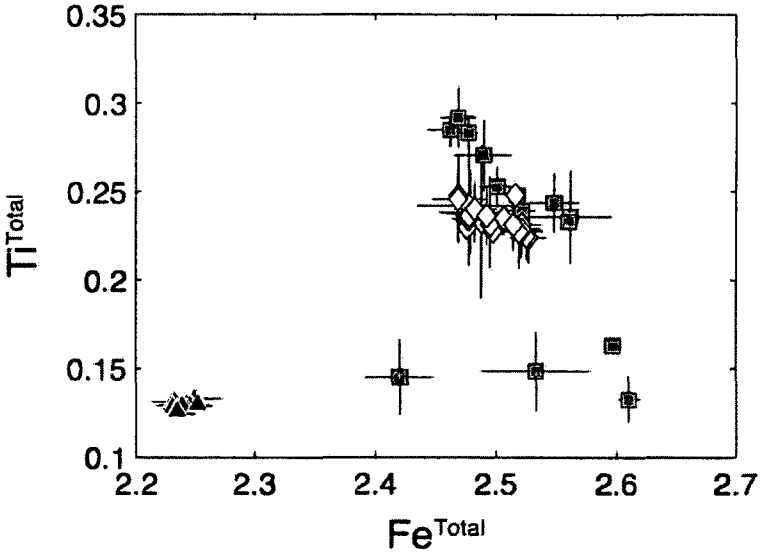

Figure 2-9: Compositions of Titanomagnetite Phenocrysts. Points represent the average composition of several analyses of an individual phenocryst (Appendix 2-7). Compositions are in atoms per formula unit, calculated using ILMAT (Lepage, 2003). Error bars represent the average variation (2 standard deviations) of each averaged analysis. Symbols as in Fig. 2-3.

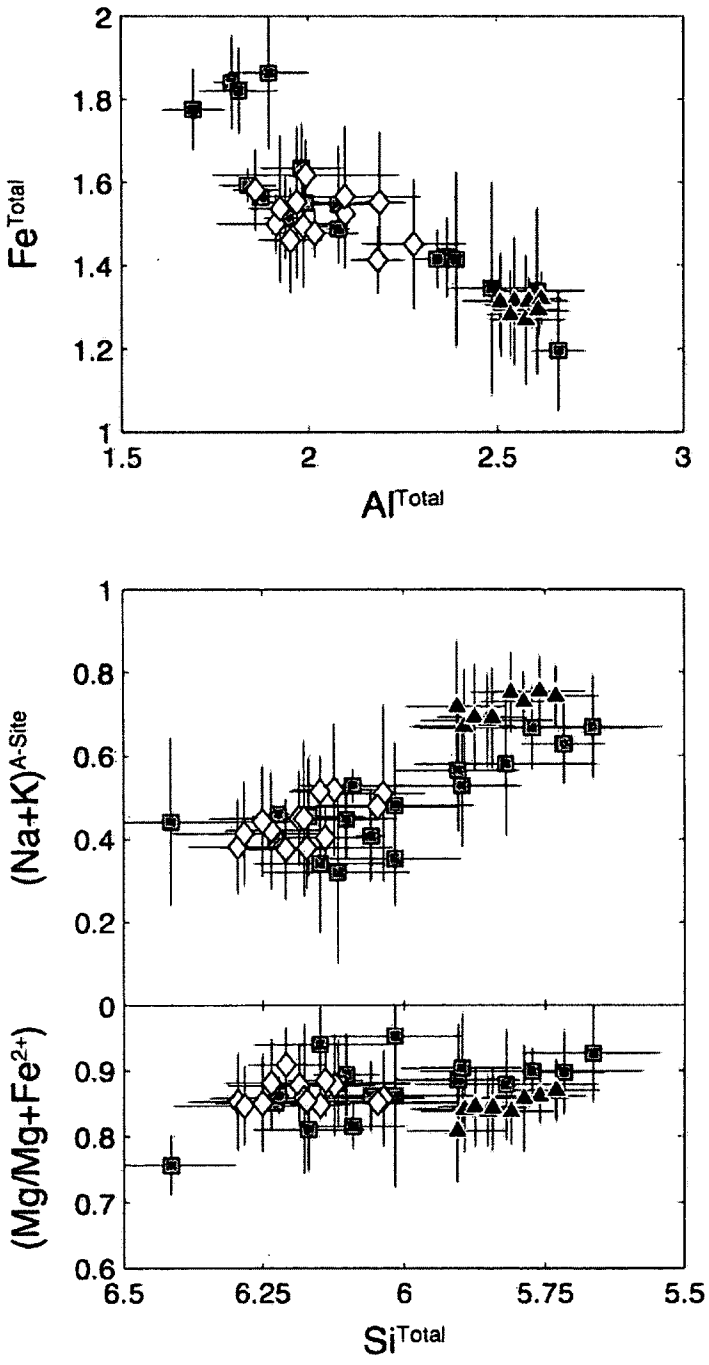

Figure 2-10: Compositions of Amphibole Phenocrysts. Points represent the average composition of several analyses of an individual phenocryst (Appendix 2-8). Error bars represent the average variation (2 standard deviations) of each averaged analysis. Compositions are in atoms per formula unit, calculated using ProbeAmph (Tindle and Webb, 1994). Symbols as in Fig. 2-3.

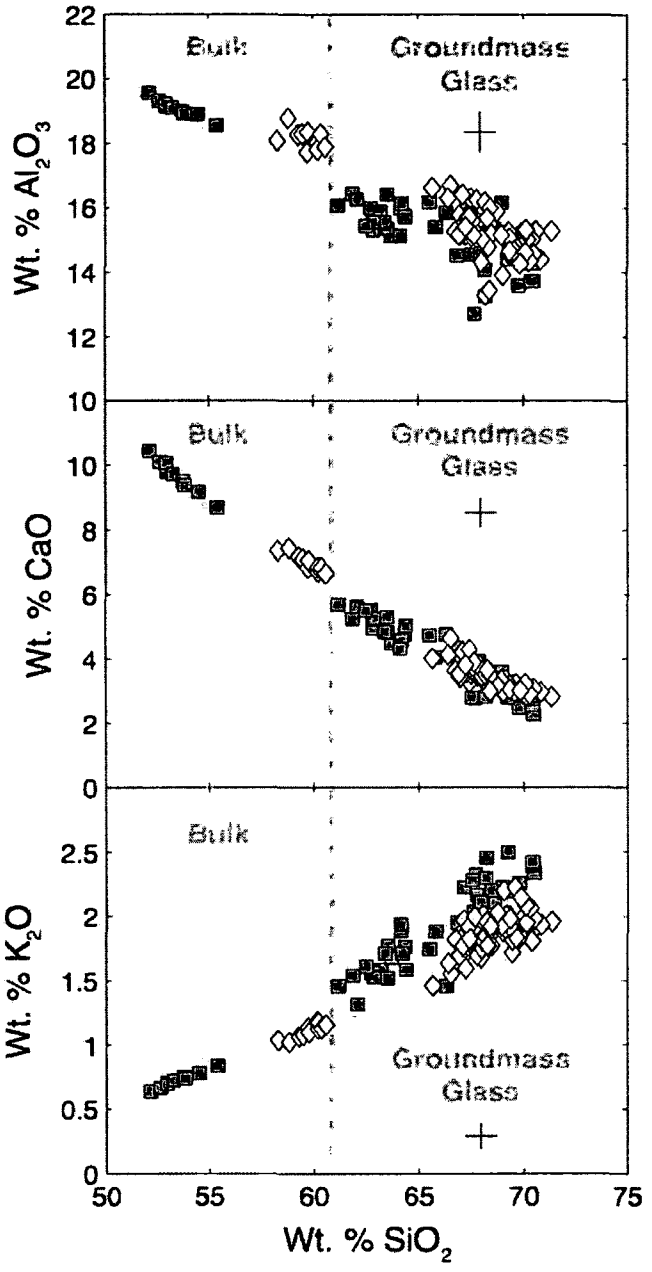

Figure 2-11: Compositions of Groundmass Glass. Andesite and basaltic andesite bulk compositions included for comparison (Appendix 2-10). Error bars represent analytical uncertainty (2 standard deviations) of groundmass glass measurements only, based on repeated measurements of the Yellowstone rhyolite glass standard VG-568 (USNM 72854; Jarosewich, 2002) and of a rhyolite glass standard synthesized by Mangan and Sisson (2000). Symbols as in Fig. 2-3.

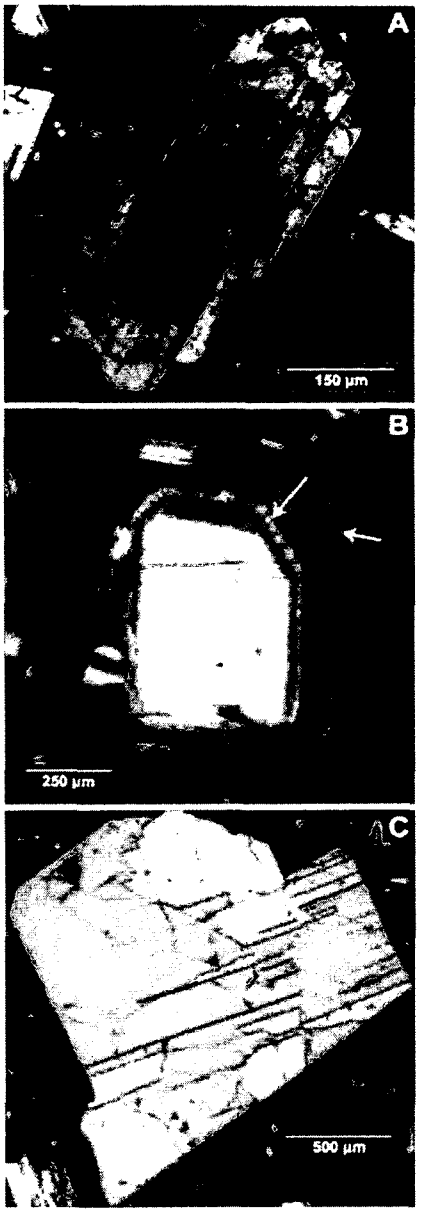

Figure 2-12: Images of Representative Plagioclase Textures. (A) Plagioclase from the basaltic andesite containing a sieved core (~An_{78}) with an un-reacted, oscillatory zoned rim (~An_{62}). (B) Plagioclase crystal from the andesite containing a high-An core (~An_{90}) surrounded by oscillatory-zoned rim, with interface of oscillating low- and high-An zones between core and rim. High-An zones (marked with white arrows) outside the core are accompanied by parallel rings of melt inclusions. Oscillatory zoning outside on the outer edge of the phenocryst is ~$An_{60\text{-}65}$. (C) Euhedral, unzoned plagioclase from the basaltic andesite with ~An_{95} core and ~An_{92} rim. All images taken with a standard petrographic microscope in cross-polarized light.

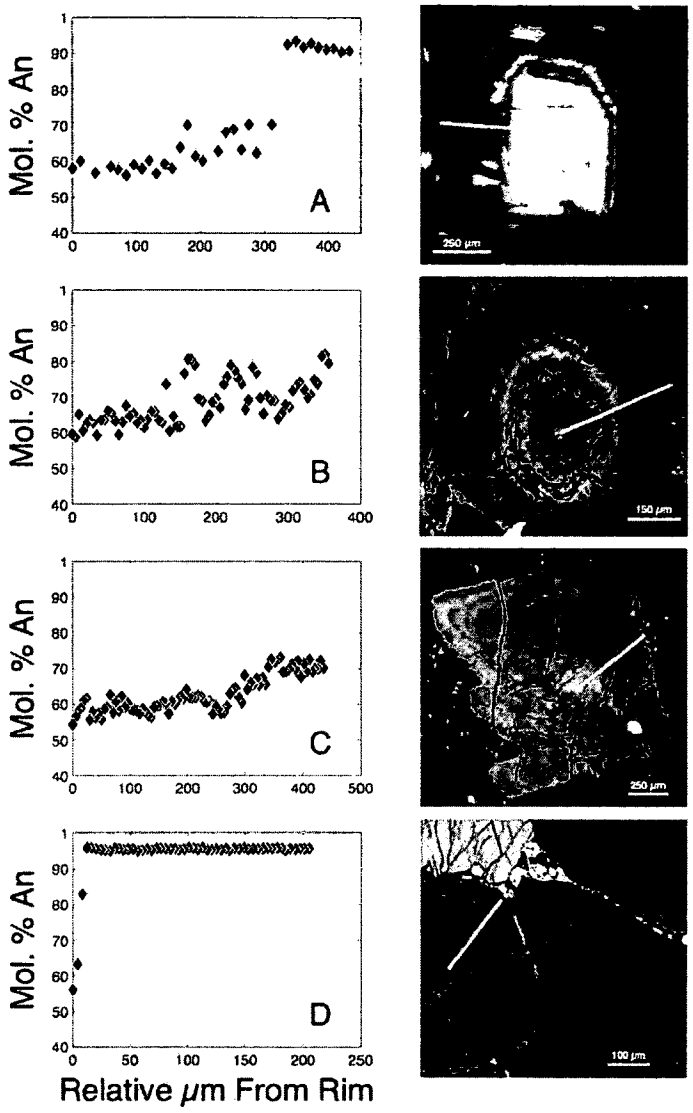

Figure 2-13: Microprobe Transects of Plagioclase Phenocrysts. Electron microprobe transects of representative plagioclase phenocrysts showing the compositional variations associated with the textures shown in Fig. 2-12. (A) High-An core as in Fig. 2-12B, with lower-An rim. (B) Normal zonation pattern, interrupted by the high-An spikes associated with dissolution boundaries such as those seen in Fig. 2-12B. These spikes occur over a narrow spatial range, with rapid onsets and returns to the overall rimward normal/oscillatory zoning trend. (C) Oscillatory zoning with an overall core-to-rim trend from high- to low-An, with no dissolution features or spikes in An content, as seen in the rims of the phenocrysts in Fig. 2-12A and 2-12B. (D) Homogenously high-An (>An_{90}) throughout the crystal, with rapid drop in An content close to the rim. Rapid drop in An content is not always observed. This texture is very similar to the unreacted, unzoned high-An phenocrysts found in the basaltic andesite (Fig. 2-12C). Analytical uncertainty is smaller than the size of the symbols. Data in Appendix 2-13.

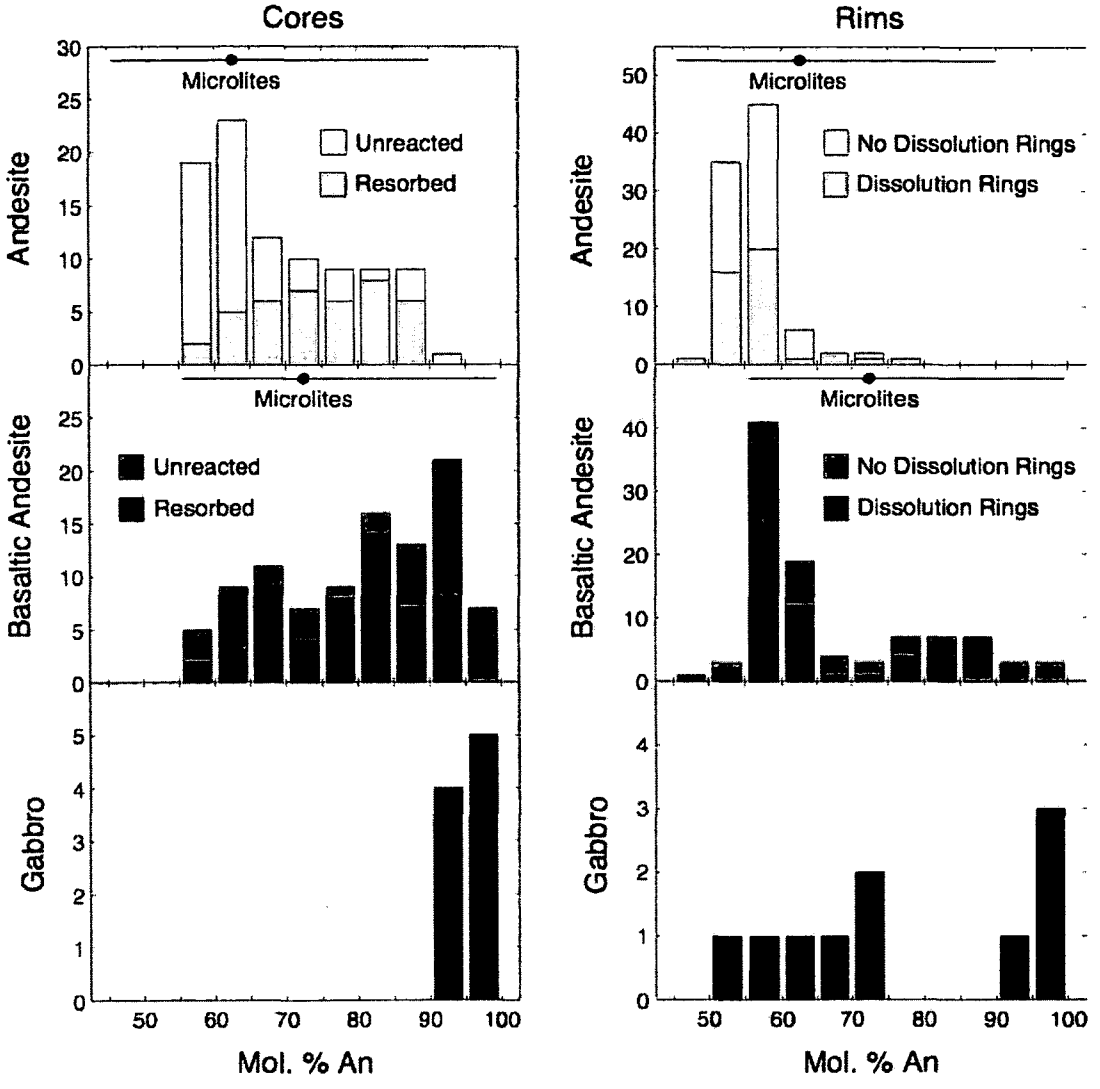

Figure 2-14: Compositions of Plagioclase Phenocryst Cores and Rims. Histograms of plagioclase core and rim compositions from eruptive products of the 2008 Kasatochi eruption (Appendix 2-11), as well as the relative abundances of dissolution features within the phenocrysts. Resorbed cores are cores that show dissolution features such as those in Fig. 2-12A. Dissolution rings are rings of melt inclusions associated with marked jumps in An content, such as those in Figs. 2-12B and 2-13B. Core and rim compositions were measured by EPMA (see text), while dissolution features were identified optically; An contents calculated using CALCMIN (Brandelik, 2009).

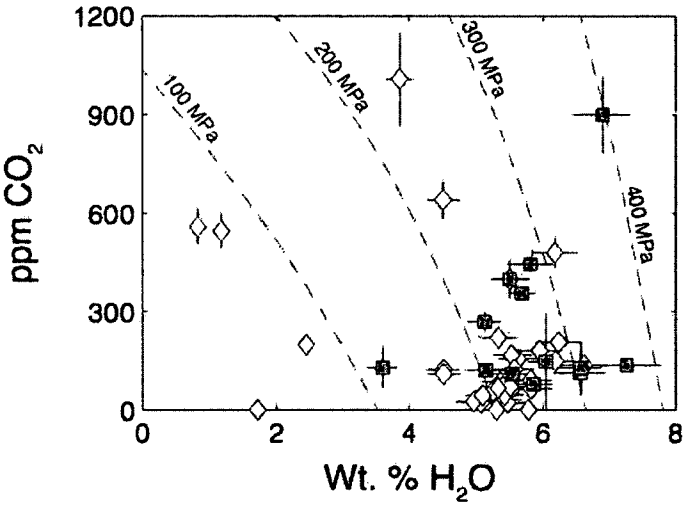

Figure 2-15: H_2O and CO_2 Concentrations of Melt Inclusions. Inclusions from the 2008 Kasatochi basaltic andesite (squares) measured by SHRIMP-RG ion probe (see text). Measurements of melt inclusions from the 2008 Kasatochi andesite by Izbekov et al. (2009) are also shown (diamonds). Isobars calculated using the H_2O-CO_2 solubility model of Papale et al. (2006). Analytical uncertainties (2 standard deviations) based on counting statistics. Individual analyses are listed in Appendix 2-12.

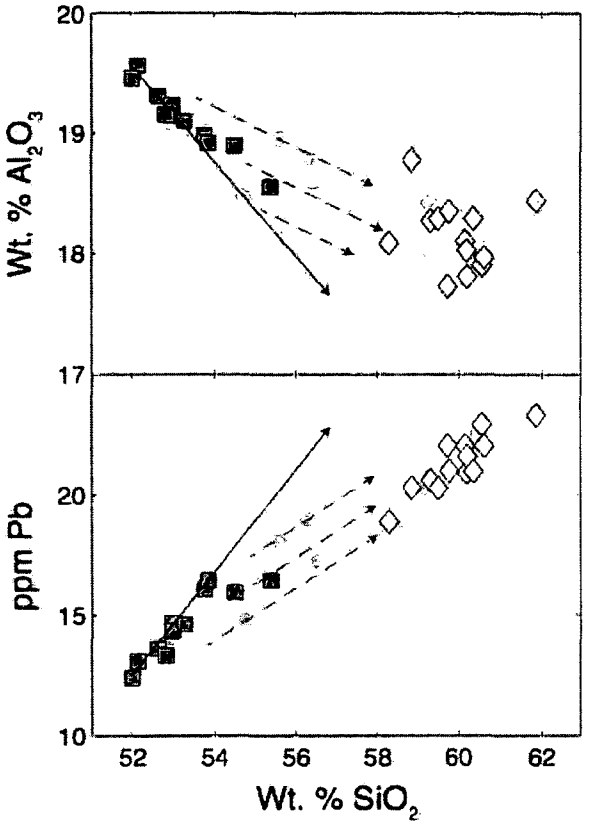

Figure 2-16: Schematic Mixing Relationships. Inferred mixing relationships between the 2008 Kasatochi andesite and basaltic andesite. Symbols as in Fig. 2-3. Solid arrows indicate the overall basaltic andesite mixing trend between end members similar in composition to the lowest- and highest-SiO_2 samples in the basaltic andesite suite. Dashed arrows represent schematic mixing relationships between various end member compositions from the andesite and basaltic andesite. Analytical uncertainty is smaller than the size of the symbols. Individual analyses are listed in Appendix 2-3.

2.9: References

Arnoult, K.M., Olson, J.V., Szuberla, C.A.L., McNutt, S.R., Garces, M.A., Fee, D. and Hedlin, M.A.H., 2010. Infrasound observations of the 2008 explosive eruptions of Okmok and Kasatochi volcanoes, Alaska. J Geophys Res-Atmos, 115: D00L15.

Bailey, E.P. and Trapp, J.L., 1986. A Reconnaissance of Breeding Birds and Mammals in the East-Central Aleutian Islands—Kasatochi to the Islands of Four Mountains—Summer 1982, with Notes on Other Species, Homer, Alaska. U.S. Fish and Wildlife Service, Report AMNWR 86/12. 83 pp.

Barclay, J., Rutherford, M.J., Carroll, M.R., Murphy, M.D., Devine, J.D., Gardner, J. and Sparks, R.S.J., 1998. Experimental phase equilibria constraints on pre-eruptive storage conditions of the Soufriere Hills magma. Geophys Res Lett, 25(18): 3437-3440. doi: 10.1029/98gl00856

Blatter, D.L. and Carmichael, I.S.E., 2001. Hydrous phase equilibria of a Mexican high-silica andesite: A candidate for a mantle origin? Geochim Cosmochim Acta, 65(21): 4043-4065.

Blundy, J., Berlo, K. and Cashman, K., 2005. Lithium transport by a magmatic volatile phase beneath Mount St. Helens volcano. Geochim Cosmochim Acta, 69(10): A151-A151.

Bluth, G.J.S., Doiron, S.D., Schnetzler, C.C., Krueger, A.J. and Walter, L.S., 1992. Global tracking of the SO_2 clouds from the June, 1991 Mount Pinatubo eruptions. Geophys Res Lett, 19(2): 151-154.

Brandelik, A., 2009. CALCMIN - an EXCEL (TM) Visual Basic application for calculating mineral structural formulae from electron microprobe analyses. Comp Geosci, 35(7): 1540-1551.

Browne, B.L., Eichelberger, J.C., Patino, L.C., Vogel, T.A., Uto, K. and Hoshizumi, H., 2006. Magma mingling as indicated by texture and Sr/Ba ratios of plagioclase phenocrysts from Unzen volcano, SW Japan. J Volcanol Geoth Res, 154(1,Äi2): 103-116. doi: 10.1016/j.jvolgeores.2005.09.022

Browne, B.L. and Gardner, J.E., 2006. The influence of magma ascent path on the texture, mineralogy, and formation of hornblende reaction rims. Earth Planet Sc Lett, 246(3-4): 161-176.

Clynne, M.A., 1999. A complex magma mixing origin for rocks erupted in 1915, Lassen Peak, California. J Petrol, 40(1): 105-132. doi: 10.1093/petroj/40.1.105

Coats, R.R., 1950. Volcanic activity in the Aleutian arc, Bulletin. US Geol Surv Num Ser, pp. 14 p.

Coats, R.R., 1956. Reconnaissance geology of some western Aleutian Islands, Alaska, Bulletin. US Geol Surv Num Ser, U.S. Govt Print Off, pp. p.83-100, ill., maps (101 fold .col. in pocket) ;124 cm.

Coombs, M.L., Eichelberger, J.C. and Rutherford, M.J., 2000. Magma storage and mixing conditions for the 1953–1974 eruptions of Southwest Trident volcano, Katmai National Park, Alaska. Contrib Mineral Petr, 140(1): 99-118.

Cottrell, E., Gardner, J.E. and Rutherford, M.J., 1999. Petrologic and experimental evidence for the movement and heating of the pre-eruptive Minoan rhyodacite (Santorini, Greece). Contrib Mineral Petr, 135(4): 315-331.

Couch, S., Harford, C.L., Sparks, R.S.J. and Carroll, M.R., 2003. Experimental constraints on the conditions of formation of highly calcic plagioclase microlites at the Soufrire Hills Volcano, Montserrat. J Petrol, 44(8): 1455-1475. doi: 10.1093/petrology/44.8.1455

Couch, S., Sparks, R.S.J. and Carroll, M.R., 2001. Mineral disequilibrium in lavas explained by convective self-mixing in open magma chambers. Nature, 411(6841): 1037-1039.

Davidson, J.P. and Tepley, F.J., 1997. Recharge in volcanic systems: evidence from isotope profiles of phenocrysts. Science, 275(5301): 826-829.

Devine, J.D., Murphy, M.D., Rutherford, M.J., Barclay, J., Sparks, R.S.J., Carroll, M.R., Young, S.R. and Gardner, J.E., 1998. Petrologic evidence for pre-eruptive pressure & temperature conditions, and recent reheating, of andesitic magma erupting at the Soufriere Hills Volcano, Montserrat, W.I. Geophys Res Lett, 25(19): 3669-3672. doi: 10.1029/98gl01330

Donovan, J.J., Kremser, D. and Fournelle, J.H., 2007. Probe for Windows User's Guide and Reference, Enterprise Edition. Probe Software Inc., Eugene, OR., 355 pp.

Ewert, J.W., Guffanti, M. and Murray, T.L., 2005. An assessment of volcanic threat and monitoring capabilities in the United States: Framework for a National Volcano Early Warning System. In: US Geol Surv Open-File Report OF 2005-1164, pp. 62.

Fee, D., Steffke, A. and Garces, M., 2010. Characterization of the 2008 Kasatochi and Okmok eruptions using remote infrasound arrays. J Geophys Res-Atmos, 115: D00L10.

Garcia, M.O. and Jacobson, S.S., 1979. Crystal clots, amphibole fractionation and the evolution of calc-alkaline magmas. Contrib Mineral Petr, 69(4): 319-327.

Geist, E.L., Childs, J.R. and Scholl, D.W., 1988. The origin of summit basins of the Aleutian Ridge - implications for block rotation of an arc massif. Tectonics, 7(2): 327-341.

George, R., Turner, S., Hawkesworth, C., Morris, J., Nye, C., Ryan, J. and Zheng, S.-H., 2003. Melting processes and fluid and sediment transport rates along the Alaska-Aleutian arc from an integrated U-Th-Ra-Be isotope study. J Geophys Res, 108(B5): 2252.

Gill, J.B., 1981. Orogenic andesites and plate tectonics. Springer Verlag, Berlin, Germany, 390 pp.

Grewingk, C., 1850. Grewingk's Geology of Alaska and the Northwest Coast of America. [edited by M.W. Falk, translated by F. Jaensch, published 2003] Fairbanks, Alaska. University of Alaska Press: 242.

Hammer, J.E., Rutherford, M.J. and Hildreth, W., 2002. Magma storage prior to the 1912 eruption at Novarupta, Alaska. Contrib Mineral Petr, 144(2): 144-162.

Housh, T.B. and Luhr, J.F., 1991. Plagioclase-melt equilibria in hydrous systems. Am Mineral, 76(3-4): 477-492.

Humphreys, M.C.S., Blundy, J.D. and Sparks, R.S.J., 2008. Shallow-level decompression crystallisation and deep magma supply at Shiveluch Volcano. Contrib Mineral Petr, 155(1): 45-61. doi: DOI 10.1007/s00410-007-0223-7

Izbekov, P., 2008. Petrology of the 2008 eruption of Kasatochi volcano, Alaska, AGU Fall Meet 2009, Abs. #A53B-0623, San Francisco, pp. 623.

Izbekov, P.E., Eichelberger, J.C., Patino, L.C., Vogel, T.A. and Ivanov, B.V., 2002. Calcic cores of plagioclase phenocrysts in andesite from Karymsky volcano: Evidence for rapid introduction by basaltic replenishment. Geology, 30(9): 799-802.

Izbekov, P.E., Eichelberger, J.C. and Ivanov, B.V., 2004. The 1996 eruption of Karymsky volcano, Kamchatka: Historical record of basaltic replenishment of an andesite reservoir. J Petrol, 45(11): 2325-2345.

Izbekov, P., Sisson, T., Wooden, J. and Bacon, C., 2009. 2008 Kasatochi Eruption: SHRIMP constraints on concentration of volatiles in melt inclusions, AGU Fall Meet 2009, Abs. #V51E-1775, San Francisco, CA, pp. 1775.

Jaggar, T., 1927. The Aleutian Islands. The Volcano Letter, 116(1).

Jarosewich, E., 2002. Smithsonian microbeam standards. J Res NIST (107): 681-685.

Johnson, D.M., Hooper, P.R. and Conrey, R.M., 1999. XRF Analysis of rocks and minerals for major and trace elements on a single low dilution Li-tetraborate fused bead. Adv X-ray Anal, 41: 843-867.

Karagulian, F., Clarisse, L., Clerbaux, C., Prata, A.J., Hurtmans, D. and Coheur, P.F., 2010. Detection of volcanic SO_2, ash, and H_2SO_4 using the Infrared Atmospheric Sounding Interferometer (IASI). J Geophys Res-Atmos, 115: D00L02.

Kay, S. and Kay, R., 1985. Aleutian tholeiitic and calc-alkaline magma series I: The mafic phenocrysts. Contrib Mineral Petr, 90(2): 276-290.

Knaack, C., Cornelius, S. and Hooper, P.R., 1994. Trace element analyses of rocks and minerals by ICP-MS, Open-File Report, Department of Geology, University of Washington.

Kristiansen, N.I., Stohl, A., Prata, A.J., Richter, A., Eckhardt, S., Seibert, P., Hoffmann, A., Ritter, C., Bitar, L., Duck, T.J. and Stebel, K., 2010. Remote sensing and

inverse transport modeling of the Kasatochi eruption sulfur dioxide cloud. J Geophys Res-Atmos, 115: D00L16.

Lange, R.A., Frey, H.M. and Hector, J., 2009. A thermodynamic model for the plagioclase-liquid hygrometer/thermometer. Am Mineral, 94(4): 494-506. doi: 10.2138/am.2009.3011

Larsen, J.F., Nye, C.J., Coombs, M.L., Tilman, M., Izbekov, P. and Cameron, C., 2010. Petrology and geochemistry of the 2006 eruption of Augustine Volcano, Professional Paper. US Geol Surv Num Ser, p. 335-382.

Le Bas, M.J., Lemaitre, R.W., Streckeisen, A. and Zanettin, B., 1986. A chemical classification of volcanic rocks based on the Total Alkali Silica diagram. J Petrol, 27(3): 745-750.

Lepage, L.D., 2003. ILMAT: an Excel worksheet for ilmenite-magnetite geothermometry and geobarometry. Comp Geosci, 29(5): 673-678.

Ludwig, K.R., 2009. SQUID2: A User's Manual (v. 2.50), Berkeley Geochronology Center Special Publication, 5, 104 pp.

Mangan, M. and Sisson, T., 2000. Delayed, disequilibrium degassing in rhyolite magma: decompression experiments and implications for explosive volcanism. Earth Planet Sc Lett, 183(3-4): 441-455. doi: Doi: 10.1016/s0012-821x(00)00299-5

Martel, C., Radadi Ali, A., Poussineau, S., Gourgaud, A. and Pichavant, M., 2006. Basalt-inherited microlites in silicic magmas: Evidence from Mount Pelée (Martinique, French West Indies). Geology, 34(11): 905-908. doi: 10.1130/g22672a.1

Miyashiro, A., 1974. Volcanic rock series in island arcs and active continental margins. Am Jour Sci, 274(4): 321-355. doi: 10.2475/ajs.274.4.321

Moore, G. and Carmichael, I.S.E., 1998. The hydrous phase equilibria (to 3 kbar) of an andesite and basaltic andesite from western Mexico: constraints on water content and conditions of phenocryst growth. Contrib Mineral Petr, 130(3-4): 304-319.

Morimoto, N., Fabries, J., Ferguson, A.K., Ginzburg, I.V., Ross, M., Seifert, F.A., Zussman, J., Aoki, K. and Gottardi, G., 1988. Nomenclature of pyroxenes. Am Mineral, 73(9-10): 1123-1133.

Murphy, M.D., Sparks, R.S.J., Barclay, J., Carroll, M.R. and Brewer, T.S., 2000. Remobilization of andesite magma by intrusion of mafic magma at the Soufriere Hills Volcano, Montserrat, West Indies. J Petrol, 41(1): 21-42.

Myers, J.D., Marsh, B.D. and Sinha, A.K., 1985. Strontium isotopic and selected trace element variations between two Aleutian volcanic centers (Adak and Atka): implications for the development of arc volcanic plumbing systems. Contrib Mineral Petr, 91(3): 221-234.

Nakamura, M., 1995. Continuous mixing of crystal mush and replenished magma in the ongoing Unzen eruption. Geology, 23(9): 807-810.

Neill, O.K., Larsen, J.F., Izbekov, P.E. and Nye, C.J. (*in prep*) Pre-eruptive magma mixing and crystal transfer in basaltic andesite from the 2008 eruption of Kasatochi Volcano, Central Aleutian Islands, Alaska.. J Volcanol Geoth Res.

Newhall, C.G. and Self, S., 1982. The Volcanic Explosivity Index (VEI) - an estimate of explosive magnitude for historical volcanism. J Geophys Res-Oc Atmos, 87(Nc2): 1231-1238.

Nielsen, C.H. and Sigurdsson, H., 1981. Quantitative methods for electron micro-probe analysis of sodium in natural and synthetic glasses. Am Mineral, 66(5-6): 547-552.

Pallister, J.S., Hoblitt, R.P., Meeker, G.P., Knight, R.J. and Siems, D.F., 1996. Magma mixing at Mount Pinatubo; petrographic and chemical evidence from the 1991 deposits. *In*: Newhall, C.G. and Punongbayan, R.S. (*eds*) Fire and Mud: Eruptions and Lahars of Mount Pinatubo, Philippines. Quezon City, Philippines: Philippine Inst Volc Seism, and Seattle: Univ Wash Press, 687-731 pp.

Papale, P., Moretti, R. and Barbato, D., 2006. The compositional dependence of the saturation surface of H_2O+CO_2 fluids in silicate melts. Chem Geol, 229(1-3): 78-95. doi: DOI 10.1016/j.chemgeo.2006.01.013

Pichavant, M., Martel, C., Bourdier, J.L. and Scaillet, B., 2002. Physical conditions, structure, and dynamics of a zoned magma chamber: Mount Pelee (Martinique, Lesser Antilles Arc). J Geophys Res-Sol Ea, 107(B5).

Prata, A.J., Gangale, G., Clarisse, L. and Karagulian, F., 2010. Ash and sulfur dioxide in the 2008 eruptions of Okmok and Kasatochi: Insights from high spectral resolution satellite measurements. J Geophys Res-Atmos, 115: D00L18.

Putirka, K.A., 2005. Igneous thermometers and barometers based on plagioclase plus liquid equilibria: Tests of some existing models and new calibrations. Am Mineral, 90(2-3): 336-346. doi: Doi 10.2138/Am.2005.1449

Roman, D., Cashman, K., Gardner, C., Wallace, P. and Donovan, J., 2006. Storage and interaction of compositionally heterogeneous magmas from the 1986 eruption of Augustine Volcano, Alaska. B Volcanol, 68(3): 240-254.

Romick, J.D., Kay, S.M. and Kay, R.W., 1992. The influence of amphibole fractionation on the evolution of calc-alkaline andesite and dacite tephra from the central Aleutians, Alaska. Contrib Mineral Petr, 112(1): 101-118.

Ruppert, N.A., Prejean, S. and Hansen, R.A., 2011. Seismic swarm associated with the 2008 eruption of Kasatochi Volcano, Alaska: Earthquake locations and source parameters. J Geophys Res, 116: B00B07.

Ruprecht, P. and Wörner, G., 2007. Variable regimes in magma systems documented in plagioclase zoning patterns: El Misti stratovolcano and Andahua monogenetic cones. J Volcanol Geoth Res, 165(3-4): 142-162.

Rutherford, M.J. and Hill, P.M., 1993. Magma ascent rates from amphibole breakdown - an experimental-study applied to the 1980-1986 Mount St-Helens eruptions. J Geophys Res-Sol Ea, 98(B11): 19667-19685.

Ryan, W.B.F., Carbotte, S.M., Coplan, J.O., O'Hara, S., Melkonian, A., Arko, R., Weissel, R.A., Ferrini, V., Goodwillie, A., Nitsche, F., Bonczkowski, J. and Zemsky, R., 2009. Global Multi-Resolution Topography synthesis. Geochem Geophys Geosyst, 10: Q03014.

Scott, W.E., Nye, C.J., Waythomas, C.F. and Neal, C.A., 2010. August 2008 eruption of Kasatochi Volcano, Aleutian Islands, Alaska-resetting an island landscape. Arct Antarct Alp Res, 42(3): 250-259.

Shcherbakov, V.D., Plechov, P.Y., Izbekov, P.E. and Shipman, J.S., 2011. Plagioclase zoning as an indicator of magma processes at Bezymianny Volcano, Kamchatka. Contrib Mineral Petr, 162(1): 83-99.

Sun, S.-s. and McDonough, W.F., 1989. Chemical and isotopic systematics of oceanic basalts: implications for mantle composition and processes. Geol Soc Lond Spec Pub, 42(1): 313-345.

Tepley, F.J., Davidson, J.P. and Clynne, M.A., 1999. Magmatic Interactions as Recorded in Plagioclase Phenocrysts of Chaos Crags, Lassen Volcanic Center, California. J Petrol, 40(5): 787-806.

Tepley, F.J., Davidson, J.P., Tilling, R.I. and Arth, J.G., 2000. Magma mixing, recharge and eruption histories recorded in plagioclase phenocrysts from El Chichón Volcano, Mexico. J Petrol, 41(9): 1397-1411.

Tindle, A.G. and Webb, P.C., 1994. Probe-Amph - a spreadsheet program to classify microprobe-derived amphibole analyses. Comp Geosci, 20(7-8): 1201-1228.

Waythomas, C.F., Scott, W.E., Prejean, S.G., Schneider, D.J., Izbekov, P. and Nye, C.J., 2010a. The 7-8 August 2008 eruption of Kasatochi Volcano, central Aleutian Islands, Alaska. J Geophys Res, 115: B00B06.

Waythomas, C.F., Scott, W.E. and Nye, C.J., 2010b. The Geomorphology of an Aleutian Volcano following a Major Eruption: the 7-8 August 2008 Eruption of Kasatochi Volcano, Alaska, and Its Aftermath. Arct Antarct Alp Res, 42(3): 260-275.

Wright, H., Bacon, C., Vazquez, J. and Sisson, T., 2012. Sixty thousand years of magmatic volatile history before the caldera-forming eruption of Mount Mazama, Crater Lake, Oregon. Contrib Mineral Petr, 1-26. doi: 10.1007/s00410-012-0787-8

Yogodzinski, G.M., Kay, R.W., Volynets, O.N., Koloskov, A.V. and Kay, S.M., 1995. Magnesian andesite in the western Aleutian Komandorsky region: Implications

for slab melting and processes in the mantle wedge. Geol Soc Am Bull, 107(5): 505-519.

Yogodzinski, G.M. and Kelemen, P.B., 1998. Slab melting in the Aleutians: implications of an ion probe study of clinopyroxene in primitive adakite and basalt. Earth Planet Sc Lett, 158(1-2): 53-65.

Yogodzinski, G.M., Vervoort, J.D., Brown, S.T. and Gerseny, M., 2010. Subduction controls of Hf and Nd isotopes in lavas of the Aleutian island arc. Earth Planet Sc Lett, 300(3-4): 226-238.

Chapter 3: Pre-Eruptive Magma Mixing and Crystal Transfer Revealed by Phenocryst and Microlite Compositions in Basaltic Andesite from the 2008 Eruption of Kasatochi[1]

"Are you going up?"
"Yes, yes, we go up."
"You may be going a lot higher than you think."

Exchange between Don Whillans and another climbing team
The Eiger, Switzerland
ca. 1962

3.1: Abstract

The 7-8 August, 2008 eruption of Kasatochi Volcano, located in the central Aleutians Islands, Alaska, produced abundant, juvenile, compositionally heterogeneous basaltic andesite (52-55 wt. % SiO_2) that has previously been interpreted to result from pre-eruptive magma mixing. The basaltic andesite contains two populations of plagioclase phenocrysts. The first, volumetrically dominant population consists of oscillatory-zoned phenocrysts with an overall normal zonation trend towards comparatively sodic rims (An_{55-65}) interrupted by dissolution features and spikes in calcium content (up to ~An_{85}). The second population consists of phenocrysts with highly

[1] Neill, O.K., Larsen, J.F., Izbekov, P.E. and Nye, C.J. (*in prep*) Pre-eruptive magma mixing and crystal transfer in basaltic andesite from the 2008 eruption of Kasatochi Volcano, Central Aleutian Islands, Alaska. To be submitted to *Journal of Volcanology and Geothermal Research*.

calcic compositions (~An_{90}). These phenocrysts contain sharp decreases in calcium content close to their rims (reaching as low as ~An_{60}) but are otherwise texturally and compositionally homogeneous. Groundmass plagioclase microlites are generally much more calcic than rims of the first phenocryst population, with more than 50% of measured microlites containing >An_{80}. Major, minor and trace element concentrations of plagioclase microlites and phenocrysts indicate that oscillatory-zoned phenocrysts derived from cooler (800-950 °C), felsic mixing magma, while unzoned, calcic phenocrysts were associated with hotter (900-1050 °C), mafic magma. The mixing of these magmas just prior eruption, followed by decompression during the eruption itself, created high effective undercoolings in the mafic end member and lead to the nucleation of high-An microlites. MgO and FeO concentrations of plagioclase microlites and high-An phenocryst rims (up to ~0.4 and ~1.3 wt. %, respectively) provide further evidence for high mixing- and eruption-induced effective undercoolings.

3.2: Introduction

3.2.1: Plagioclase Microlites in Volcanic Systems

Plagioclase microlites are small (<100 μm) crystals of plagioclase feldspar, which are generally assumed to crystallize in response to the high effective undercooling created by degassing and decompression during the final ascent of magma from shallow crustal

storage regions to the surface (e.g. Westrich et al., 1988; Geschwind and Rutherford, 1995; Hammer and Rutherford, 2002; Martel and Schmidt, 2003; McCanta et al., 2007; Brugger and Hammer, 2010). Crystallization during magmatic ascent is the last phase of crystallization before an erupted magma freezes. If all microlites are assumed to grow during ascent, their abundance and texture may reflect the ascent rate of the magma from depth (e.g. Hammer and Rutherford, 2002). Also, microlites growing in such an environment would grow from the most evolved, relatively low-Ca, high-Na/high-K liquids within the system, and therefore microlite compositions would be compositionally similar or even higher in Na and K than the rim compositions of plagioclase phenocrysts (e.g. Blundy and Cashman, 2001).

There are, however, systems that do not conform to this general model, containing microlites that are more anorthitic than the dominant phenocryst rim compositions. In these cases, microlites may have been inherited from a pre-eruptive mixing end member. For example, Martel et al. (2006) reported microlites with compositions up to ~An_{90}, well in excess of phenocryst rim compositions (An_{50-60}), in a study of Mount Pelée, Martinique. Mount Pelée, like Kasatochi, had produced andesite and basaltic andesite in the same eruptive sequence, and Martel et al. (2006) inferred that the highly calcic microlites were inherited from basaltic replenishment of the magmatic system immediately prior to eruption. In a study of Soufriere Hills Volcano, Montserrat, Couch et al. (2003) suggested that high-An microlites crystallized due to convective self-mixing of the Soufriere Hills magma system, whereby hotter, more calcic liquid ascended rapidly

within the magma chamber, causing the crystallization of high-An microlites, which were then mixed with cooler, more evolved andesite at the top of the system.

Basaltic andesite clasts from the 2008 eruption of Kasatochi Volcano, Alaska, also contain a population of microlites that are more calcic than the rims of the dominant phenocryst population. Herein, the plagioclase phenocryst and microlite populations of the 2008 Kasatochi basaltic andesite are characterized to determine the origins and conditions of formation of the individual populations. The goal of this study is to decipher whether the high-An microlites seen in the 2008 Kasatochi basaltic andesite were derived from basaltic replenishment, similar to a model for their formation at Mount Pelée.

3.2.2: Geologic Setting

Kasatochi Island, located in the Central Aleutian Islands, is a 3-km wide island stratovolcano, rising ~300 m above sea level. The Kasatochi volcanic cone surrounds a crater ~1 km wide, which contains a brackish crater-lake. Deposits from eruptions prior to 2008 consist of a basal unit of interbedded lahars, lava flows, pyroclastic deposits and hyaloclastites; a middle series of lava flows ranging in composition from basalt to andesite; and an uppermost interbedded pyroclastic surge/flow unit (Waythomas et al., 2010a). Due to the island's remote location and the lack of historical eruptions, no geologic studies targeting Kasatochi existed prior to 2008, though studies of the island's flora and fauna had been ongoing since the 1980's (Williams et al., 2010, and references

therein). Geologic studies of the island were limited to preliminary surveys and mapping of the area (e.g. Coats, 1956) and chemical analyses of one basaltic sample, originally reported in Kay and Kay (1985) and used in subsequent studies of arc petrogenesis in the Aleutians (e.g. Yogodzinski et al., 1995; Yogodzinski and Kelemen, 1998).

Anomalously strong seismic activity was detected at Kasatochi on 6 August, 2008, and on 7 August the first ash plume was detected, indicating the onset of explosive activity. The eruption continued for ~21 hours after the first ash plume, punctuated by 5 main explosive events (Arnoult et al., 2010; Fee et al., 2010). Detailed descriptions of the eruption are provided by Waythomas et al. (2010a; 2010b) and Scott et al. (2010), but to summarize, the eruption produced ash plumes which reached up to 18 km above sea level, released more seismic energy than any volcanic eruption ever recorded by the Alaska Volcano Observatory, the agency responsible for monitoring Aleutian volcanoes, and was the single largest point-source release of SO_2 gas since the 1991 eruptions of Cerro Hudson in Chile and Pinatubo in the Philippines. In addition, the eruption produced voluminous pyroclastic flows and surges, leaving tephra deposits up to 30 m thick, which increased the area of the diameter of the island by ~800 m.

The 2008 eruptive products have been fully described and interpreted petrologically and geochemically, as described in Neill et al. (*in prep*); a brief summary of the findings of that study is presented here. The 2008 eruption produced two main juvenile lithologies: a white, pumiceous, medium-K, borderline calk-alkaline andesite (Miyashiro, 1974) ranging from ~58-62 wt. % SiO_2 (Fig. 3-1); and a denser, grey-brown,

medium-K, tholeiitic basaltic andesite ranging from ~52-55 wt. % SiO_2 (Fig. 3-1). Banded clasts, representing mechanical mixtures between the andesite and basaltic andesite, are also common throughout the 2008 pyroclastic deposits. All juvenile products of the 2008 eruption contain a phase assemblage of (in approximately descending order of volumetric abundance) plagioclase, clinopyroxene, orthopyroxene, amphibole and titanomagnetite.

Andesite compositions do not vary systematically in all components; while andesite large-ion lithophile and high field strength element concentrations form linear arrays in most element vs. SiO_2 diagrams, other components, such as the heavy rare-earth elements and P_2O_5, show little systematic variations (Fig. 3-1). However, basaltic andesite samples lie along approximately linear arrays in element-element diagrams (Fig. 3-1), likely the result of mixing directly prior to eruption. As the basaltic andesite compositional trends do not intersect with andesite concentrations in certain components (e.g. P_2O_5, Er, Fig. 3-1), the basaltic andesite and andesite must have resided in physically and chemically separate storage regions until directly prior to eruption, and the mixing that affected the basaltic andesite involved end members similar to the most mafic and most felsic basaltic andesite compositions. This study is based on the samples described in Neill et al. (*in prep*), and includes relevant subsets of the data from that chapter, as well as new characterizations of the basaltic andesite plagioclase populations that shed further light on pre-eruptive mixing and crystal transfer in the basaltic andesite. Readers should note that all appendices are included electronically on the compact disc accompanying this dissertation.

3.3: Analytical Methods

Compositions of amphibole, titanomagnetite and groundmass glass were analyzed by wavelength-dispersive x-ray spectrometry using the 4-spectrometer CAMECA SX-50 electron microprobe, housed at the Advanced Instrumentation Laboratory of the University of Alaska Fairbanks. Analytical conditions, standards and uncertainties for electron microprobe analyses may be found in Appendix 3-1. Concentrations were obtained from raw counts using a ZAF intensity correction. Amphibole and titanomagnetite analyses were conducted with a focused beam, while groundmass glass analyses were conducted with the beam defocused to a radius of ~10 μm to minimize Na, K, Al and Si migration during analyses (e.g. Morgan and London, 1996). Na loss was corrected using a variation of the procedures of Nielsen and Sigurdsson (1981) via ProbeForEPMA software (Donovan et al., 2007).

Compositions of plagioclase phenocrysts and microlites were analyzed by electron microprobe using two separate analytical procedures. A routine optimized for speed and accurate determination of anorthite content was used for an initial survey of plagioclase phenocryst cores and rims (hereafter referred to as the "Major" routine). A second set of phenocrysts, and all plagioclase microlites, were then analyzed using higher currents and longer counting times in order to obtain more accurate analyses of the minor elements Fe and Mg (reported as oxides FeO and MgO, with all Fe reported as Fe^{2+}). In the second routine (referred to as the "Trace" routine), the electron beam was defocused to ~3 μm and Na peak counting time was reduced to 10 seconds to minimize alkali

migration; no significant alkali migration was detected. Detection limits for FeO and MgO, calculated using ProbeForEPMA software as described by Donovan et al. (2007), were 0.03 and 0.009 wt. %, respectively. Beam conditions, calibration standards and typical analytical uncertainties for both the Major and Trace routines are reported in Appendix 3-1. For the purposes of this study, the term microlite will refer to crystals <100 μm in length, while the term "phenocryst" will refer to crystals within the sample >300 μm in length. Microprobe analyses of microlites were performed as close to the rims of the microlites as possible.

3.4: Plagioclase in the 2008 Kasatochi Basaltic Andesite

3.4.1: Plagioclase Phenocrysts

There are two distinct populations of plagioclase phenocrysts in the basaltic andesite. The first population (referred to herein as Group 1 phenocrysts) consists of oscillatory-zoned plagioclase phenocrysts with an overall normal zonation trend sometimes interrupted by spikes in An content (Fig. 3-2). These spikes in An content are commonly associated with dissolution features and are interpreted as markers of periodic mafic recharge into a well-buffered silicic system. Prior studies have documented that an influx of mafic material, possibly bringing heat and increased H_2O contents, causes the outer rim of plagioclase phenocrysts to dissolve, followed by the growth of higher-An

plagioclase on the outside of the dissolution surface (e.g. Tsuchiyama, 1985; Davidson and Tepley, 1997; Clynne, 1999; Tepley et al., 1999; Izbekov et al., 2004; Ruprecht and Wörner, 2007). Once the system re-equilibrates, the overall normal zonation trend resumes rimward of the dissolution boundaries. Approximately 70% of Group 1 phenocrysts have rim compositions between An_{55-65} (Fig. 3-3). Group 1 phenocrysts also commonly contain high-An cores, which may represent crystals that were initially brought into the system by the mafic injections that caused the dissolution features.

The second major phenocryst population (Group 2) consists of high-An ($>An_{80}$, Fig. 3-2), texturally homogenous plagioclase phenocrysts with no dissolution features beyond scattered small (<10 μm) melt inclusions. Compared to Group 1 phenocrysts, however, Group 2 phenocrysts contain very few compositional variations within individual crystals. Some crystals have cores with $>An_{90}$, which is higher than the dominant composition, though the boundaries of these zones are not marked by any observable textural features (Fig. 3-2). Also, An contents in the rims of Group 2 phenocrysts frequently decrease sharply <30 μm from the rim or less (Fig. 3-2). Group 2 phenocrysts account for ~30% of the overall basaltic andesite plagioclase phenocryst population.

3.4.2: Plagioclase Microlites

Plagioclase microlite compositions vary across a wide range of An contents (An_{55-95}, Fig. 3-3), but the modal composition ($\sim An_{85}$) is approximately 25 mol. % higher than

the modal rim composition (~An_{60}) of the volumetrically dominant Group 1 phenocryst population. Only ~10% of microlites have An contents equivalent to the compositional mode of the Group 1 rims (An_{55-65}, Fig. 3-3), while ~50% of microlites have An contents >An_{80}. Larger microlites show some degree of zonation, with lower-An rims (An_{57-79}) surrounding higher-An cores (An_{80-87}; Fig. 3-4), though rims are generally smaller than can be analyzed quantitatively.

3.4.3: Plagioclase MgO and FeO Concentrations

Iron and magnesium contents of Group 1 plagioclase phenocrysts do not vary within individual grains by more than analytical uncertainty. Group 1 plagioclase core and rim FeO and MgO contents are approximately equivalent, even in crystals with high-An cores (Appendix 3-2; Fig. 3-2), and the spikes in An content common in Group 1 phenocrysts are also not correlated with any significant change in FeO or MgO (Fig. 3-2). While analytical uncertainties associated with both FeO and MgO measurements are relatively large, all Group 1 phenocryst cores and rims contain between 0.4 and 0.65 wt. % FeO, while MgO concentrations of Group 1 phenocrysts are generally near 0.05 wt. % (Appendices 3-2, 3-3).

FeO and MgO contents of Group 2 phenocryst cores generally match those of Group 1, containing between ~0.4 and ~0.65 wt. % FeO and MgO concentrations ~0.05 wt. % (Appendix 3-2). Systematic changes in FeO and MgO contents within individual grains are generally lacking (Fig. 3-2). However, the abrupt drop in An content seen in

the outermost few tens of microns of Group 2 phenocrysts corresponds to spikes in both FeO and MgO, reaching up to 1.3 wt. % FeO and 0.4 wt. % MgO (Figs. 3-2, 3-5). Microlite FeO and MgO contents vary much more than those measured in transects of Group 1 phenocrysts. Only ~20% of measured microlites contain <0.65 wt. % FeO, with the maximum FeO reaching ~1.3 wt. %. There is also a negative correlation between anorthite content and MgO and FeO content in both microlites and Group 2 phenocryst rims, although more sodic microlites with low-Fe/low-Mg contents do exist (Fig. 3-5).

3.5: Compositions of Groundmass Glass and Mafic Minerals

Groundmass glass compositions in the basaltic andesite are heterogeneous, varying from ~60-70 wt. % SiO_2, ~13-17 wt. % Al_2O_3, and ~1.2-2.6 wt. % K_2O (Fig. 3-6). MgO concentrations reach a maximum of 3 wt. %, while FeO concentrations are between ~2.5 and ~8 wt. %. Groundmass glass compositions qualitatively mirror trends in bulk-rock compositions, varying along scattered linear trends, with both MgO and FeO correlating positively with CaO.

Mafic phenocrysts from all 2008 lithologies do not display significant zonation within individual crystals, although unlike in other lithologies from the 2008 eruption, basaltic andesite titanomagnetite and amphibole show significant inter-grain compositional variations across the respective suites of measured phenocrysts.

Titanomagnetite compositions are bimodal. The first group contains relatively low Ti contents with variable Fe contents, which do not vary by more than analytical uncertainty (Fig. 3-7). Phenocrysts in the second group contain much higher Ti and show a negative correlation between Ti and Fe (Fig. 3-7). Amphibole compositions also appear bimodal, with low-Fe and Si/high-Al and high-Fe and Si/low-Al groups, though the distinction is at the limits of analytical uncertainty (Fig. 3-8). Even if the bimodality is ignored as an analytical artifact, amphibole phenocrysts in the basaltic andesite vary over a much larger compositional range than amphibole from other lithologies from the 2008 Kasatochi eruption.

3.6: Pre-Eruptive Mixing Revealed by Phenocryst and Microlite Populations

3.6.1: Plagioclase Phenocrysts and Microlites Inherited from Mixing End Members

Microlite and Group 2 phenocryst compositions are out of equilibrium with measured groundmass glass compositions. Equilibrium Ca-Na partition coefficients between plagioclase and melt vary with magmatic H_2O content, but based on the range of these partition coefficients and measured Ca/Na molar ratios of groundmass glasses, plagioclase crystallizing from liquids equivalent in composition to groundmass glasses would have equilibrium Ca/Na molar ratios not exceeding ~3.1, even at high H_2O (Fig. 3-9). The average microlite and Group 2 phenocryst Ca/Na ratios are ~4.8 and ~7.1, respectively, with 33 of 61 measured microlites and 23 of 29 measured Group 2 rims having Ca/Na ratios greater than 3.1. By contrast, the average Group 1 phenocryst Ca/Na

ratio is ~1.8, with only with 5 of 72 measured Group 1 rims having Ca/Na ratios greater than 6. Group 1 phenocryst rims likely grew from a liquid similar in composition to the measured groundmass glass, but most of the Group 2 rims and microlites likely grew in a liquid that was significantly more mafic. The liquid that produced the Group 2 phenocrysts may also have had higher dissolved H_2O, but given the range of measured glass Ca/Na ratios, melt H_2O concentrations would have to be unreasonably high (>8 wt. %) to account for the full range of Group 2 phenocryst and microlite Ca/Na ratios, and therefore differences in composition of the crystallizing liquid would also be necessary to produce the observed compositions.

Bulk-rock chemical trends indicate that compositional variations at Kasatochi were the product of pre-eruptive two-component magma mixing (Fig. 3-1; discussed in depth in Chapter 2). This mixing did not involve the 2008 Kasatochi andesite, which lies well away from bulk compositional trends defined by the basaltic andesite (Fig. 3-1). Instead, the high-Si component was likely a medium-to-high SiO_2 basaltic andesite or low-Si andesite, similar to or more silicic than the more felsic basaltic andesite samples (>55 wt. % SiO_2; Fig. 3-1), while the more mafic component was likely basaltic, similar to or more mafic than the lowest-Si basaltic andesite compositions (<53 wt. % SiO_2; Fig. 3-1). These two components are referred to henceforth as the felsic end member and the mafic end member, respectively. The disparate plagioclase phenocryst populations reflect the compositional disparity between the two components in this mixing relationship, with the Group 1 phenocrysts (having grown in more felsic liquids) being inherited from the felsic end member and Group 2 phenocrysts from the more mafic end member.

The comparably high An contents of plagioclase microlites and Group 2 plagioclase phenocrysts suggests that at least a large portion of plagioclase microlites in the 2008 Kasatochi basaltic andesite crystallized from the same magma as the Group 2 phenocrysts (Fig. 3-2). The high FeO and MgO contents, which increase with decreasing An content of both microlites and Group 2 rims relative to Group 1 rims (Fig. 3-5), and the disequilibrium between microlites and measured groundmass glass compositions (Fig. 3-9) support this inference. However, a small portion of microlites contain low FeO and MgO contents even at An contents $<An_{70}$ (Fig. 3-5). This distinction is even more obvious in the FeO/MgO ratios of plagioclase phenocryst rims and microlites, which generally decrease with An content, but also fall along two separate trends, with most Group 1 rims having higher FeO/MgO ratios than Group 2 phenocrysts at a given An content (Fig. 3-10). Microlite FeO/MgO ratios generally fall to low FeO/MgO as An decreases, consistent with their formation in a similar environment to Group 2 phenocryst rims, but a few microlites have FeO/MgO ratios similar to or even higher than Group 1 phenocrysts (Fig. 3-10), and they appear to create a second, high FeO/MgO trend with increasing An content that lies above the lower FeO/MgO trend. Therefore, Group 2 plagioclase phenocrysts and most microlites in the 2008 Kasatochi basaltic andesite were inherited from the more mafic mixing end member, while Group 1 phenocrysts, along with a few microlites, were likely inherited from the felsic end member.

3.6.2: Mafic Phenocrysts Inherited from Mixing End Members

If pre-eruptive mixing was responsible for the bulk compositional trends (Fig. 3-1), high-An plagioclase microlites and the presence of multiple plagioclase phenocryst populations, the compositions of the mafic phenocryst populations may also be expected to also reflect this mixing, as the overall phenocryst population of the basaltic andesite will reflect the contribution of pre-existing mafic phenocrysts from the mafic and felsic end members described in the previous section (e.g., Izbekov et al., 2004). The compositions of the high-Ti titanomagnetite closely match titanomagnetite compositions of the 2008 Kasatochi andesite, while the low-Al amphibole compositions also overlap with amphibole compositions from the andesite (Fig. 3-7). These correlations suggest that the high-Ti titanomagnetite and low-Al amphibole grew in P-T-X conditions similar to those of the 2008 Kasatochi andesite, which would more likely be found in the felsic end member than the mafic. Furthermore, the contrasting compositions of the mafic phenocryst populations may help illuminate relative differences in temperature between the felsic and mafic end members. In the absence of coexisting rhombohedral Fe-Ti oxides, temperatures recorded by the two titanomagnetite compositional populations cannot be determined quantitatively. However, if the andesite was indeed colder than the basaltic andesite, as suggested in Chapter 2, and compositions of the low-Al amphibole and the high-Ti magnetite compositions match those of the andesite, then it seems likely that the low-Al amphibole and the high-Ti magnetite formed in a magma that was colder, meaning that the felsic end member was colder than the mafic end member.

Although amphibole is abundant in the 2008 Kasatochi eruptive products, current amphibole-based thermobarometers are not applicable to the Kasatochi basaltic andesite. Models based on amphibole aluminum contents (e.g. Hammarstrom and Zen, 1986; Johnson and Rutherford, 1989; Anderson and Smith, 1995) or plagioclase-amphibole equilibria (e.g. Holland and Blundy, 1994) cannot be used, as the Kasatochi system is not saturated in quartz or biotite, as is required by such models. Also, while new models based solely on amphibole compostions continue to grow in popularity (Ridolfi et al., 2010; Ridolfi and Renzulli, 2012), they are applicable only to calc-alkaline systems and are specifically contraindicated for use in theoleiitic systems such as the 2008 Kasatochi basaltic andesite (Fig. 3-1). However, amphibole compositions can still be examined in a semi-quantitative way to help to illuminate the relative temperature conditions of their formation, as their compositions will still be partially dependent on the temperature-sensitive substitution reactions that have been defined previously (Hammarstrom and Zen, 1986; Johnson and Rutherford, 1989; Blundy and Holland, 1990; Schmidt, 1992; Holland and Blundy, 1994; Anderson and Smith, 1995; Anderson, 1996; Bachmann and Dungan, 2002; Anderson et al., 2008). In general, decreasing temperature will lower the A-site alkali content and decrease the tetrahedral site occupancy of aluminum (in favor of silica) in an amphibole through the edenite exchange reaction, defined below:

$$^{IV}Si + {}^{A}[\text{Empty Site}] = {}^{IV}Al + {}^{A}(Na + K) \qquad \text{(Eq. 3-1)}$$

Decreasing temperature will also lower amphibole calcium and tetrahedral aluminum contents with a simultaneous increase in silica and octahedrally coordinated sodium

through what Bachmann and Dungan (2002) termed the "plagioclase exchange" reaction, defined as:

$$^{IV}Si + {}^{M4}Na = {}^{IV}Al + {}^{M4}Ca \qquad \text{(Eq. 3-2)}$$

Consistent with the influence of these reactions, the amphiboles from the 2008 Kasatochi basaltic andesite show positive correlations between tetrahedral aluminum and both Ca and A-site alkali contents (Fig. 3-8). These positive correlations suggests that the low-Al amphibole group formed under cooler conditions than the high-Al group (cf. Fig. 5 of Bachmann and Dungan, 2002, and associated discussion). This, in turn, further strengthens the inference that the low-Al amphibole group is likely associated with the lower temperature magma that produced the Group 1 plagioclase phenocrysts, while the high-Al amphibole group is likely associated with Group 2 plagioclase phenocrysts and the majority of plagioclase microlites, hosted within higher temperature magma. The 2008 Kasatochi basaltic andesite phase assemblage is therefore comprised of two separate phenocryst populations, each being contributed by their respective mixing end member.

3.6.3: Temperature Constraints on Mixing End Members

The compositions of the mafic phenocrysts provide constraints only on the relative temperature differences between the felsic and mafic mixing end members of the 2008 Kasatochi basaltic andesite. Absolute temperature constraints may be partially

determined using the plagioclase-liquid hygrometer/thermometer of Lange et al. (2009), which can be applied to estimate temperatures of plagioclase crystallization from a melt of know composition and dissolved H_2O concentration. Ion microprobe measurements of volatile contents in melt inclusions from the basaltic andesite yield H_2O contents of ~5-7 wt. % (Izbekov et al., 2009; see also Chapter 2). Group 2 phenocrysts and microlites are not in equilibrium with the groundmass glass (Fig. 3-9), and, in the absence of constraints on the composition of liquid in equilibrium with these crystals, the Lange model cannot be applied. The Group 1 phenocrysts, however, are in equilibrium with groundmass glass compositions, and therefore the Lange et al. (2009) hygrometer can be used to determine pre-eruptive magmatic temperatures for the felsic mixing end member containing the Group 1 phenocrysts. The most primitive and most evolved measured compositions of groundmass glass are used as proxies for the most primitive and most evolved crystallizing liquid from which Group 1 plagioclase phenocrysts could reasonably be expected to grow. A comparison of natural plagioclase compositions with those predicted by the Lange et al. (2009) hygrometer reveals that the range of measured An contents of Group 1 phenocryst rims agree with predicted compositions at temperatures between 800 and 950 °C (Fig. 3-11), a plausible (albeit wide) range of pre-eruptive magmatic temperatures for the felsic mixing end member.

Without constraints on equilibrium liquid composition, such a method for estimating temperature for the mafic end member based on Group 2 phenocrysts is inappropriate. However, if the mafic end member was hotter than the felsic as the mafic phenocryst populations indicate (see Section 3.6.2), the lower temperature boundaries of

the mafic end member are constrained by the upper boundaries of the felsic end member to ~900° C. Furthermore, no amphibole phenocrysts from the 2008 Kasatochi basaltic andesite display reaction rims, oxidation, opacitization or any other disequilibrium textures, indicating that magmatic temperatures never exceeded those at which amphibole is stable. Therefore the upper temperature limits of amphibole stability in magmas similar to the mafic end member may used to constrain maximum magmatic temperatures of the mafic mixing end member.

Previous experimental phase equilibria studies of Volcan Colima in Mexico and Westdahl Volcano in the central Aleutian islands, basaltic andesite systems similar to Kasatochi, suggest that amphibole would not be stable at pressures up to 300 MPa, or at temperatures much in excess of 1000° C (Moore and Carmichael, 1998; Rader, 2010). Furthermore, the experiments of Gaetani et al. (1994) on basaltic andesite from the central Lau basin did not find amphibole at temperatures >1000° C at pressures up to 200 MPa, and the experiments of Pichavant et al. (2002) on basaltic andesite from Mount Pelée did not find amphibole at temperatures >1000° C at 400 MPa. Experiments on more mafic compositions produce amphibole at slightly higher temperatures, but not exceeding 1050° C at pressures up to 300 MPa (Barclay and Carmichael, 2004; Nicholis and Rutherford, 2004). It seems unlikely that pristine amphibole crystals such as those found in the 2008 Kasatochi basaltic andesite could exist at temperatures exceeding 1050 °C, and therefore 1050°C is taken as the upper limit for plausible magmatic temperatures for the mafic end member.

3.7: Origins of High-An Plagioclase Microlites

3.7.1: Latent Heat Release Leads to More Calcic Microlites?

Crystallization of groundmass microlites is an exothermic process which has been shown to raise the temperatures of ascending magmas by up to 100 °C (e.g. Couch et al., 2003; Blundy et al., 2006; Hale et al., 2007; Pallister et al., 2008) and as such could cause the compositions of crystallizing plagioclase to become more anorthitic due to latent heat released during ascent-driven groundmass crystallization raising magmatic temperatures. Latent heat release must therefore be considered as a possible mechanism for the formation of high-An microlite crystallization in the 2008 Kasatochi basaltic andesite. The maximum latent heat released by plagioclase microlite crystallization can be estimated from the thermodynamic properties of the anorthite and albite end members by the relationship:

$$L = \frac{\Delta H_m}{C_p} \qquad \text{(Eq. 3-3)}$$

where ΔH_m is the enthalpy of melting of the plagioclase, C_p is the plagioclase heat capacity and L is change in temperature due to latent heat release (cf. Couch et al., 2003; Pallister et al., 2008).

The ΔH_m for pure albite and pure anorthite are 59280 J mol^{-1} and 81000 J mol^{-1}, respectively (Robie et al., 1978), while C_p (in J mol^{-1} K^{-1}) can be estimated for anorthite and albite as a function of temperature (T, in degrees K) using the following equations from Berman (1988):

$$C_P^{An} = 439.37 - 3734.1T^{-0.5} + (0.31702 * 10^9)T^{-3} \quad \text{(Eq. 3-4)}$$

$$C_P^{Ab} = 393.64 - 2415.5T^{-0.5} - (7.8928 * 10^6)T^{-2} + (1.07064 * 10^9)T^{-3} \quad \text{(Eq. 3-5)}$$

While Eq. 3-3 provides only an estimate of the maximum temperature change due to latent heating, L can be determined as a function of plagioclase An content at different groundmass crystallinities. Depending on the amount of groundmass crystallization, the maximum change in temperature due to the formation of high-An plagioclase microlites would not exceed ~25 °C and could be as low as ~10 °C (Fig. 3-12), unlike in other systems where more albitic plagioclase is crystallizing and heat release is more extreme (cf. Couch et al., 2003; Pallister et al., 2008). Even a latent heat release of 25 °C would increase equilibrium An contents by only as much as ~10 mol. %, depending on T and magmatic H_2O (Fig. 3-11), which is insufficient to cause the discrepancies in An content between the modal compositions of the microlites and Group 1 phenocrysts. Furthermore, adiabatic cooling due to degassing and vapor bubble expansion during magmatic ascent can also counteract the effects of latent heat release (e.g. Sparks and Pinkerton, 1978; Sahagian and Proussevitch, 1996; Zhang, 1999; Mastin and Ghiorso, 2001). To summarize, while it is significant in other volcanic systems, latent heat released by groundmass crystallization was likely negligible in the 2008 Kasatochi basaltic andesite and was probably not a significant factor in the formation of the high-An microlites.

3.7.2: Mixing-Induced Microlite Crystallization

When two magmas mix, the thermal contrast between the two mixing end members can lead to cooling within the hotter magma, leading to high effective undercoolings, which in turn cause a shift from a crystallization regime dominated by growth on pre-existing phenocrysts to a regime dominated by the nucleation and growth of microlites (e.g. Westrich et al., 1988; Geschwind and Rutherford, 1995; Hammer and Rutherford, 2002; Martel and Schmidt, 2003; McCanta et al., 2007; Brugger and Hammer, 2010). This has been the basis for previous models for the formation of anomalously high-An microlites in other volcanic systems, with the difference in temperature between end members during magma mixing responsible for the nucleation of high-An microlites in the hotter, more mafic of the two end members. At Soufriere Hills, the convective rise of hotter, andesitic material brought it into contact with cooler, more silicic dacite, causing nucleation of microlites in the andesite (Couch et al., 2003). At Mount Pelée, the mixing of newly injected basalt with cooler andesite caused the basalt to cool and nucleate high-An microlites (Martel et al., 2006). In both cases, the microlites that grew in the mafic magma were to anorthitic too be in equilibrium with the groundmass melts of the hybridized magmas that were eventually erupted.

A similar mechanism seems likely to have operated at Kasatochi. When the hot, mafic magma containing the Group 2 phenocrysts came into contact with cooler, more silicic magma containing the Group 1 phenocrysts, the difference in temperature between the two would have induced cooling within the mafic end member and could have driven

a burst of nucleation of plagioclase microlites, crystallizing from the same high-Ca liquid from which the Group 2 phenocrysts had previously been growing. The rapid growth of microlites and the progressive assimilation of the more silicic material would then both cool the magma further and drive melt evolution to less calcic compositions, which would in turn drive microlite compositions to more albitic compositions as the liquid becomes more sodic. This would lead to the formation of both new, more sodic microlites and more sodic rims on large microlites and Group 2 phenocrysts. Syn-eruptive crystallization due to decompression and degassing would further promote the growth of more sodic compositions (e.g. Brugger and Hammer, 2010).

3.7.3: Minor and Trace Element Variations in Phenocryst Rims and Microlites

The equilibrium plagioclase-liquid partition coefficient (K_D) for Mg is essentially constant regardless of plagioclase compositions or magmatic intensive properties (Longhi et al., 1976; Sato, 1989; Phinney, 1992; Bindeman et al., 1998; Aigner-Torres et al., 2007), and therefore the negative relationship between An and MgO contents in microlites and Group 2 phenocryst rims and the sharp increases in MgO at the rims of Group 2 phenocrysts are not a direct result of mixing-induced cooling alone. While mixing between the felsic and mafic end members could increase plagioclase MgO concentrations by increasing the abundance of MgO in the crystallizing liquid, it is unlikely that this alone could lead to the elevated MgO concentrations seen in Kasatochi microlites and Group 2 phenocryst rims. To produce the negative correlation between An

and MgO, the post-mixing liquid would have to be both more magnesian and less calcic, a scenario inconsistent with both bulk rock and groundmass glass compositional trends (Figs. 3-1, 3-6).

A more plausible scenario can be found in the model suggested by the seminal paper of Bottinga et al. (1966), whereby rapid growth rates create a boundry layer of melt around the crystal, which will become progressively more depleted in compatible elements (such as Ca), which are taken up by the plagioclase, and enriched incompatible elements rejected by the growing crystal such as Fe and Mg. As rapid, high-undercooling crystallization progresses and the crystal grows, these boundary layers will become more and more depleted in Ca and enriched in Fe and Mg. This model has been previously invoked to explain rimward increases in FeO and MgO contents and decreases in An content in plagioclase phenocrysts from Parinacota Volcano in Chile by Ginibre et al. (2002). Similar to the scenario described at Parinacota, the inverse correlation between An content and FeO and MgO in the Group 2 phenocryst rims and microlites in the 2008 Kasatochi basaltic andesite (Figs. 3-2, 3-5), as well as the zonation observed in some larger microlites (Fig. 3-4), are probably products of this boundry layer effect, reflecting these relative changes in Ca, Fe and Mg activity in the melt boundry layers surrounding these crystals. As both high-An microlites and Group 2 phenocrysts have these rims (Figs. 3-2, 3-4), it seems likely that these rims formed primarily in response to the high undercoolings created by syneruptive decompression and degassing after the initial mixing event that led to the formation of the high-An microlites.

Unlike Mg, the K_D for Fe is expected to depend strongly on magmatic oxygen fugacity (fO_2) and temperature (Longhi et al., 1976; Sato, 1989; Phinney, 1992; Wilke and Behrens, 1999; Sugawara, 2001; Lundgaard and Tegner, 2004; Aigner-Torres et al., 2007). Iron K_D's for plagioclase will increase sharply with increasing fO_2. It will, however, decrease with increasing temperature, an effect that is negligible at reducing conditions (where all available Fe is Fe^{2+}) but significant at more oxidizing conditions where Fe^{3+} is available. While dependences of Fe partitioning into plagioclase on An content have been documented (Bindeman et al., 1998), such a correlation does not appear consistently in the Kasatochi basaltic andesite plagioclase. An content is dependent on temperature and more strongly on p_{H2O}, the partial pressure of H_2O in the system (e.g. Lange et al, 2009). Since p_{H2O} exerts a partial control on fO_2, correlated variations between plagioclase An and Fe concentrations more likely result from both An content and Fe partitioning changing simultaneously in response to a change in T, fO_2 and/or p_{H2O}, rather than Fe partitioning changing in repsonse to flucations in An content.

This distinction is especially germane to the Kasatochi system, in which plagioclase Fe contents do not consistently depend on An content, as shown by the uniformly low FeO contents of Group 1 phenocrysts cores. Even the $>An_{80}$ cores and spikes in An content common in Group 1 plagioclase, which were also created by influx of matrix material (see Chapter 2), are not correlated with statistically significant positive or negative changes in FeO or MgO (Figs. 3-2, 3-5). This suggests that while previous influxes of mafic material were different enough in composition to cause dissolution and re-growth on top of the dissolution surfaces, the magnitudes of these forcings were

insufficient to cause significant changes in Fe partitioning or to induce the rapid growth rates necessary for the formation of the boundary layers as described above.

Interestingly, despite microlite and Group 2 phenocryst rim FeO and MgO contents increasing with decreasing An contents, FeO/MgO ratios actually *decrease* slightly as microlites become more sodic (Fig. 3-10), suggesting that the Fe K_D decreased in response to either a decrease in fO_2 or an increase in temperature. An increase in temperature seems unlikely, given that latent heat release is negligible (Fig. 3-11) and that the mafic end member, the source of most of the microlites and the Group 2 phenocrysts, would cool down, rather than heat up, during mixing. A decrease in fO_2 is more realistic and could have been induced if the felsic end member was stored under more reducing conditions than the mafic. Also, Kasatochi was the largest point source release of SO_2 since the 1991 eruptions of Pinatubo in the Phillipines and Cerro Hudson in Chile, and several studies have shown that the decompression and degassing of H_2O and S-rich systems may cause decreases in fO_2 of >1 log unit due to changes in liquid-vapor redox equilibria (Burgisser and Scaillet, 2007; Burgisser et al., 2008).

3.8: Summary

Basaltic andesite from the 2008 eruption of Kasatochi Volcano displays significant heterogeneity in bulk composition, which has been interpreted as being the

result of magma mixing just prior to eruption. Compositions of plagioclase phenocrysts, mafic phenocrysts and plagioclase microlites support this inference, suggesting that the phenocryst population of the 2008 Kasatochi basaltic andesite is derived from two different sources. Group 1 plagioclase phenocrysts, which are oscillatory zoned and have relatively sodic rims (An_{55-65}), likely crystallized in the silicic mixing end member at temperatures of 800-950 °C, along with low-Al amphibole and high-Ti titanomagnetite phenocrysts. Group 2 plagioclase phenocrysts, which are dominantly >An_{80} and texturally and compositionally homogenous except for abrupt shifts to more sodic compositions <30 μm from their rims, likely crystallized in the mafic end member at higher temperatures (900-1000 °C), along with high-Al amphibole and low-Ti titanomagnetite phenocrysts.

Microlites in the 2008 Kasatochi basaltic andesite are highly calcic, with compositions similar to Group 2 phenocryst rims and out of equilibrium with measured groundmass glass compositions. The undercooling imposed on the mafic magma due to contact with the silicic magma likely triggered a burst of plagioclase microlite nucleation in the mafic magma, leading to the growth of high-An microlites. As the magma crystallized and more silicic material was entrained, microlites became more sodic and thin sodic rims formed on the exteriors of Group 2 phenocrysts. The high effective undercoolings created by the mixing were exacerbated by decompression-induced degassing, causing the formation of boundary layers rich in incompatible elements (e.g., Fe, Mg) and depleted in compatible elements (e.g., Ca) around microlites and Group 2

phenocrysts, leading to the formation of more sodic rims on Group 2 phenocrysts and leading to higher Fe and Mg concentrations in more sodic microlites and Group 2 rims.

3.9: Acknowledgments

This manuscript benefited greatly from insightful discussions with C. Cameron, J. Pallister, K. Putirka, K. Severin and K. Spaleta. The authors also thank the interdisciplinary team studying ecosystem response to the eruption of Kasatochi for their assistance in the field, J. Williams and the U.S. Fish and Wildlife Service for coordinating trips to Kasatochi, and the crew of the M/V *Tiĝlax̂* for providing safe passage to and from the island. Fieldwork for this study was supported by the U.S. Fish and Wildlife Service and by the North Pacific Research Board Project #923. Analytical work was supported by the American Recovery and Reinvestment Act, by the UAF Advanced Instrumentation Laboratory, by a Jack Kleinman Grant for Volcano Research from the Community Foundation of Southwest Washington, and by the United States Geological Survey Volcano Hazards Program through the Alaska Volcano Observatory, a cooperative program of the University of Alaska Fairbanks, the Alaska Department of Geological and Geophysical Surveys, and the USGS.

3.10: Figures

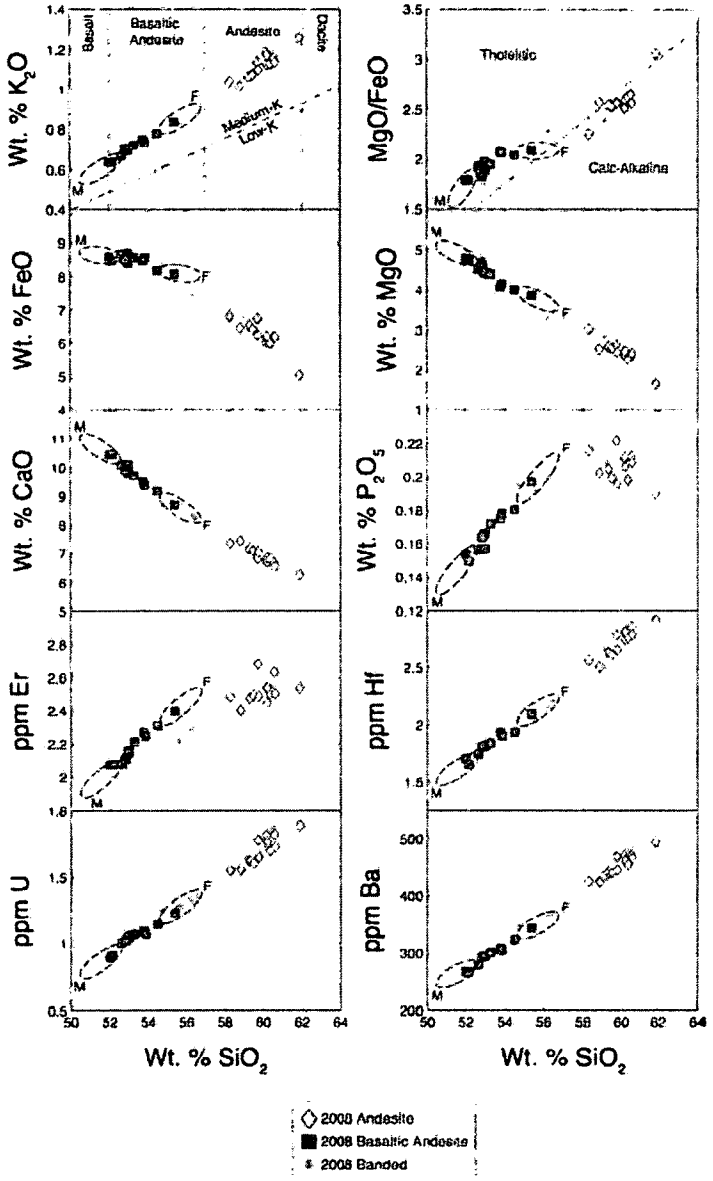

Figure 3-1: Bulk Compositions. Bulk major oxide, minor oxide and trace element vs. SiO_2 diagrams for eruptive products of the 2008 eruption of Kasatochi. Data from Appendix 2-2. SiO_2 vs. K_2O classification diagram after Le Bas et al. (1986), with low-K/medium-K boundary from Gill (1981). SiO_2 vs. MgO/FeO classification diagram after Miyashiro (1974). Dashed fields represent schematic end member compositions for pre-eruptive basaltic andesite mixing trends (see Section 3.6.1), with fields labeled "M" representing the mafic end member and "F" representing the felsic end member.

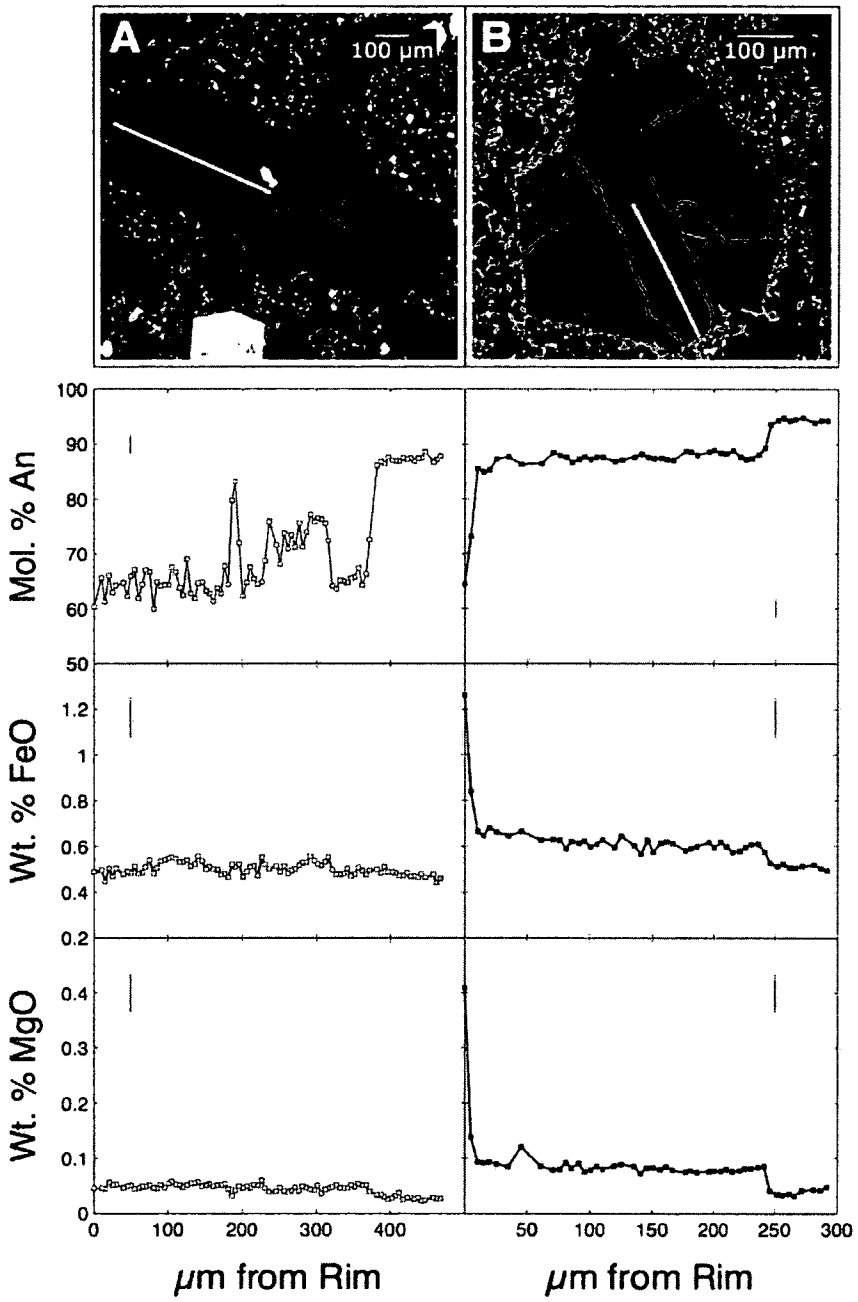

Figure 3-2: Representative Electron Microprobe Transects of Plagioclase Phenocrysts. Backscatter electron images and core-rim compositional profiles of representative (A) Group 1 and (B) Group 2 plagioclase phenocrysts from the 2008 Kasatochi basaltic andesite. Error bars indicate analytical uncertainty (2 standard deviations) calculated from repeated measurements of the Lake County, Oregon, Labradorite plagioclase standard (USNM 115900; Jarosewich, 2002). Transects were measured using the "Trace" analytical routine (see text). Data in Appendix 3-8.

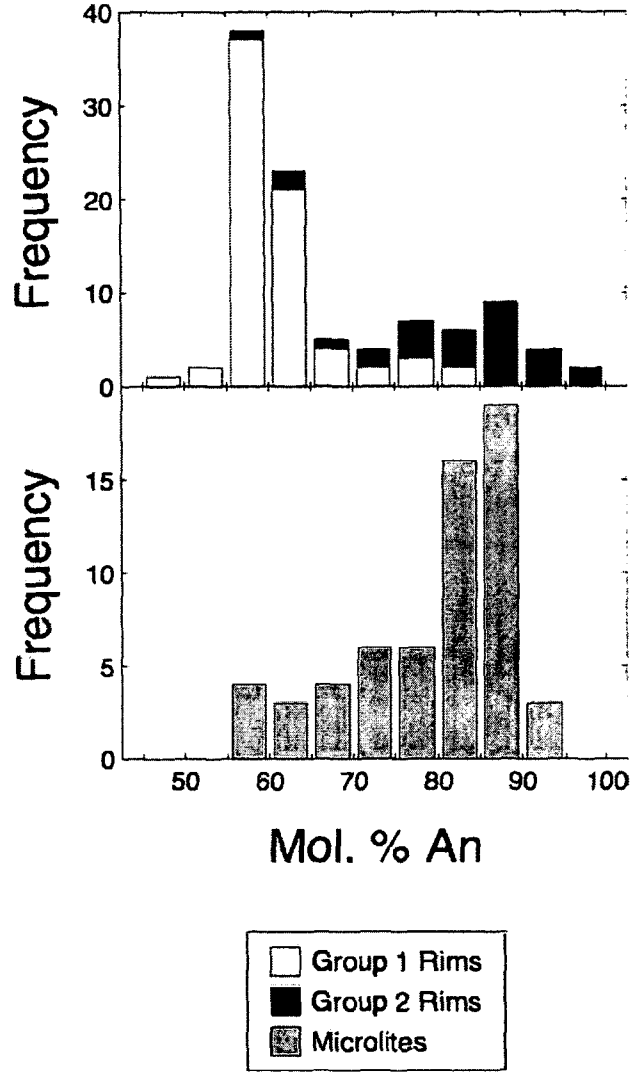

Figure 3-3: Plagioclase Phenocryst and Microlite Compositions. Histogram of An contents for Group 1 and Group 2 plagioclase phenocryst rims (top) and plagioclase microlites (bottom) from the 2008 Kasatochi basaltic andesite. Individual analyses reported in Appendix 3-3 (phenocryst rims) and Appendix 3-4 (microlites).

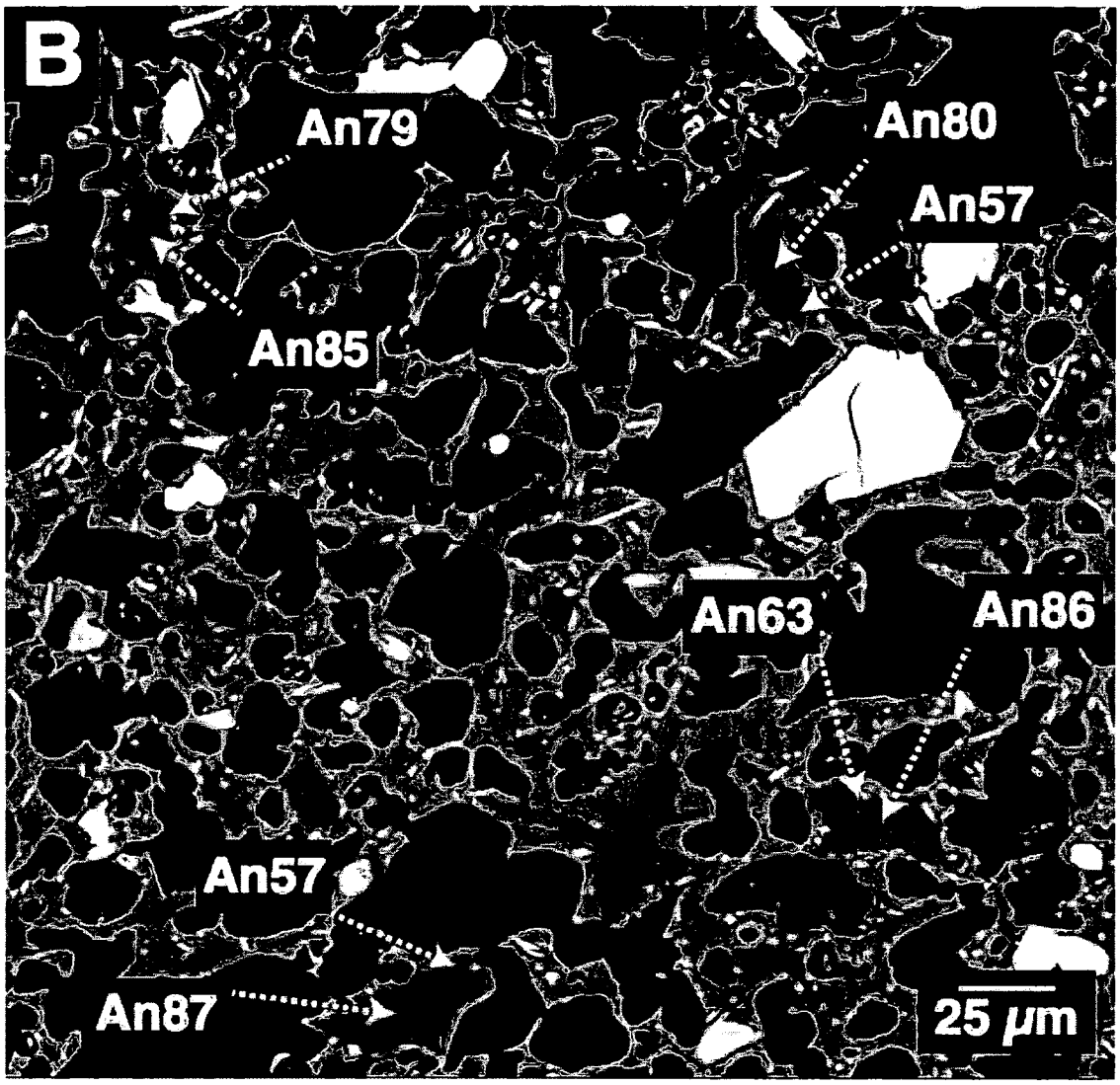

Figure 3-4: Backscatter Electron Image of Zoned Plagioclase Microlites. Microlites display high-An cores and lower-An rims.

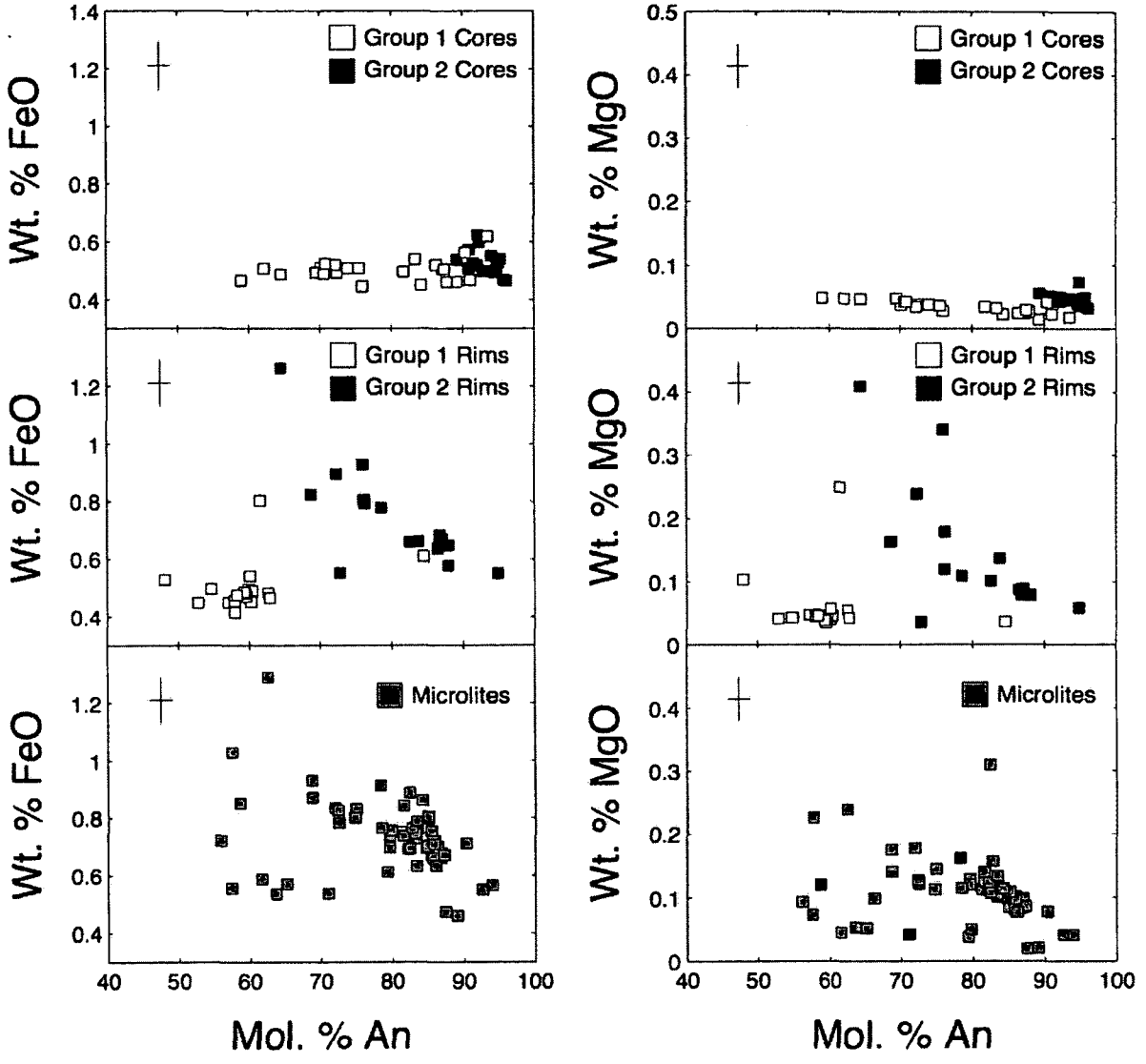

Figure 3-5: Plagioclase Iron and Magnesium Concentrations. FeO and MgO contents, plotted as a function of An content, of Group 1 and Group 2 plagioclase phenocryst cores (top), rims (middle) and microlites (bottom) from the 2008 Kasatochi basaltic andesite. Error bars indicate analytical uncertainty (2 standard deviations) calculated from repeated measurements of the Lake County, Oregon, Labradorite plagioclase standard (USNM 115900; Jarosewich, 2002). FeO and MgO were measured using the "Trace" analytical routine (see text). Individual analyses reported in Appendix 3-2 (phenocryst cores), Appendix 3-3 (phenocryst rims), and Appendix 3-4 (microlites).

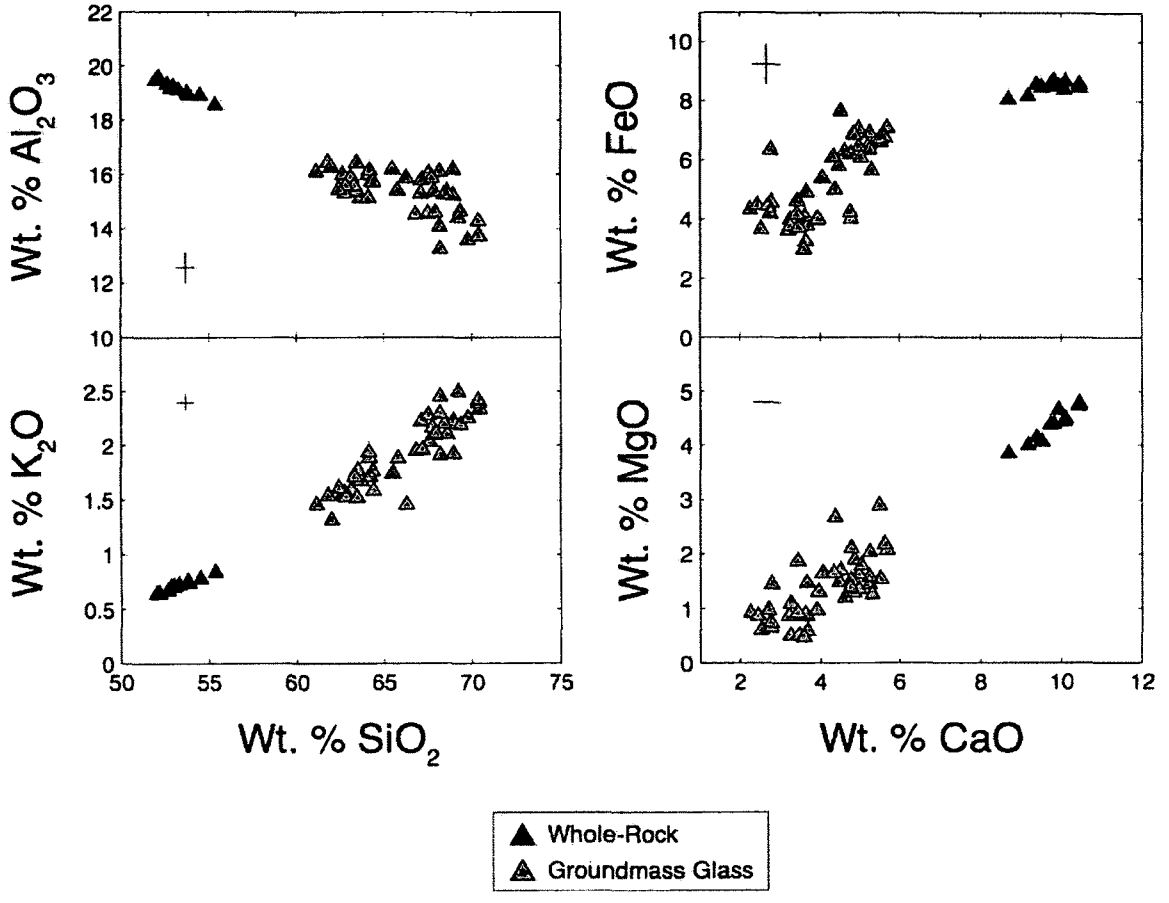

Figure 3-6: Groundmass Glass Compositions. Error bars indicate analytical uncertainty (2 standard deviations) calculated from repeated measurements of the VG-568 Yellowstone Rhyolite glass standard (USNM 72854; Jarosewich, 2002). Whole rock analyses included for comparison. Error bars refer only to groundmass glass measurements; analytical uncertainty of bulk compositional analyses and MgO analyses of groundmass glass are smaller than the size of the symbols. Individual analyses reported in Appendix 3-5.

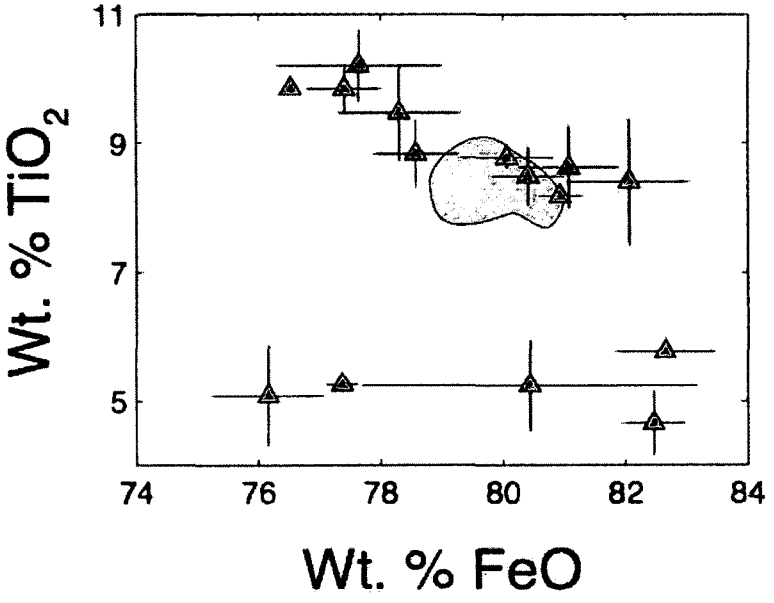

Figure 3-7: Titanomagnetite Phenocryst Compositions. Points represent the average composition of several analyses of an individual phenocryst, with error bars representing the variation (2 standard deviations) of each averaged analysis. Grey field represents the range of titanomagnetite compositions from the 2008 Kasatochi andesite, reported in Chapter 2 (Appendix 2-7). Individual analyses reported in Appendix 3-6.

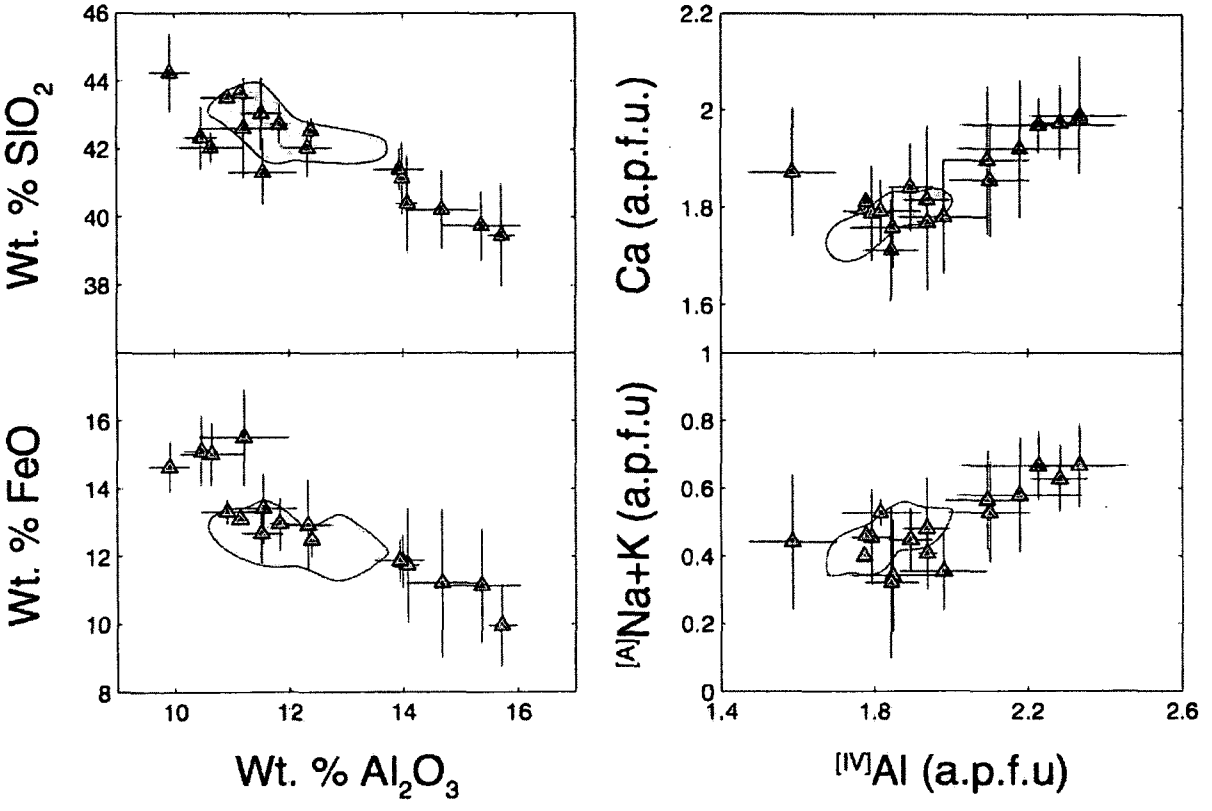

Figure 3-8: Amphibole Phenocryst Compositions. Structural formulae are reported in atoms per formula unit (a.p.f.u.), calculated using ProbeAmph (Tindle and Webb, 1994). $^{[A]}$Na+K refers to the total number of atoms of Na and K in the amphibole A-site, while $^{[IV]}$Al refers to the amount of tetrahedrally-coordinated aluminum atoms. Points represent the average composition of several analyses of an individual phenocryst, with error bars representing the variation (2 standard deviations) of each averaged analysis. Grey field represents the range of amphibole compositions from the 2008 Kasatochi andesite, reported in Chapter 2 (Appendix 2-8). Individual analyses reported in Appendix 3-7.

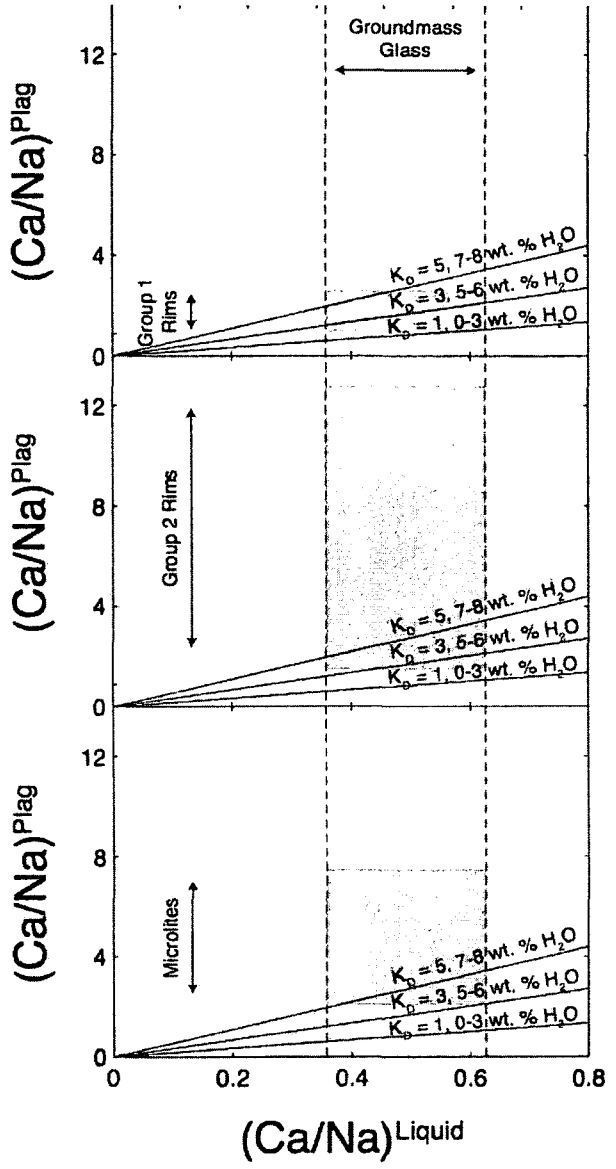

Figure 3-9: Plagoclase Ca/Na Ratios. Ca/Na molar ratios of Group 1 plagioclase phenocryst rims (top), Group 2 plagioclase phenocryst rims (middle) and plagioclase microlites (bottom) from the 2008 Kasatochi basaltic andesite, compared to Ca/Na of measured groundmass glass compositions. Grey fields represent measured compositions (average, ±1 standard deviation) of the given plagioclase population. Vertical dashed field represents measured groundmass glass compositions (average, ±1 standard deviation). Lines represent equilibrium plagioclase-liquid Ca/Na distribution coefficients at different magmatic H_2O concentrations (after Fig. 4 of Martel et al., 2006, and references therein).

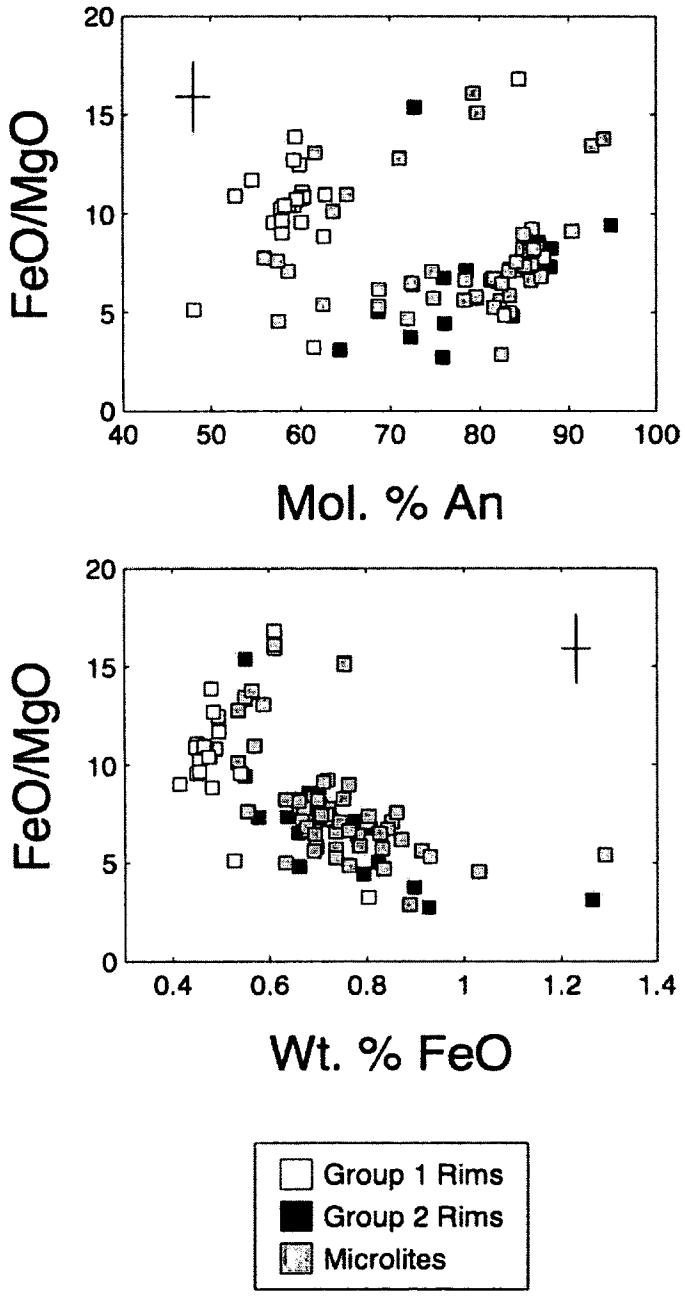

Figure 3-10: Plagioclase FeO/MgO Ratios. FeO/MgO of plagioclase phenocryst rims and microlites, plotted as a function of An content (top) and Fe content (bottom) from the 2008 Kasatochi basaltic andesite. All iron is reported as FeO. Error bars indicate analytical uncertainty (2 standard deviations) calculated from repeated measurements of the Lake County, Oregon, Labradorite plagioclase standard (USNM 115900; Jarosewich, 2002). FeO and MgO were measured using the "Trace" analytical routine (see text).

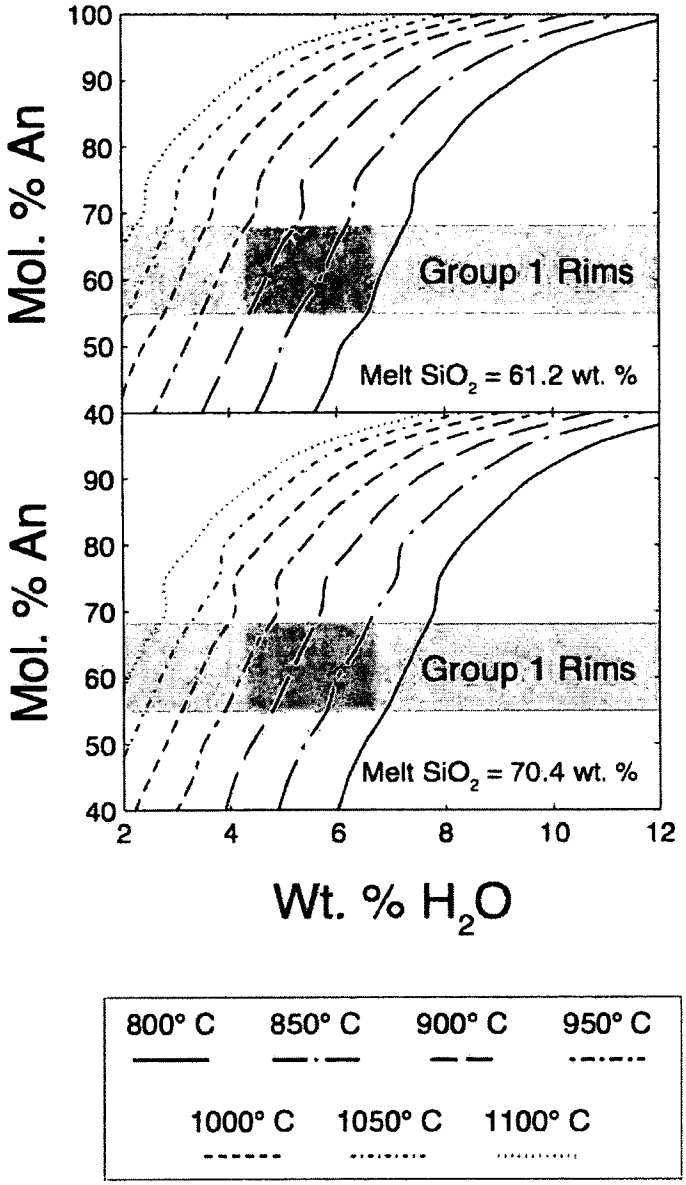

Figure 3-11: Plagioclase-Liquid Hygrometry. Natural compositions of Group 1 phenocryst rims compared with compositions predicted by the plagioclase-liquid hygrometer of Lange et al. (2009). Compositions based on plagioclase crystallizing from liquids with compositions of the most mafic (top) and most felsic (bottom) groundmass glass composition measured in the basaltic andesite. Lines show compositions predicted by the Lange et al. (2009) hygrometer, as a function of melt H_2O content, crystallizing at temperatures indicated. Vertical grey fields represent range of natural pre-eruptive melt H_2O compositions (average, ±1 standard deviation; Izbekov et al., 2009; P.E. Izbekov, *unpub. data*). Horizontal fields represent measured An contents of Group 1 phenocrysts (average, ±1 standard deviation).

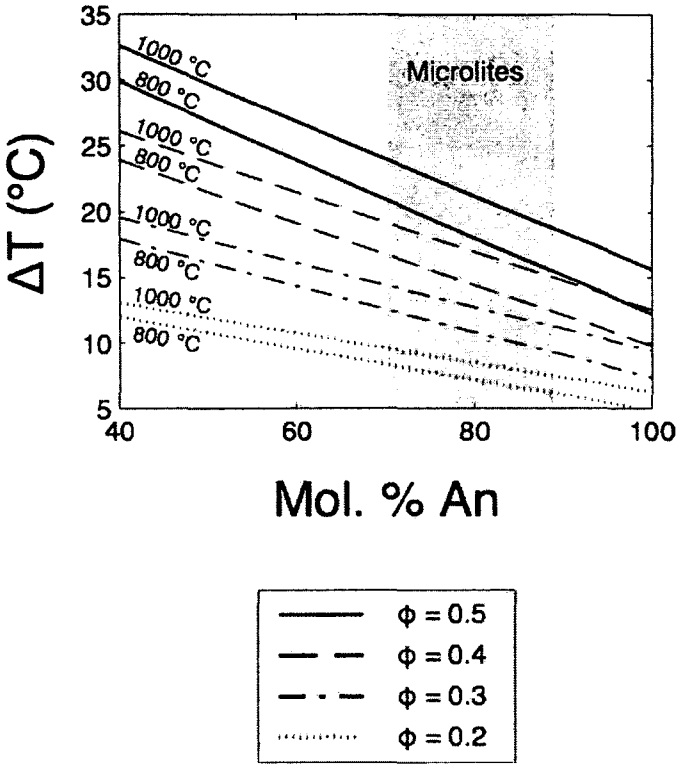

Figure 3-12: Predicted Latent Heat Release from Microlite Crystallization. Modeled increases in magmatic temperature due to latent heat released by crystallization of plagioclase, as a function of the composition of the crystallizing plagioclase. See text for full description of calculations. Latent heat is calculated for a range of groundmass crystal fractions (ϕ). Vertical grey fields represent the range of natural plagioclase microlite compositions (average, ±1 standard deviation).

3.12: References

Aigner-Torres, M., Blundy, J., Ulmer, P. and Pettke, T., 2007. Laser-ablation ICP-MS study of trace element partitioning between plagioclase and basaltic melts: an experimental approach. Contrib Mineral Petr, 153(6): 647-667. doi: 10.1007/s00410-006-0168-2

Anderson, J.L., 1996. Status of thermobarometry in granitic batholiths. T Roy Soc Edin-Earth, 87: 125-138.

Anderson, J.L. and Smith, D.R., 1995. The effects of temperature and fO_2 on the al-in-hornblende barometer. Am Mineral, 80(5-6): 549-559.

Anderson, J.L., Barth, A.P., Wooden, J.L. and Mazdab, F., 2008. Thermometers and thermobarometers in granitic systems. Rev Mineral Geochem, 69: 121-142. doi: Doi 10.2138/Rmg.2008.69.4

Arnoult, K.M., Olson, J.V., Szuberla, C.A.L., McNutt, S.R., Garces, M.A., Fee, D. and Hedlin, M.A.H., 2010. Infrasound observations of the 2008 explosive eruptions of Okmok and Kasatochi volcanoes, Alaska. J Geophys Res-Atmos, 115: D00L15. doi: 10.1029/2010jd013987

Barclay, J. and Carmichael, I.S.E., 2004. A hornblende basalt from western Mexico: Water-saturated phase relations constrain a pressure-temperature window of eruptibility. J Petrol, 45(3): 485-506. doi: Doi 10.1093/Petrology/Egg091

Bachmann, O. and Dungan, M.A., 2002. Temperature-induced Al-zoning in hornblendes of the Fish Canyon magma, Colorado. Am Mineral, 87(8-9): 1062-1076.

Berman, R.G., 1988. Internally-consistent thermodynamic data for minerals in the system Na_2O-K_2O-CaO-MgO-FeO-Fe_2O_3-Al_2O_3-SiO_2-TiO_2-H_2O-CO_2. J Petrol, 29(2): 445-522. doi: 10.1093/petrology/29.2.445

Bindeman, I.N., Davis, A.M. and Drake, M.J., 1998. Ion microprobe study of plagioclase-basalt partition experiments at natural concentration levels of trace elements. Geochim Cosmochim Acta, 62(7): 1175-1193.

Blundy, J. and Cashman, K., 2001. Ascent-driven crystallisation of dacite magmas at Mount St Helens, 1980-1986. Contrib Mineral Petr, 140(6): 631-650.

Blundy, J., Cashman, K. and Humphreys, M., 2006. Magma heating by decompression-driven crystallization beneath andesite volcanoes. Nature, 443(7107): 76-80. doi: Doi 10.1038/Nature05100

Blundy, J.D. and Holland, T.J.B., 1990. Calcic amphibole equilibria and a new amphibole-plagioclase geothermomemeter. Contrib Mineral Petr, 104(2): 208-224.

Bottinga Y., Kudo A., and Weill D., 1966. Some observations on oscillatory zoning and crystallization of magmatic plagioclase. Am Mineral, 51: 792-806.

Brugger, C.R. and Hammer, J.E., 2010. Crystallization kinetics in continuous decompression experiments: implications for interpreting natural magma ascent processes. J Petrol, 51(9): 1941-1965. doi: 10.1093/petrology/egq044

Burgisser, A. and Scaillet, B., 2007. Redox evolution of a degassing magma rising to the surface. Nature, 445(7124): 194-197. doi: 10.1038/nature05509

Burgisser, A., Scaillet, B. and Harshvardhan, 2008. Chemical patterns of erupting silicic magmas and their influence on the amount of degassing during ascent. J Geophys Res-Sol Ea, 113(B12). doi: 10.1029/2008jb005680

Clynne, M.A., 1999. A complex magma mixing origin for rocks erupted in 1915, Lassen Peak, California. J Petrol, 40(1): 105-132. doi: 10.1093/petroj/40.1.105

Coats, R.R., 1956. Reconnaissance geology of some western Aleutian Islands, Alaska, Bulletin. US Geol Surv Num Ser. U.S. Govt. Print. Off., pp. p.83-100, ill., maps (101 fold .col. in pocket) ;124 cm.

Couch, S., Harford, C.L., Sparks, R.S.J. and Carroll, M.R., 2003. Experimental constraints on the conditions of formation of highly calcic plagioclase microlites at the Soufrire Hills Volcano, Montserrat. J Petrol, 44(8): 1455-1475. doi: 10.1093/petrology/44.8.1455

Davidson, J.P. and Tepley, F.J., 1997. Recharge in volcanic systems: evidence from isotope profiles of phenocrysts. Science, 275(5301): 826-829.

Donovan, J.J., Kremser, D. and Fournelle, J.H., 2007. Probe for Windows User's Guide and Reference, Enterprise Edition. Probe Software Inc., Eugene, OR.

Fee, D., Steffke, A. and Garces, M., 2010. Characterization of the 2008 Kasatochi and Okmok eruptions using remote infrasound arrays. J Geophys Res-Atmos, 115: D00L10. doi: 10.1029/2009jd013621

Gaetani G.A., Grove T.L. and Bryan, W.B., 1994. Experimental phase relations of basaltic andesite from Hole 839B under hydrous and anhydrous conditions. In: Hawkins, J., Parson, L., Allan, J., et al. (eds) Proc Ocean Drill Prog, Sci Res, 135: 557–563.

Geschwind, C.H. and Rutherford, M.J., 1995. Crystallization of microlites during magma ascent - the fluid-mechanics of 1980-1986 eruptions at Mount-St-Helens. B Volcanol, 57(5): 356-370.

Gill, J.B., 1981. Orogenic andesites and plate tectonics. Springer Verlag, Berlin, Germany, 390 pp.

Ginibre, C., Wörner, G. and Kronz, A., 2002. Minor- and trace-element zoning in plagioclase: implications for magma chamber processes at Parinacota volcano, northern Chile. Contrib Mineral Petr, 143(3): 300-315. doi: 10.1007/s00410-002-0351-z

Hale, A.J., Wadge, G. and Mühlhaus, H.B., 2007. The influence of viscous and latent heating on crystal-rich magma flow in a conduit. Geophys J Int, 171(3): 1406-1429. doi: 10.1111/j.1365-246X.2007.03593.x

Hammarstrom, J.M. and Zen, E.A., 1986. Aluminum in hornblende - an empirical igneous geobarometer. Am Mineral, 71(11-12): 1297-1313.

Hammer, J.E., Cashman, K.V. and Voight, B. (2000) Magmatic processes revealed by textural and compositional trends in Merapi dome lavas. J. Volcanol Geoth Res, 100, 165-192.

Hammer, J.E. and Rutherford, M.J., 2002. An experimental study of the kinetics of decompression-induced crystallization in silicic melt. J Geophys Res-Sol Ea, 107(B1) doi: 10.1029/2001jb000281

Holland, T.J.B. and Blundy, J.D., 1994. Nonideal interactions in calcic amphiboles and their bearing on amphibole-plagioclase thermometry. Contrib Mineral Petr, 116(4): 433-447.

Izbekov, P.E., Eichelberger, J.C. and Ivanov, B.V., 2004. The 1996 eruption of Karymsky volcano, Kamchatka: Historical record of basaltic replenishment of an andesite reservoir. J Perol, 45(11): 2325-2345.

Izbekov, P., Sisson, T., Wooden, J. and Bacon, C., 2009. 2008 Kasatochi Eruption: SHRIMP constraints on concentration of volatiles in melt inclusions, AGU Fall Meet, Abs. #V51E-1775, San Francisco, CA, pp. 1775.

Jarosewich, E., 2002. Smithsonian microbeam standards. J Res NIST (107): 681-685.

Johnson, M.C. and Rutherford, M.J., 1989. experimental calibration of the aluminum-in-hornblende geobarometer with application to Long-Valley Caldera (California) volcanic rocks. Geology, 17(9): 837-841.

Kay, S. and Kay, R., 1985. Aleutian tholeiitic and calc-alkaline magma series I: The mafic phenocrysts. Contrib Mineral Petr, 90(2): 276-290. doi: 10.1007/bf00378268

Lange, R.A., Frey, H.M. and Hector, J., 2009. A thermodynamic model for the plagioclase-liquid hygrometer/thermometer. Am Mineral, 94(4): 494-506. doi: 10.2138/am.2009.3011

Le Bas, M.J., Lemaitre, R.W., Streckeisen, A. and Zanettin, B., 1986. A chemical classification of volcanic rocks based on the Total Alkali Silica diagram. J Petrol, 27(3): 745-750.

Lepage, L.D., 2003. ILMAT: an Excel worksheet for ilmenite-magnetite geothermometry and geobarometry. Computers & Geosciences, 29(5): 673-678. doi: 10.1016/S0098-3004(03)00042-6

Longhi, J., Walker, D. and Hays, J.F., 1976. Fe and Mg in plagioclase. In: Proc 7th Lunar Sci Conf: 1281-1300.

Lundgaard, K. and Tegner, C., 2004. Partitioning of ferric and ferrous iron between plagioclase and silicate melt. Contrib Mineral Petr, 147(4): 470-483. doi: 10.1007/s00410-004-0568-0

Martel, C. and Schmidt, B.C., 2003. Decompression experiments as an insight into ascent rates of silicic magmas. Contrib Mineral Petr, 144(4): 397-415. doi: 10.1007/S00410-002-0404-3

Martel, C., Radadi Ali, A., Poussineau, S., Gourgaud, A. and Pichavant, M., 2006. Basalt-inherited microlites in silicic magmas: Evidence from Mount Pelée (Martinique, French West Indies). Geology, 34(11): 905-908. doi: 10.1130/g22672a.1

Mastin, L.G. and Ghiorso, M.S., 2001. Adiabatic temperature changes of magma-gas mixtures during ascent and eruption. Contrib Mineral Petr, 141(3): 307-321.

McCanta, M.C., Rutherford, M.J. and Hammer, J.E., 2007. Pre-eruptive and syn-eruptive conditions in the Black Butte, California dacite: Insight into crystallization kinetics in a silicic magma system. J Volcanol Geoth Res, 160(3-4): 263-284. doi: 10.1016/J.Jvolgeores.2006.10.004

Miyashiro, A., 1974. Volcanic rock series in island arcs and active continental margins. Am Journ Sci, 274(4): 321-355. doi: 10.2475/ajs.274.4.321

Moore, G. and Carmichael, I.S.E., 1998. The hydrous phase equilibria (to 3 kbar) of an andesite and basaltic andesite from western Mexico: constraints on water content and conditions of phenocryst growth. Contrib Mineral Petr, 130(3-4): 304-319.

Morgan, G.B. and London, D., 1996. Optimizing the electron microprobe analysis of hydrous alkali aluminosilicate glasses. Am Mineral, 81(9-10): 1176-1185.

Nielsen, C.H. and Sigurdsson, H., 1981. Quantitative methods for electron micro-probe analysis of sodium in natural and synthetic glasses. Am Mineral, 66(5-6): 547-552.

Nicholis, M.G. and Rutherford, M.J., 2004. Experimental constraints on magma ascent rate for the Crater Flat volcanic zone hawaiite. Geology, 32(6): 489-492. doi: 10.1130/g20324.1

Pallister, J.S., Thornber, C.R., Cashman, K.V., Clynne, M.A., Lowers, H.A., Mandeville, C.W., Brownfield, I.K. and Meeker, G.P., 2008. Petrology of the 2004-2006 Mount St. Helens lava dome - implications for magmatic plumbing and eruption triggering. *in*: D.R. Sherrod, W.E. Scott and P.H. Stauffer (*eds*), A Volcano Rekindled: The Renewed Eruption of Mount St. Helens, 2004-2006. U.S. Geol Surv Prof Pap 1750, pp. 647-702.

Phinney, W.C., 1992. Partition-coefficients for iron between plagioclase and basalt as a function of oxygen fugacity - implications for Archean and Lunar anorthosites. Geochim Cosmochim Acta, 56(5): 1885-1895.

Pichavant, M., Martel, C., Bourdier, J.L. and Scaillet, B., 2002. Physical conditions, structure, and dynamics of a zoned magma chamber: Mount Pelee (Martinique, Lesser Antilles Arc). J Geophys Res-Sol Ea, 107(B5). doi: 10.1029/2001JB000315

Rader, E.L., 2010. Mineral stability in H_2O-undersaturated magmas: experiments on basaltic andesite from Westdahl Volcano. University of Alaska Fairbanks, M.Sc. Thesis, 94 pp.

Ridolfi, F., Renzulli, A. and Puerini, M., 2010. Stability and chemical equilibrium of amphibole in calc-alkaline magmas: an overview, new thermobarometric formulations and application to subduction-related volcanoes. Contrib Mineral Petr, 160(1): 45-66. doi: Doi 10.1007/S00410-009-0465-7

Ridolfi, F. and Renzulli, A., 2012. Calcic amphiboles in calc-alkaline and alkaline magmas: thermobarometric and chemometric empirical equations valid up to 1,130°C and 2.2 GPa. Contributions to Mineralogy and Petrology, 163(5): 877-895. doi: 10.1007/s00410-011-0704-6

Robie, R.A., Hemingway, B.S. and Fisher, J.R., 1978. Thermodynamic properties of minerals and related substances at 298.15 K and 1 bar (105 pascals) pressure and at higher temperatures, Bulletin. US Geol Surv Num Ser., 456 pp.

Ruprecht, P. and Wörner, G., 2007. Variable regimes in magma systems documented in plagioclase zoning patterns: El Misti stratovolcano and Andahua monogenetic

cones. J Volcanol Geoth Res, 165(3-4): 142-162. doi: 10.1016/j.jvolgeores.2007.06.002

Sahagian, D.L. and Proussevitch, A.A., 1996. Thermal effects of magma degassing. J Volcanol Geoth Res, 74(1-2): 19-38. doi: 10.1016/s0377-0273(96)00047-9

Sato, H., 1989. Chemistry of basalts of ODP Hole 111-504B, Supplement to: Sato, Hiroaki (1989): Mg-Fe partitioning between plagioclase and liquid in basalts of Hole 504B, ODP Leg 111: a study of melting at 1 ATM. In: Becker, K; Sakai, H; et al. (eds.), Proc Ocean Drill Prog, Sci Res, 111, 17-26, doi:10.2973/odp.proc.sr.111.113.1989

Schmidt, M.W., 1992. Amphibole composition in tonalite as a function of pressure - an experimental calibration of the Al-in-hornblende barometer. Contrib Mineral Petr, 110(2-3): 304-310.

Scott, W.E., Nye, C.J., Waythomas, C.F. and Neal, C.A., 2010. August 2008 eruption of Kasatochi Volcano, Aleutian Islands, Alaska-Resetting an island landscape. Arct Antarct Alp Res, 42(3): 250-259. doi: Doi 10.1657/1938-4246-42.3.250

Sparks, R.S.J. and Pinkerton, H., 1978. Effect of degassing on rheology of basaltic lava. Nature, 276: 385-386.

Sugawara, T., 2001. Ferric iron partitioning between plagioclase and silicate liquid: thermodynamics and petrological applications. Contrib Mineral Petr, 141(6): 659-686.

Tepley, F.J., Davidson, J.P. and Clynne, M.A., 1999. Magmatic interactions as recorded in plagioclase phenocrysts of Chaos Crags, Lassen Volcanic Center, California. J Petrol, 40(5): 787-806. doi: 10.1093/petroj/40.5.787

Tindle, A.G. and Webb, P.C., 1994. Probe-Amph - a spreadsheet program to classify microprobe-derived amphibole analyses. Comp Geosci, 20(7-8): 1201-1228.

Tsuchiyama, A., 1985. Dissolution kinetics of plagioclase in the melt of the system diopside-albite-anorthite, and origin of dusty plagioclase in andesites. Contrib Mineral Petr, 89(1): 1-16. doi: 10.1007/bf01177585

Waythomas, C.F., Scott, W.E., Prejean, S.G., Schneider, D.J., Izbekov, P. and Nye, C.J., 2010a. The 7-8 August 2008 eruption of Kasatochi Volcano, central Aleutian Islands, Alaska. J Geophys Res, 115: B00B06. doi: 10.1029/2010jb007437

Waythomas, C.F., Scott, W.E. and Nye, C.J., 2010b. The geomorphology of an Aleutian volcano following a major eruption: the 7-8 August 2008 eruption of Kasatochi Volcano, Alaska, and its aftermath. Arct Antarct Alp Res, 42(3): 260-275. doi: Doi 10.1657/1938-4246-42.3.260

Westrich, H.R., Stockman, H.W. and Eichelberger, J.C., 1988. Degassing of rhyolitic magma during ascent and emplacement. J Geophys Res-Sol Ea, 93(B6): 6503-6511.

Wilke, M. and Behrens, H., 1999. The dependence of the partitioning of iron and europium between plagioclase and hydrous tonalitic melt on oxygen fugacity. Contrib Mineral Petr, 137(1-2): 102-114.

Williams, J.C., Drummond, B.A. and Buxton, R.T., 2010. Initial effects of the August 2008 volcanic eruption on breeding birds and marine mammals at Kasatochi Island, Alaska. Arct Antarct Alp Res, 42(3): 306-314. doi: Doi 10.1657/1938-4246-42.3.306

Yogodzinski, G.M., Kay, R.W., Volynets, O.N., Koloskov, A.V. and Kay, S.M., 1995. Magnesian andesite in the western Aleutian Komandorsky region: Implications for slab melting and processes in the mantle wedge. Geol Soc Am Bull, 107(5): 505-519. doi: 10.1130/0016 7606(1995)107<0505:maitwa>2.3.co;2

Yogodzinski, G.M. and Kelemen, P.B., 1998. Slab melting in the Aleutians: implications of an ion probe study of clinopyroxene in primitive adakite and basalt. Earth Planet Sc Lett, 158(1-2): 53-65. doi: Doi: 10.1016/s0012-821x(98)00041-7

Zhang, Y., 1999. Exsolution enthalpy of water from silicate liquids. J Volcanol Geoth Res, 88(3): 201-207. doi: 10.1016/s0377-0273(98)00115-2

Chapter 4: Evolution of the Magmatic System of Bezymianny Volcano, Kamchatka, Russia: Insights from Compositional Analyses of Melt Inclusions[1]

> And yet my eyes are drawn towards the mountain in the east
> Fascinates and captivates and gives my heart no peace
> The mountain holds the sunrise in the prison of the night
> 'Til bursting forth from rocky chains, the valley floods with light
>
> *Rush,* "The Fountain of Lamneth"
> *Caress of Steel, Mercury Records, 1975*

4.1: Abstract

Bezymianny Volcano, located in the central Kamchatka Peninsula, Russia, experienced a climactic eruption in 1956 driven by the failure of the volcanic edifice, which has been followed by over 60 years of nearly continuous explosive and effusive activity. Measurements by electron microprobe and SHRIMP ion probe of major, trace lithophile, and volatile element concentrations in melt inclusions from the 1956 eruption and from eruptions in 1984-2010 help to reveal the evolution of the magmatic system at Bezymianny. Melt inclusions also reveal low-pressure crystallization of magma at shallow storage levels (~2-4 km) due to degassing brought on by decompression. Also, as has been seen previously at other volcanoes, inclusions trapped at shallow levels below

[1] Neill, O.K., Izbekov, P.I., Vazquez, J.A., Shcherbakov, V.D., Plechov, P.Yu., Wooden, J.L., Lopez, T.M., and Bacon, C.R. (*in prep*) Evolution of the magmatic system of Bezymianny Volcano, Kamchatka, Russia: Insights from compositional analyses of melt inclusions. To be submitted to *Journal of Volcanology and Geothermal Research.*

Bezymianny show significant enrichment in lithium (up to 120 ppm). Lithium enrichment at low pressures is dominantly found in inclusions from eruptions between 1984 and 1997, but is largely absent from inclusions from 2001-2010. Low-pressure lithium enrichment is probably the result of the ascent of magmatic volatiles from deep in the magma system below Bezymianny leading the saturation of Li-rich fluids at shallow depths, a process which seems to be restricted after 2001.

4.2: Introduction

After ~1000 years of quiescence (Braitseva et al., 1991), Bezymianny volcano, part of the Klyuchevskoy Volcanic Group (KVG) in the central Kamchatka Peninsula, Russia (Fig. 4-1), re-awakened in the fall of 1955 with the emplacement of a cryptodome in the volcanic edifice. On 30 March, 1956, in an event strikingly similar to the 1980 eruption of Mount St. Helens, Washington, the growth of this cryptodome eventually de-stabilized the edifice, causing the flank of the edifice to fail (Gorshkov, 1959; Gorshkov and Bogoyavlenskaya, 1965; Bogoyavlenskaya et al., 1985; Belousov and Bogoyavlenskaya, 1988; Belousov et al., 2007). This sector collapse generated a laterally directed explosion, followed by a Plinian eruption that produced ~0.8 km^3 of andesitic tephra, and left a horseshoe-shaped crater at the center of the volcano, opening to the southwest (Gorshkov, 1959; 1963; Bogoyavlenskaya et al., 1985; Bogoyavlenskaya et al., 1991; Braitseva et al., 1991; Belousov, 1996; Belousov et al., 2007).

Girina (*in review*) provides a comprehensive review of post-1956 eruptive activity at Bezymianny; a brief summary is presented here. Since 1956, eruptive activity has centered around the growth of an exogenous andesitic lava dome in the center of the crater, punctuated by intermittent low-level explosive activity. From 1956-1977, dome growth was nearly continuous, punctuated by explosive events generating both ash plumes and pyroclastic flows. From 1977 until the early 2000's, dome growth became more sporadic. Eruptive events would include explosive activity as well as the extrusion and collapse of spines from the dome area. Beginning in the early 2000's, while explosive events continued in a similar manner, extrusive activity transitioned from spine extrusion to lava flows originating from a central vent area at the top of the dome. Explosive eruptions have been strikingly regular since the early 2000's, averaging ~1-2 per year. As of 2011, the edifice has been nearly entirely rebuilt (Fig. 4-1).

The 1956 eruption of Bezymianny produced high-silica (~61 wt. % SiO_2) andesite that was remarkably homogenous in composition, despite being the product of multiple eruptive regimes (e.g. Belousov, 1996; Ozerov et al., 1997). Since then, eruptive products have become increasingly more mafic, with clasts from the 2010 eruption containing ~56 wt. % SiO_2 in addition to mafic enclaves with ~52-55 wt. % SiO_2 (Izbekov et al., 2010; Turner et al., *in review*). Previous authors (Ozerov et al., 1997; Izbekov, 2009; Izbekov et al., 2010; Shcherbakov et al., 2011; Turner et al., *in review*) have suggested that this evolution is the result of the progressive influx and mixing of mafic magma, possibly related to the magmatic feeding system of Klyuchevskoy Volcano, the massive basaltic cone ~10 km to the northeast.

The purpose of this study is to investigate the evolution of the Bezymianny magmatic system using the major, trace lithophile and volatile element concentrations of melt inclusions, which are small volumes of melt trapped within a growing crystal (Fig. 4-2). While melt inclusion compositions may be modified post-entrapment (see Kent, 2008, and references therein), they can effectively record pre-eruptive liquid compositions in a way that interstitial liquid compositions cannot, due to modifications of the interstitial liquids by crystallization and degassing during ascent and eruption. The compositions of melt inclusions have been used to investigate magmatic processes at depth, such as the locations of magma storage regions based on the equilibrium solubility of volatile species in silicic melt, as well the chemical evolutions of magmas prior to eruption, both in terms of volatile and non-volatile elements (e.g. Tolstykh et al., 1998; Wallace et al., 1999; Danyushevsky et al., 2002; Tolstykh et al., 2003; Liu et al., 2006; Humphreys et al., 2008). Conversely, they can be used to track more dynamic processes such as degassing, volatile flux through a magmatic system, and syn-eruptive crystallization (e.g. Berlo et al., 2004; Blundy and Cashman, 2005; Blundy et al., 2005; Kent et al., 2007; Blundy et al., 2008; Edmonds, 2008). By analyzing melt inclusions from a series of eruptions from 1956 to 2010, this study seeks to characterize how processes of both melt evolution and volatile movement have changed as Bezymianny has evolved since 1956.

4.3: Methods

4.3.1. Sample Collection and Preparation

Samples from the 1956 and 2006-2010 Bezymianny eruptions were collected from juvenile blocks in pyroclastic flows from each eruption of interest, while samples from eruptions from 1984-2005 were provided by A.B. Belousov, M.G. Belousova, G.E. Bogoyavlenskaya, O.A. Girina, A.P. Maximov, P.R. Kyle and M.E. Zelensky. Samples were collected from juvenile blocks with evidence for post-eruptive cooling such as cracks and viscous tearing features that distinguish them from accidental material incorporated into those pyroclastic flows. For clarity, in figures presenting melt inclusion compositions, data has been grouped into three different categories based on eruption chronology: (1) inclusions from the 1956 climactic eruption; (2) inclusions from the 1984-2000 eruptive period, characterized by exogenous dome growth between explosive events; (3) inclusions from the 2001-2010 eruptive period, characterized by lava flows and explosive eruptions emanating from a central vent at the top of the rebuilt Bezymianny edifice. Samples are fully described in Appendix 4-1. As in previous chapters, all appendices are included electronically on the compact disc accompanying this dissertation.

Melt inclusions hosted in plagioclase and pyroxene were prepared for analysis by secondary ion mass spectrometry (SIMS) by first lightly crushing selected samples and picking individual plagioclase and pyroxene crystals and then removing any glass adhered to the outsides of selected crystals in an unltrasonic bath of 10% molar HF acid

solution. Crystals containing melt inclusions were then mounted in CrystalBond© mounting compound and ground down to expose individual inclusions. Crystals were then polished on the exposed surface, removed from the CrystalBond© mounts and soaked in acetone to remove CrystalBond© and any contaminants from polishing and mounting compounds. These crystals were then pressed into indium contained in aluminum mounts and gold-coated in preparation for SIMS analyses. Indium mounts were preferred to epoxy to minimize background C and OH counts, as those elements may be released from the epoxy under the high vacuum of the SIMS sample chamber. Only glassy inclusions without interstitial microlites, cracks, capillary channels or signs of decrepitation and were chosen for SIMS analyses to minimize effects of post-entrapment volatile loss or modification of the trapped liquid (e.g. Lowenstern, 1995).

4.3.2. Secondary Ion Mass Spectrometry (SIMS)

Melt inclusions were analyzed for H_2O, Li, Be, B, CO_2, F, S, Cl, Rb and Sr by SIMS using the SHRIMP-RG (Super-High Resoulution Ion Microprobe with Reverse Geometry) located at the Stanford University/USGS SUMAC facility. Analyses employed a primary 20 μm diameter beam of $^{16}O_2$- ions, with a current of ~2 nA and an accelerating potential of 10.5 kV. Individual masses were measured in four counting cycles, acquiring on-peak counts for ^{7}Li, ^{9}Be, ^{11}B, $^{16}O^{1}H$, ^{12}C, ^{19}F, $^{28}Si^{1}H$, ^{30}Si, ^{32}S, ^{35}Cl, ^{85}Rb and ^{88}Sr, monitor isotopes of major elements ^{26}Mg, ^{42}Ca, $^{27}Al^{16}O$ and ^{57}Fe, and off-peak background counts on both sides of the $^{28}Si^{1}H$ peak. Mass resolution was 7000 at

10% peak height. Counting times per cycle were 2 s for Mg, Si, Ca, Fe, Rb and Sr, 4 s for Li, Be, B, and F, 5 s for $^{16}O^{1}H$ and on- and off-peak measurements of $^{28}Si^{1}H$, 10 s for S and Cl, and 30 s for C. Samples were pre-ablated for ~60 s to remove gold coating and any remaining surface contaminants.

A suite of glass standards was measured to create calibration curves of peak count rates normalized against counts of ^{30}Si, against standard concentrations normalized to SiO_2 concentrations. Anhydrous standards included NIST SRM 611 and SRM 613 (Pearce et al., 1997), Macusani glass (Pichavant et al., 1988), and natural volcanic glasses RLS-37 and RLS-158 (MacDonald et al., 1992). H_2O and CO_2 standards included materials synthesized by Mangan and Sisson (2000). Analytical uncertainties from internal errors were calculated for each analytical spot based counting statistics using the SQUID2 data reduction program of Ludwig (2009). Analytical uncertainty from external errors, such as errors in standard concentrations and repeated standard analyses, were calculated for each analysis using a modified York regression (York, 1969) with the corrections of Mahon (1996). Error bars in figures are plotted as 1 standard deviation, reporting whichever uncertainty (internal or external) is larger.

Ablation pits that intersected the host mineral were identified visually, by monitoring counts of Mg, Si, Ca, Fe, Sr and Rb for anomalously high variability across the four counting cycles, and by energy dispersive spectrometry of the ablation pits using an EDAX energy-dispersive spectrometer on the CAMECA SX-50 electron microprobe located at the UAF Advanced Instrumentation Laboratory. Concentrations obtained from

these contaminated analytical spots are not reported. Also, the CO_2 concentrations of some analyses were anomalously high (>6000 ppm), accompanied by highly variable count rates across the four counting cycles. Wright et al. (2012), who used nearly identical analytical and sample preparation procedures, report a similar finding and suggest that small amounts of carbon surface contamination are not fully removed during cleaning of the crystals or pre-ablation, and that only CO_2 measurements where the variability in count rates is low can be considered reliable. In accordance with the recommendations of Wright et al. (2012), only CO_2 measurements with internal analytical uncertainties (1 standard deviation) <10% of calculated concentration, or that contain less CO_2 than the detection limit of ~50 ppm calculated by Wright et al. (2012), are reported. Standard values and calibration curves may be found in Appendix 4-2 and Figure 4-3, respectively, while internal and external uncertainties, along with calculated concentrations, are reported in Appendix 4-3.

4.3.3: Electron Probe Microanalysis (EPMA)

Major oxide and minor oxide concentrations of individual melt inclusions were analyzed by wavelength-dispersive x-ray spectrometry, using the AIL CAMECA SX-50 4-sprectrometer electron microprobe. Analyses were performed using a 15 kV accelerating potential and 10 nA beam, defocused to ~10 μm to minimize Si, Al, Na and K migration during analyses. Effects of elemental migration were further minimized by counting Al, Na and K first and by using Time-Dependent Intensity corrections through

ProbeForEPMA software (Nielsen and Sigurdsson, 1981; Donovan et al., 2007). Concentrations were obtained from raw intensities using a ZAF intensity correction. EPMA analyses were performed after SIMS analyses to avoid compromising SIMS analyses of light elements due to electron beam damage (Humphreys et al., 2006). Further details of EPMA procedures may be found in Appendix 4-4, while EPMA data is reported alongside SHRIMP data in Appendix 4-3.

4.4: Compositions of Bezymianny Melt Inclusions

4.4.1: Major and Minor Oxides, Rb and Sr

Melt inclusion compositions are dacitic to rhyolitic, with ~68-78 wt. % SiO_2, 0.1-2 wt. % MgO and ~2.2-4.7 wt. % K_2O, while Rb and Sr concentrations range from ~35-85 ppm and ~40-200 ppm, respectively (Fig. 4-4). The positive correlation between SiO_2 and Rb reflects the overall incompatibility of Rb in andesites, while the negative correlation between Sr and SiO_2 is indicative of the compatibility of Sr due to plagioclase crystallization (cf., Bacon and Druitt, 1988). More silicic melt inclusions tend to be hosted in plagioclase rather than pyroxene. No measured pyroxene-hosted inclusions contained more than ~76 wt. % SiO_2, with generally <55 ppm Rb and >100 ppm Sr, while plagioclase-hosted inclusions reach ~79 wt. % SiO_2 (Fig. 4-4). At a given SiO_2 content, pyroxene- and plagioclase-hosted inclusions do not differ in major and minor

oxide concentrations past the limits of analytical uncertainty (Fig. 4-4), and therefore inclusion compositions are not corrected for post-entrapment crystallization (cf., Danyushevsky et al., 2002).

Bulk compositions of Bezymianny samples have become progressively more mafic over time (Fig. 4-5; Izbekov, 2009; Izbekov et al., 2010; Turner et al., *in review*). While the range of melt inclusion major-oxide and trace element compositions does not vary greatly with time, they do somewhat reflect the bulk compositional trend, as SiO_2 concentration does slightly decrease with time and all but two of 15 inclusions with >75 wt. % SiO_2 are from prior to 2001 (Fig. 4-5). There is, however, significant overlap between the sample sets, and more mafic compositions are equally common before and after 2001. Inclusions from 1956 have some of the highest SiO_2 and K_2O contents measured, along with relatively low Mg and Ca. There are no systematic differences in in Rb and Sr between inclusions from 1984-1997 and from 2001-2010, though inclusions from 1956 have some of the lowest Sr and highest Rb concentrations of the entire sample set (Fig. 4-4).

4.4.2: H_2O, CO_2 and S

Inclusions from the 1956 eruption are relatively high in H_2O, with concentrations from ~1.2-3.8 wt. % H_2O (Fig. 4-5), similar to the melt inclusion H_2O concentrations determined by Tolstykh et al. (1999). From 1984-2010, maximum H_2O concentrations generally increase with time, from a maximum of ~2 wt. % H_2O in 1984 to ~4.2 wt. % in

2010 (Fig. 4-5). CO_2 data is limited by the analytical issues described previously, but only four of 33 acceptable CO_2 analyses have concentrations >200 ppm (Fig. 4-6). The two highest CO_2 inclusions (910 and 432 ppm) are both hosted in plagioclase from the 9 May, 2006 eruption. Sulfur concentrations are generally <150 ppm, with only 12 of 82 inclusions exceeding 150 ppm S (Fig. 4-7). Of those 12 high-S inclusions, nine are hosted in pyroxene, while seven are from 2001-2010 and one is from 1956. While there is no monotonic correlation between H_2O and either CO_2 or S, high CO_2 and high-S inclusions generally have higher H_2O, and the maximum CO_2 and S concentrations at a given H_2O concentration increase as H_2O concentrations increase (Figs. 4-6, 4-7), consistent with S and CO_2 concentrations being controlled by magmatic degassing. In addition, inclusions with higher concentrations of highly incompatible elements (e.g. K, Rb) tend to be slightly less H_2O rich (Figs. 4-8, 4-9). CO_2 and S also both correlate negatively with Rb (Fig. 4-8) and K_2O (Fig. 4-7; CO_2 not shown). No inclusions with >50 ppm Rb contain >200 ppm CO_2, and only two inclusions with >50 ppm Rb contain >100 ppm S.

4.4.3: Li, Be and B

While the analytical uncertainties on measured lithium concentrations are comparatively large, some interpretation is still possible. Lithium concentrations follow two trends relative to H_2O concentrations (Fig. 4-9), with one trend dominated by low-Li (<50 ppm) inclusions reaching H_2O concentrations >2.5 wt. %, while the other reaches higher Li concentrations (up to ~110 ppm) with low H_2O (<2.5 wt. %, Fig. 4-9). Of the

82 inclusions measured in this study, 22 have >50 ppm Li and 17 have >2.5 wt. % H_2O, but only six inclusions contain both >50 ppm Li and >2.5 wt. % H_2O. Inclusions from 1956 are dominantly low in both Li and H_2O; of the two 1956 inclusions with >2.5 wt. % H_2O, one lies along the main low-Li/high-H_2O trend, while the other has anomalously high Li (~80 ppm, Fig. 4-9). In addition to being low in H_2O, 17 out of 22 measured inclusions (~77%) with >50 ppm Li are from 1984-2000, while 19 of 23 inclusions (~82%) with >50 ppm Li are hosted in plagioclase. These findings exceed what would be expected due to sampling bias, as only 49 of the 82 measured inclusions (~58%) are from 1984-2000 and only 53 of the 82 inclusions (~65%) are hosted in plagioclase.

Variations in beryllium concentrations barely exceed analytical uncertainty, remaining between ~4.5-5.5 ppm across all inclusions (Fig 4-9). Previous studies have suggested that Be behaves as an incompatible lithophile element (similar to B) and is generally unaffected by degassing or fluid movement (e.g. Ryan and Langmuir, 1988; Stix et al., 1995; Stix and Layne, 1996), although Humphreys et al. (2008) suggest that variations in Be concentrations are not inherited from source characteristics at Shiveluch Volcano in Kamchatka. At Bezymianny, Be does not co-vary with Rb (Fig. 4-10) or B (not shown) and displays only a statistically dubious negative correlation with H_2O (Fig. 4-9), suggesting that any systematic variations in Be concentration are below detection.

Inclusions from all eruptions contain dominantly ~15-50 ppm B, although six inclusions (one from 1984-2000, five from 2001-2010) have higher concentrations, with a maximum of ~90 ppm (Fig. 4-9). Boron concentrations show a slightly negative

correlation with H_2O (Fig. 4-9) and a more robust positive correlation with Rb, although inclusions from 1956 have average B concentrations despite being significantly higher in Rb (Fig. 4-10). Boron has been frequently considered an incompatible lithophile trace element in volcanic systems, and concentrations in magmas are generally thought to derive from mantle source characteristics, modified by mixing and fractional crystallization during pre-eruptive melt evolution (e.g. Ryan and Langmuir, 1993; Straub and Layne, 2002; Clift et al., 2003; Straub et al., 2004; Humphreys et al., 2008). As boron concentrations correlate positively with other incompatible lithophile elements such as Rb (Fig. 4-10) and K (not shown), boron seems to behave like an incompatible lithophile element at Bezymianny, in agreement with the aforementioned studies. B/Be ratios range from a minimum of ~5 to a maximum of ~23 (Fig. 4-10). Such low B/Be ratios indicate that the influence of sediments or fluids during primary melting may be minor (Morris et al., 1990), although Auer et al. (2009) suggest that such a heterogeneous, fluid-modified mantle wedge may contribute to oxygen isotope heterogeneities in the greater Klyuchevskoy group.

4.4.4: Halogens

Fluorine concentrations are generally ~50-800 ppm, although two inclusions contain ~1600 ppm F (Fig. 4-9). Chlorine concentrations are between ~600-2000 ppm, with one inclusion having an anomalously low Cl concentration of ~180 ppm (Fig. 4-9). Lower-Cl inclusions tend to be found in pyroxene; 11 of the 17 inclusions with <1000

ppm Cl are pyroxene-hosted (Fig. 4-9). Neither Cl nor F concentrations decrease systematically with decreasing inclusion H_2O content, suggesting that Cl and F are not significantly removed from the melt by degassing (Fig. 4-9). Chlorine is also significantly enriched in low-S melt inclusions (Fig. 4-7), with only four of 42 inclusions with >1200 ppm Cl containing >100 ppm S, further suggesting that Cl is not significantly affected by degassing. Chlorine concentrations show a broadly positive correlation with Rb, although, as with B, inclusions from 1956 typically have average Cl concentrations despite being high in Rb (Fig. 4-10). Fluorine concentrations are not correlated with Rb concentrations (Fig. 4-10).

4.5: Discussion

4.5.1: Melt Inclusion Entrapment Pressures and Depths

The solubility of H_2O and CO_2 in silicate melts is highly pressure dependent, and therefore H_2O-CO_2 solubility models can be used to calculate the total pressures (P_{Total}) at which the melt inclusions were entrapped (e.g. Newman and Lowenstern, 2002). As CO_2 concentrations were not determined for all inclusions, P_{Total} cannot be determined for the entire dataset. However, pressure can be expressed as the partial pressure of H_2O (p_{H2O}), which can, in turn, serve as a proxy for the depth at which a melt inclusion was entrapped. p_{H2O} can only serve as a qualitative proxy for depth, and any "true" depths

calculated based on a lithostatic geobaric gradient are underestimates relative to pressures calculated based on H_2O-CO_2 solubility. However, trends in melt inclusion compositions relative to P_{Total} and relative to p_{H2O} do not differ significantly (Figs. 4-11, 4-12), and therefore the *relative* depths of inclusion entrapment can be estimated from p_{H2O}.

P_{Total} and p_{H2O} were calculated using the VolatileCalc H_2O-CO_2 solubility model (Newman and Lowenstern, 2002), assuming a magmatic temperature of 900° C (Kadik et al., 1986; Shcherbakov et al., *in press*). P_{Total} was calculated for all inclusions with acceptable CO_2 concentrations, while p_{H2O} was calculated for all inclusions. Entrapment pressures are dominantly low, with only five inclusions entrapped at P_{Total} >100 MPa (Fig. 4-6). Of these seven inclusions, three are from 2001-2010 and hosted in plagioclase, while two are pyroxene-hosted inclusions from 1956. The maximum calculated P_{Total} from all Bezymianny inclusions is ~230 MPa, corresponding to a depth ~8 km, assuming a crustal density of 2700 kg m^{-3}. Interestingly, Kadik et al. (1986) suggest that, at H_2O-saturated conditions, initial H_2O contents of Bezymianny magmas would be in the range of 5-6 wt. %, ~1 wt. % more than the maximum measured H_2O from all inclusions measured in this study, which indicates that either magma at Bezymianny loses significant volatiles before melt inclusion entrapment begins or that $X_{H2O} < 1$ in the deep Bezymianny magma system.

4.5.2: Shallow Magmatic Storage, Crystallization and Degassing at Bezymianny

Both geochemical (e.g. Kadik et al., 1986; Ozerov et al., 1997; Tolstykh et al., 1999; Al'meev et al., 2002) and geophysical studies (e.g. Fedotov et al., 2010; Thelen et al., 2010) suggest depths of primary magmatic storage at Bezymianny volcano of >20 km or >500 MPa. Such depths are well in excess of even the maximum calculated inclusion entrapment pressures, indicating that either the melt inclusions lost H_2O and CO_2 post-entrapment, or that melt inclusion entrapment at Bezymianny takes place in shallower parts of the Bezymianny magma system. Inclusions with obvious cracks, capillaries or signs of decrepitation were avoided in the initial sample preparation (cf. Lowenstern, 1995). In addition, diffusive loss of H_2O is less problematic in plagioclase- and pyroxene-hosted inclusions than in inclusions hosted in olivine (e.g. Danyushevsky et al., 2002). Therefore, pressures estimated from melt inclusion H_2O and CO_2 concentrations probably reflect actual entrapment pressures during crystallization and are not artificially low due to post-entrapment H_2O and CO_2 loss during magmatic ascent. Thelen et al. (2010) observed an aseismic zone 1-2 km below the edifice, which they suggest may be associated with a shallow magma or fluid staging area. The depth of this storage area is in good agreement with melt inclusion entrapment pressures. Furthermore, Lopez et al. (*in review*) suggest that low SO_2/H_2O and CO_2/H_2O ratios, measured in fumaroles on the surface of the Bezymianny dome, result from the degassing of a shallow magma body.

In light of both these studies and the low entrapment pressures recorded by melt inclusions, it seems probable that magma at Bezymianny does not travel directly from deeper storage regions to the surface, but is staged at ~2-4 km below the edifice prior to eruption. The dominantly low H_2O (<1.5 wt. %), CO_2 (<200 ppm) and S (<150 ppm) concentrations in melt inclusions reflect degassing during ascent to and/or storage in this shallow magmatic region. Based on the moderate SO_2 fluxes and persistent volcanic plume emanating from the Bezymianny edifice, Lopez et al. (*in review*) suggest that this degassing is open-system, whereby volatiles are allowed to fully segregate from the magma and degas at the surface. A model of the Bezymianny sub-surface magmatic plumbing system that includes a shallowly-stored, degassing magma body is not only supported by the volatile concentrations in melt inclusions measured in this study, but is consistent with models of the shallow magmatic plumbing system at Bezymianny proposed in the aforementioned studies.

If post-entrapment volatile loss from melt inclusions is negligible, low-pressure entrapment of melt inclusions will therefore either result from crystallization during magmatic ascent as the magma degasses due to decompression or during storage at shallow depths beneath the volcanic edifice. Inclusions trapped at low pressures during rapid ascent will trap liquids with relatively low H_2O and CO_2 concentrations, but the concentrations of non-volatile elements will not be significantly modified by decompression-driven crystallization, as the kinetics of degassing are far faster than those of crystallization (cf. Fig. 3 of Blundy and Cashman 2005). At Bezymianny, inclusions with low incompatible element concentrations (<3 wt. % K_2O, <50 ppm Rb), which are

found across the entire range of entrapment pressures and S concentrations (Figs. 4-7, 4-8, 4-11), probably represent inclusions that were formed during magmatic ascent, when degassing is rapid but ascent is fast enough to prevent extensive modifications to lithophile element concentrations of interstitial liquids by crystallization. However, inclusions with the highest incompatible element concentrations are volatile-poor, found only at low pressures (p_{H2O} < 50 MPa and P_{Total} < 100 MPa, Fig. 4-11). If ascent is slow, or the magma is allowed to reside at shallow depths for a significant period of time, the increase in liquidus temperatures triggered by H_2O loss from melt at low pressures will drive rapid crystallization and microlite nucleation (e.g. Geschwind and Rutherford, 1995; Hammer and Rutherford, 2002), driving interstitial liquids towards more evolved, incompatible-rich compositions.

High S concentrations (>100 ppm) are only found in inclusions with <3 wt. % K_2O and in only two inclusions with >50 ppm Rb (none with >60 ppm), while K_2O and Rb concentrations increase sharply at S concentrations <100 ppm (Figs. 4-7, 4-8). The strong negative correlations between the incompatible lithophile elements and S concentrations further suggest significant degassing-driven crystallization, as S is another volatile species that partitions into vapor during decompression and degassing (e.g., Metrich and Wallace, 2008). As described above and in Blundy and Cashman (2005), inclusions that were entrapped at shallow levels in the magmatic system experienced significant decompression-driven crystallization, and have higher concentrations of incompatible elements like K and Rb. These inclusions also trapped melts that had degassed due to decompression, and therefore have low S concentrations. By contrast,

inclusions that have been entrapped with high S concentrations had not decompressed, were relatively un-degassed. These inclusions had also experienced less pre-eruptive crystallization and therefore have lower K_2O and Rb concentrations.

As discussed in Section 4.4.1, more incompatible element-rich inclusions, which are entrapped at low-p_{H2O}, are dominantly entrapped in plagioclase (Fig. 4-11). This is unsurprising, as the highly silicic nature of these liquids means that low-pressure crystallization will be dominated by plagioclase (e.g. Blundy and Cashman, 2001; Brugger et al., 2003). Pyroxene crystals will therefore tend to trap more mafic liquids (e.g. Fig. 4-4), as essential components for pyroxene growth such as Fe and Mg will become less and less available as the melts evolve.

4.5.3: Mechanisms for Low-Pressure Lithium Enrichment

Many Bezymianny melt inclusions record relatively high Li concentrations (>50 ppm) at low pressures (Fig. 4-12), a phenomenon that has been documented extensively at Mount St. Helens (Berlo et al., 2004; Blundy et al., 2005; Kent et al., 2007; Blundy et al., 2008). The aforementioned authors have ascribed this enrichment to "gas streaming" (to use the term of Kent et al., 2007), which refers the upward flow of magmatic vapor released from the deep magma system, which carries volatile species to the shallow magmatic storage zone. The decompression of this vapor can then lead to separation of the ascending vapor into a fluid and an H_2O-rich gas phase. Lithium partitions preferentially in the fluid relative to the vapor at magmatic P-T conditions (Webster et al.,

1989), and therefore the shallowly stored magma will be enriched in Li. Melt inclusions entrapped in shallow storage areas will then record low volatile concentrations with high concentrations of Li by entrapping these gas-streaming-enriched liquids, while at the same time being depleted in H_2O, CO_2 and S, which will be lost to degassing (Figs. 4-12, 4-13). Humphreys et al. (2008) also observed similar Li enrichment in melt inclusions from Shiveluch Volcano, located ~80 km north of Bezymianny in central Kamchatka, and suggested a similar mechanism to that described for Mount St. Helens.

Lithium enrichment is dominantly found in plagioclase-hosted inclusions, to a degree greater than would be expected from sampling bias (Fig: 4-13: see Section 4.4.3). This may also reflect the dominance of plagioclase crystallization over pyroxene crystallization at low pressures and more evolved compositions. If plagioclase is the dominant crystallizing phase during the later stages of low-P_{H2O} crystallization, then the evolved, Li-enriched melts will dominantly be sampled by inclusions trapped in plagioclase. Lithium enrichment in plagioclase-hosted inclusions may also be exacerbated post-entrapment, as diffusion of Li through plagioclase phenocrysts is rapid (Giletti and Shanahan, 1997; Blundy et al., 2008).

There is also evidence from other fluid-mobile species for gas streaming at Bezymianny. Chlorine is another species that will be a significant component in the ascending magmatic vapor (Webster, 1997; Webster, 2004; Webster et al., 2009), which is also enriched in Bezymianny melt inclusions at low pressures, albeit less systematically than Li (Fig. 4-12). A number of inclusions are enriched in Cl in low-S

melt inclusions (Fig. 4-7). While this may be partially due to the negative correlation between Cl solubility and pressure in silicic magma, at $P_{Total} < 200$ MPa, silicic magmas with <2000 ppm Cl will not be Cl-saturated (Metrich and Rutherford, 1992; Signorelli and Carroll, 2001), and therefore Cl variations cannot simply derive from Cl lost to fluids or vapor due to variations in Cl solubility. Also, Humphreys et al. (2008) further suggest that the presence of these fluids led to the positive co-variation between Li and Na_2O contents in Shiveluch melt inclusions, as Na will commonly associate with chloride species common in hydrothermal fluids (e.g. Webster, 1997; Webster, 2004; Williams-Jones and Heinrich, 2005). There is a similar (albeit weak) positive correlation between Li and Na_2O in Bezymianny inclusions, and the shape of the Li-Na_2O trends at Bezymianny and Shiveluch are similar (Fig. 4-13; cf. Fig. 12 of Humphreys et al, 2008).

While the low-pressure Li enrichment seen in Bezymianny melt inclusions is likely due to gas streaming, and therefore at least superficially mirrors that at Mount St. Helens, the systems are not strictly analogous. If a separate volatile phase carries Li to the surface, it will also carry the U-series decay product ^{222}Rn, which is in turn a parent isotope of ^{210}Pb. Magma that receives significant volatile enrichment will show excess (relative to equilibrium) ^{210}Pb activity relative to the activity of the stable isotope ^{226}Rn, while magma that has lost significant gas will show ^{210}Pb deficiencies (e.g. Gauthier and Condomines, 1999; Gauthier et al., 2000; Berlo et al., 2004; Turner et al., 2004; Berlo et al., 2006; Reagan et al., 2006; Turner et al., 2007; Kayzar et al., 2009). At Mount St. Helens, samples with elevated melt inclusion Li concentrations at low pressures also show significant ^{210}Pb excesses caused by gas streaming (Berlo et al., 2004; 2006; Kent

et al., 2007). However, while ^{210}Pb excesses are pervasive at Mount St. Helens, they are conspicuous by their absence at Bezymianny, which lead both Turner et al. (2007) and Kayzar (2012) to conclude that gas streaming either does not occur at Bezymianny, or occurs on timescales too rapid to form significant ^{210}Pb excesses.

Li is not a compatible element in any major crystallizing mineral phase found at Bezymianny, and could therefore possibly behave as an incompatible element and be enriched in the melt by crystallization in a manner similar to Rb or K (described above), but Li's strong affinity for fluids relative to melt (Webster et al., 1989), and the lack of co-variation between Li and Rb (Fig. 4-10) or any other non-volatile component do not support this. A well-developed near-surface hydrothermal system could potentially contribute Li to shallowly stored magma via fluid movement, but the compositions of gases released by fumarolic activity at Bezymianny do not show evidence for any subsurface hydrothermal system (Lopez et al., *in review*). It seems more probable that gas streaming is enriching the shallowly-stored Bezymianny magma in Li in a manner similar to that described by the aforementioned authors, but that this streaming is happening over much more rapid timescales than at Mount St. Helens to prevent the formation of significant ^{210}Pb excesses. Measureable (^{210}Pb)/(^{226}Rn) disequilibria can only established at both Bezymianny and Mount St. Helens over timescales longer than months (Berlo et al., 2006; Kayzar, 2012), and therefore gas flux into the shallow magma system must take place over times on the order of weeks prior to eruption.

The amount of time necessary to produce Li enrichment by gas streaming can be constrained by modelling length scales and rates of diffusion of Li through plagioclase crystals into melt inclusions through Fick's Second Law. Length scales of diffusion may be estimated by:

$$L_D = 2 * \sqrt{Dt} \qquad \text{(Eq. 4-1)}$$

where L_D is the length scale over which diffusion is occurring, t is time and D is the diffusion coefficient. Length scales are calculated using $D = 1.178 \times 10^{-11}$ m^2 s^{-1}, the average of the distribution coefficients for Li diffusion through pure anorthite (2.73×10^{-11} m^2 s^{-1}) and pure albite (8.2×10^{-12} m^2 s^{-1}) at high temperatures determined by Giletti and Shanahan (1997). Length scales of >2 mm, approximately the diameter of the average plagioclase phenocryst in Bezymianny eruptive products, may be obtained in <1.5 days.

A more robust assessment of the time necessary to produce the observed Li enrichment may be found in solving Fick's Second Law in one dimension to model diffusion of Li through a plagioclase crystal into a melt inclusion, using the equation:

$$\frac{C_1 - C(x,t)}{C_1 - C_2} = erf\left(\frac{x}{2\sqrt{Dt}}\right) \qquad \text{(Eq. 4-2)}$$

where t is the timescale over which the diffusion occurs, x is the distance of the melt inclusion from the crystal boundary, $C(x,t)$ is the time- and distance-dependent concentration of Li due to diffusion, C_1 is the Li concentration of the surrounding melt, C_2 is the initial Li concentration of the melt inclusion, D is the diffusion coefficient

(1.178×10^{14} m^2 s^{-1}, from Giletti and Shanahan, 1997, as above) and *erf* is the error function. Diffusion is modeled for distances between the melt inclusion and the edge of the crystal (x) of between 100 μm and 2000 μm, where 2000 μm represents an approximate radius for larger plagioclase phenocrysts at Bezymianny, and therefore a substantial overestimate of actual distances between inclusions and crystal rims. Models assume an infinite external reservoir with constant Li concentrations (C_1) of 100, 150 and 200 ppm Li, values near the maximum measured Li concentration (~110 ppm), and initial Li concentrations in melt inclusions (C_2) of 5 ppm, just below the minimum measured concentration. If it is assumed that all low-pressure Li enrichment results from diffusion of Li into plagioclase-hosted inclusions, Li diffusion from the surrounding melt would increase Li concentrations of these inclusions to >50 ppm in <4 days. This is true even at the lowest value of C_0 (100 ppm) and a distance between melt inclusion and crystal rim of 1000 μm, which is up to 5 times the minimum distance between any measured inclusion and the edge of its host grain. Diffusion over more reasonable distances (x) would produce such enrichment in 1 day or less (Fig. 4-14). Increasing C_0 to values greater than the maximum melt inclusion Li concentration only shortens these timescales (Fig. 4-14).

This diffusion modeling exercise is undoubtedly oversimplified. In direct contradiction to the assumption of the previous paragraph, high Li concentrations are not the result of diffusion alone, as some pyroxene crystals, through which Li diffuses much more slowly, also record high Li (Fig. 4-13). The measured Li concentrations reflect a combination of the entrapment of gas-streaming-enriched, high-Li liquid and some

degree of post-entrapment diffusion into inclusions hosted in plagioclase. However, these conditions will only reduce the times necessary to produce Li enrichment in Bezymianny melt inclusions via diffusion, meaning that these timescales must be considered overestimates. Enrichment of the shallow magmatic system in Li by gas streaming is therefore not contradicted by the lack of measured (^{210}Pb)/(^{226}Rn) disequilibria reported by Turner et al. (2007) and Kayzar (2012), as the time scales necessary to create the observed Li enrichment are on the order of hours to days, significantly shorter than the 1 month or longer necessary to create measureable (^{210}Pb)/(^{226}Rn) disequilibria. This does imply, however, that unlike Mount St. Helens, eruptions at Bezymianny were preceded by a pulse of gas streaming only a few days prior to the actual explosive event, and that the eruption cleared the shallow magma system of gas-streaming-enriched magma. Also, unlike at Mount St. Helens, gas streaming was minimal during repose periods between eruptions.

4.5.4: Temporal Variations and Models for the Bezymianny Magma System

Low-pressure Li enrichment is dominantly found in inclusions from samples from the 1984-2000 eruptive period, while inclusions from 2001-2010 entrap liquids that are less enriched in Li and include the most H_2O-rich inclusions in the sample set (Fig. 4-12). This may result from one or more of several different processes. Eruptions at Bezymianny may no longer be fed by magma that spent significant time in shallow storage regions and instead are dominated by magma brought directly to the surface from

deeper in the Bezymianny plumbing system. Conversely, magma may still be stored at shallow depths prior to eruption but is no longer being affected by gas streaming, either due to reduced gas fluxes or insufficient residence time at low pressure for significant degassing and influx of volatiles from the deep magmatic system due to gas streaming. If magma was no longer being stored at shallow depths, however, inclusions from 2001-2010 would not show significant pressure-dependent variations in K or Rb, as the magma would not have enough time to crystallize and enrich the residual liquids in these incompatible elements. This is not the case, as 2001-2010 Bezymianny melt inclusions show K and Rb enrichment at low pressures indistinguishable from previous years. This suggests that magma has been allowed to crystallize and degas at low pressures throughout the post-1956 eruptive history of the volcano but has not experienced significant Li enrichment since 2001, and therefore it is the nature of the upward gas streaming, not magma storage, that has changed.

If the locations of magmatic storage beneath Bezymianny are not changing significantly, why is gas streaming being restricted? Turner at al. (*in review*) suggest that the 1956 eruption was dominantly fed by shallowly-stored silicic magma, and that eruptive products of Bezymianny are becoming progressively more mafic due to the increasing dominance of a mafic mixing end-member from the deep magmatic system over silicic components. If the gas streaming is also sourced in the deep, mafic magma system, the cessation of gas streaming may indicate that the new mafic magma is dry or is beginning to run out of volatiles to supply gas streaming. The general increase in inclusion H_2O concentrations in more recent eruptions (Fig. 4-5) contradicts the former

scenario, but Kayzar (2012) reported a decrease in (^{210}Pb)/(^{226}Rn) ratios between 2005 and 2007 to values below equilibrium, indicating that the magma had lost volatiles prior to eruption. Gas streaming prior to 2001 may have depleted the deep magmatic source in volatiles to a sufficient degree to prevent to the segregation of a separate fluid phase at Bezymianny. Volatile depletion would be reflected in the decreasing (^{210}Pb)/(^{226}Rn) ratios found by Kayzar (2012) and the cessation of shallow Li enrichment.

Changing stress patterns in the crust around Bezymianny may also play a role in restricting gas streaming. Geodetic measurements of Bezymianny and the surrounding area indicates a pattern of long-term subsidence of the Klyuchevskoy volcanic group dating back to at least 1978, which is partially (though not completely) due to the increased loading of the area by material erupted from Bezymianny and Klyuchevskoy over the past 55 years (Fedotov et al., 1992; Grapenthin et al., *in review*). Numerous studies (e.g. Sigvaldason et al., 1992; Jull and McKenzie, 1996; Albino et al., 2010; Sigmundsson et al., 2010; Tuffen, 2010; Hooper et al., 2011) have suggested that decreasing the surface loads at volcanoes will promote increased magmatic output, both by promoting decompression melting and by reducing the compressive stress on shallow crustal magmatic pathways, allowing these pathways to expand and allow larger volumes of magma to pass through them.

At Bezymianny, the reverse of this process may be in play. Could the system have been "sealed" prior to the 1956 eruption by old magma and the load of the pre-1956 edifice, and only the clearing of the system by the 1956 eruption allowed upward volatile

movement into the shallow system? If so, this may in part explain why low-pressure Li enrichment is prevalent in 1984-2000 samples, but minor in 1956 and 2000-2010 samples (Fig. 4-12), as the 1984-1997 eruptive period represented a period when the system was most "open," and gas streaming was at a maximum. The subsidence of the Klyuchevskoy group and surrounding areas and the increased surface loads at Bezymianny and Klyuchevskoy may have then increased the compressive stress on the Bezymianny magma system and restricted the Li enrichment of the shallow magmatic storage regions by choking pathways for gas streaming. Further modeling of the stress field under Bezymianny is necessary to constrain how the continued regional subsidence and loading are affecting volatile and magma movement.

4.6: Conclusions

Measurements of major, trace and volatile elements concentrations in melt inclusions from Bezymianny allow for several major conclusions. Similar to the trend in bulk rock compositions, melt inclusion compositions become slightly less silicic over time, reflecting the increasing influence of mafic magma being introduced into the system from depth. H_2O concentrations generally increase in inclusions from eruptions after 1956, reaching a maximum of ~4.2 wt. %. Based on H_2O - CO_2 solubility, the maximum pressure of melt inclusion entrapment was ~230 MPa, but inclusions dominantly record pressures <50-100 MPa, in good agreement with previous conclusions

from geophysical and geochemical data that the Bezymianny plumbing system includes a zone of a shallow magmatic storage 2-4 km below the surface. Magma stored in this shallow region degasses, which triggers extensive crystallization, as seen in the low H_2O, CO_2 and S concentrations and marked increases in the concentrations of incompatible elements (K, Rb) with decreasing pressure (cf. Blundy and Cashman, 2005).

Inclusions trapped at shallow levels beneath Bezymianny show significant enrichment in Li, likely due to the ascent of a separate volatile fluid phase from deep in the Bezymianny magmatic system, similar to the gas streaming observed at Mount St. Helens (cf. Kent et al., 2007). Unlike at Mount St. Helens, however, no $(^{210}Pb)/(^{226}Ra)$ disequilibria have been reported at Bezymianny, as would be expected for a system that had experienced gas enrichment for long periods prior to eruption. This indicates that gas streaming at Bezymianny occurs only immediately prior to eruption, rather than over long periods (>1 month; e.g., Berlo et al., 2006; Kayzar, 2012). Modeling of Li diffusion through plagioclase indicates that timescales not more than a few days are necessary for significant Li enrichment to be found in melt inclusions, and therefore it seems likely that any gas streaming at Bezymianny is transient and occurs only a few days prior to eruptions.

Low-pressure Li enrichment is dominantly found in inclusions from samples from eruptions between 1984 and 1997, while inclusions from 2001-2010 are dominantly low in Li. While inclusions continue to be trapped at low pressures, modification of shallowly-stored magma by upward movement of volatiles seems to have diminished at

Bezymianny in recent years. This may be due to increased compressional stresses, imposed by the subsidence of the KVG and surrounding areas, restricting pathways for upward volatile movement, though this hypothesis requires further investigation. The composition trends in melt inclusions in the Bezymianny system are similar to those seen at Mount St. Helens (cf. Blundy et al., 2008), though the cessation of low-pressure Li enrichment with time is, at this point, unique to Bezymianny. Whether a similar cessation occurs at Mount St. Helens remains to be seen.

4.7: Acknowledgments

The authors gratefully acknowledge O.A. Girina, R.N. Grapenthin, T.M. Lopez, S.J. Turner and their co-authors for sharing early drafts of manuscripts, and for their willingness to discuss the data and conclusions therein. S.M.H. de Angelis, B.V. Ivanov, J.F. Larsen, C.J. Nye, S.V. Ushakov and M.E. West are thanked for enlightening discussions, while A.B. Belousov, M.G. Belousova, G.E. Bogoyavlenskaya, O.A. Girina, A.P. Maximov, P.R. Kyle and M.E. Zelensky generously provided samples used in this study. The authors also thank the staff of the Stanford/SUMAC facility for use of the SHRIMP facilities, K.P. Severin and the UAF Advanced Instrumentation Laboratory for the use of EPMA, K.I. Mahon for sharing an executable York regression script, and the members of the NSF-sponsored PIRE-Kamchatka project for their assistance during field campaigns at Bezymianny. This study was funded by NSF PIRE – Kamchatka Award

OISE 0530278 to J.C. Eichelberger, by the UAF Advanced Instrumentation Laboratory, and by the Alaska Volcano Observatory, a collaborative program of the University of Alaska Fairbanks, the Alaska Department of Geological and Geophysical Surveys, and the United States Geological Survey.

4.8: Figures

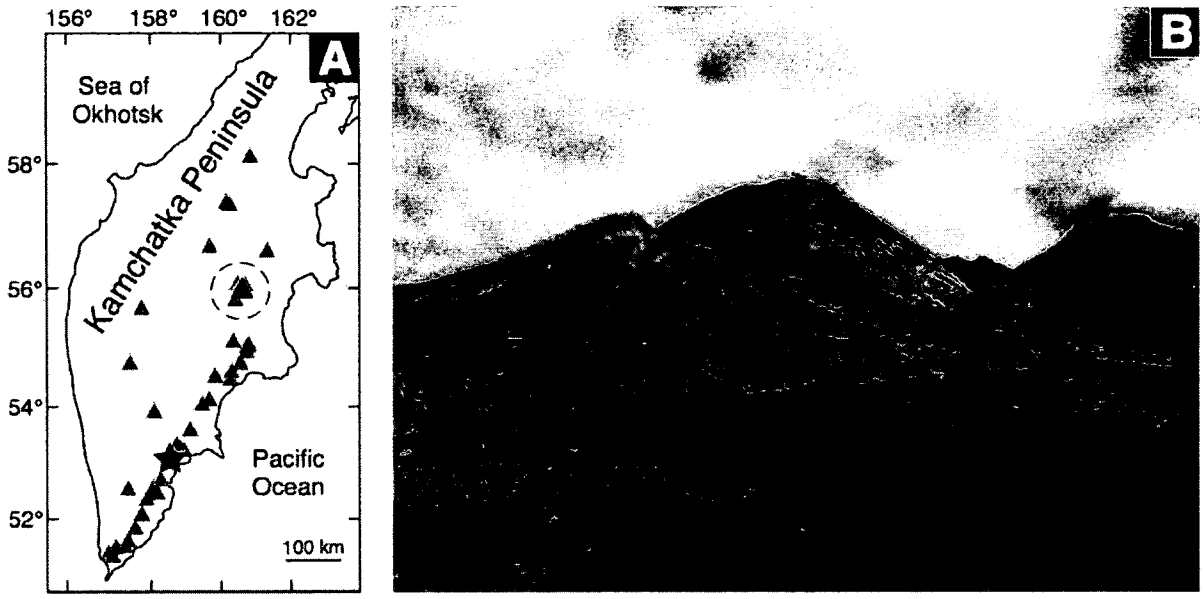

Figure 4-1: Location Map and Photo of Bezymianny. (A) Regional location map of Kamchatka. *Dashed circle* indicates the location of the Klyuchevskoy Volcanic Group (KVG), *black triangle* indicates Bezymianny Volcano, *grey triangles* indicate other major Kamchatkan volcanoes active during the Holocene. Map adapted from the Institute of Volcanology and Seismology, Far East Branch of the Russian Academy of Sciences (http://www.kscnet.ru/ivs/volcanoes/holocene/main/map/holocene.jpg, last accessed 20 July, 2012). (B) Photo taken 13 July, 2010, by O.K. Neill from a ridge east of Bezymianny, showing the growing lava dome inside the crater created by the collapse of the edifice during the climactic 1956 eruption. An actively extruding lava flow (dark area) can be seen on south side of the dome. Base of visible edifice to the top of the dome is ~1000 m. Kamen Volcano is at right.

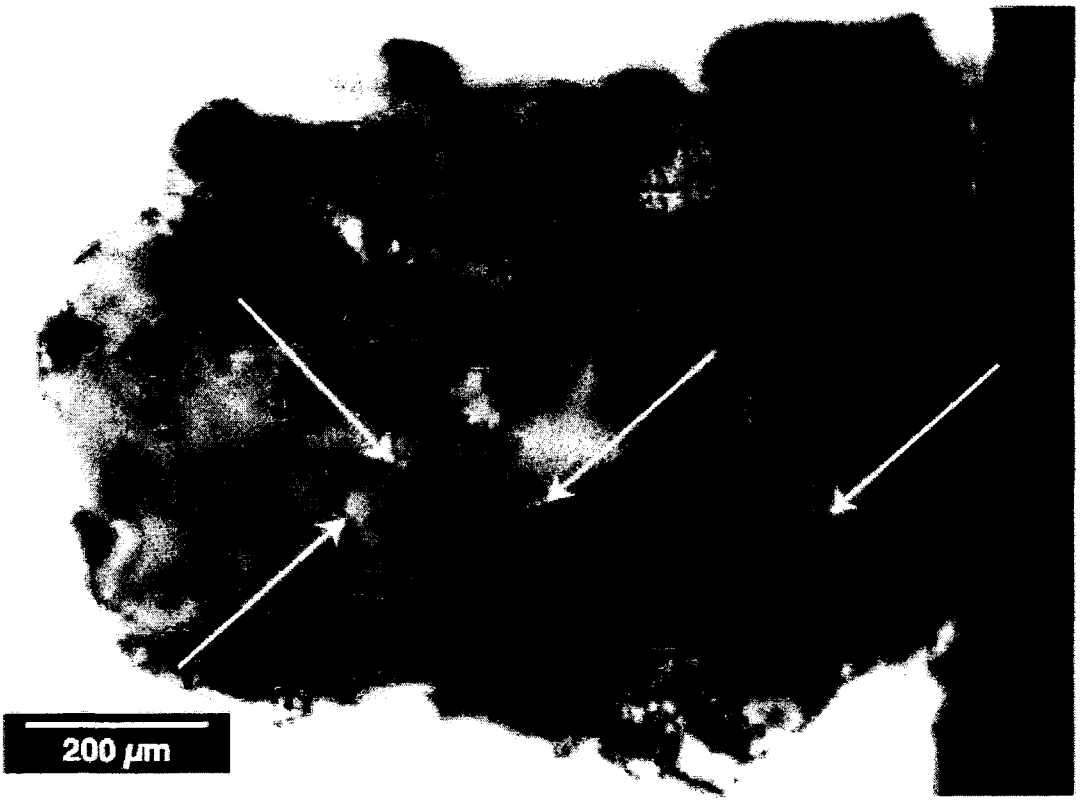

Figure 4-2: Representative Photomicrograph of Melt Inclusions. Inclusions (indicated by white arrows) are hosted in a pyroxene phenocryst from the 11 January, 2005 eruption of Bezymianny.

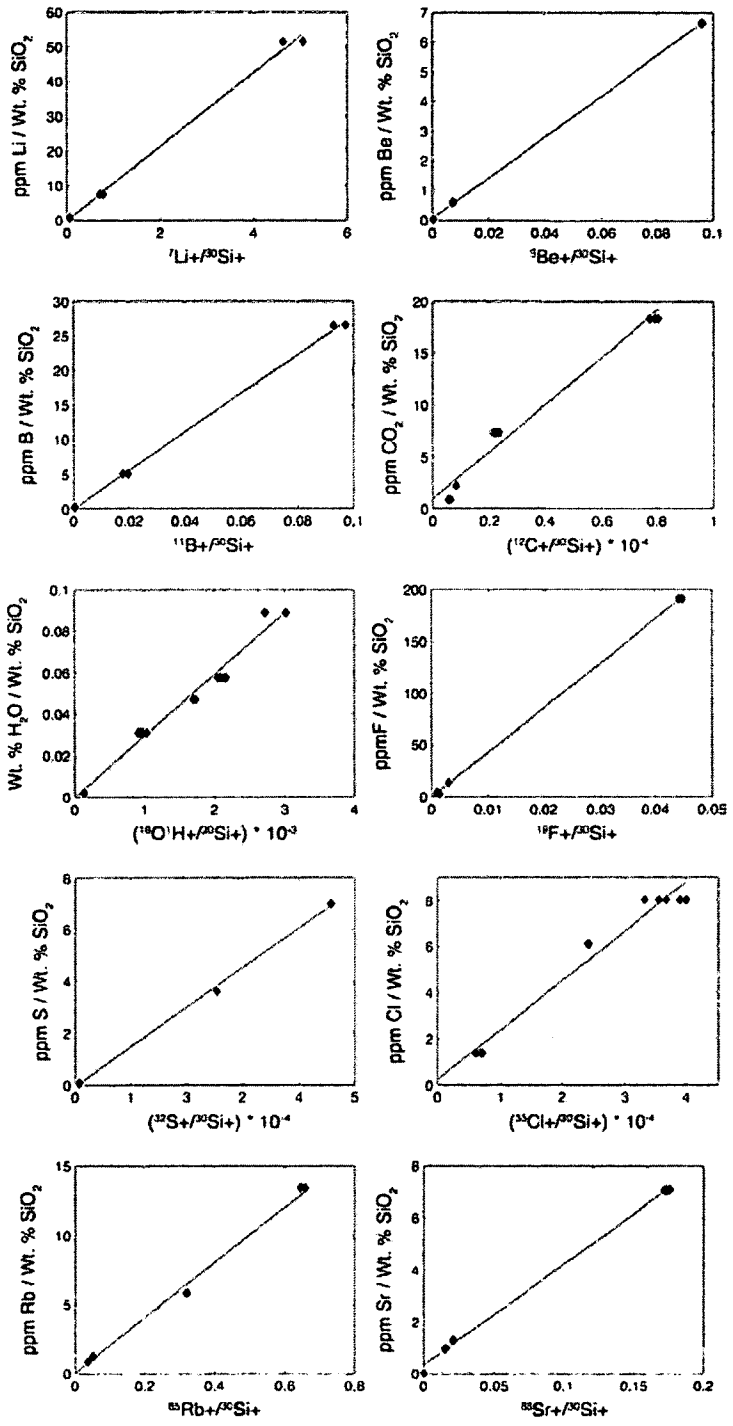

Figure 4-3: SIMS Calibration Curves. Calibration curves created from measurements of glass standards used to calculate concentrations from SHRIMP ion microprobe measurements of melt inclusions. Standard concentrations are given in Appendix 4-2.

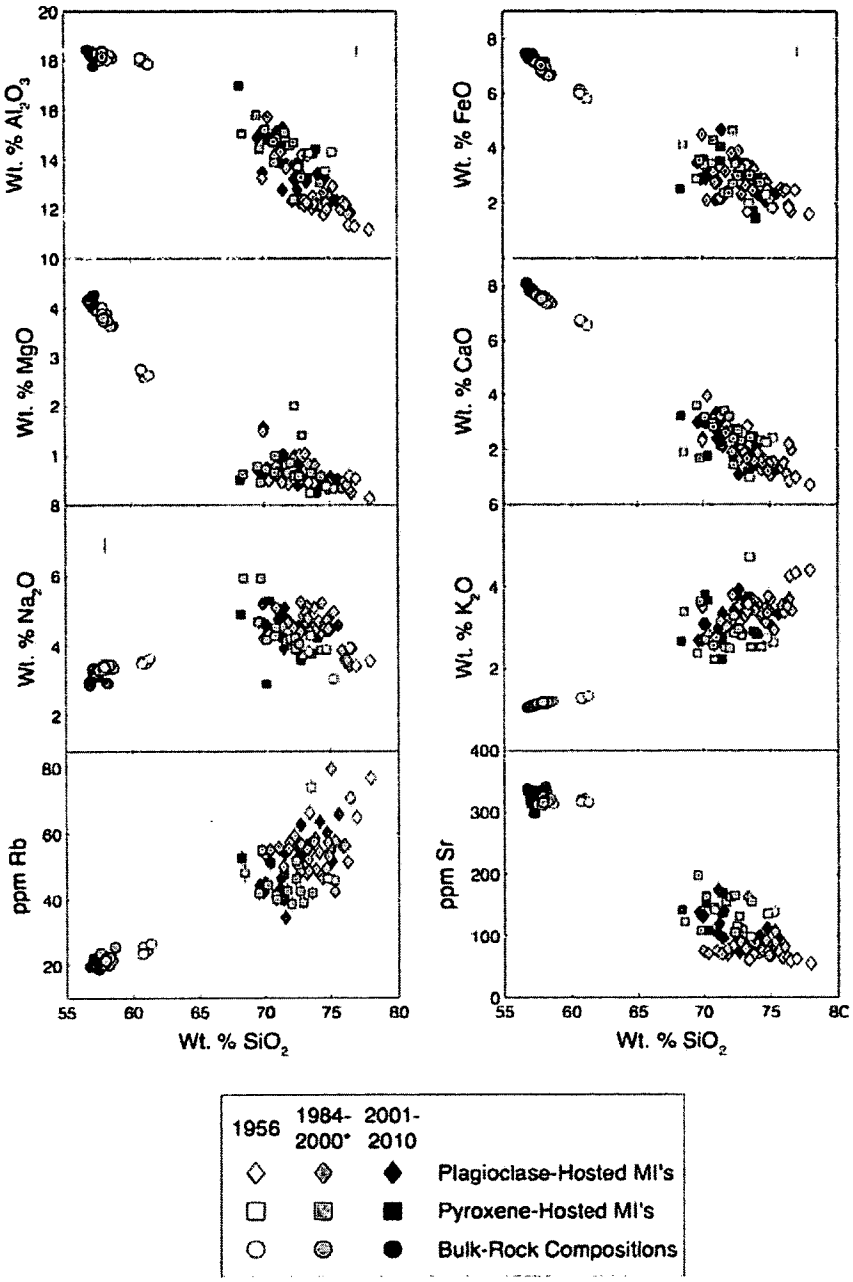

Figure 4-4: Major, Minor and Trace Element vs. SiO_2 Variation Diagrams. Compositions of both bulk samples and melt inclusions from Bezymianny are shown. Bulk compositions taken from Turner et al. (*in review*). All measurements of MI's by EPMA except for Rb and Sr, which were measured by SHRIMP. Error bars indicate analytical uncertainty (one standard deviation) of melt inclusion measurements (both SHRIMP and EPMA) only; where error bars are absent, uncertainty is smaller than the size of the symbols. Analytical uncertainty of bulk compositions is also within symbol size.

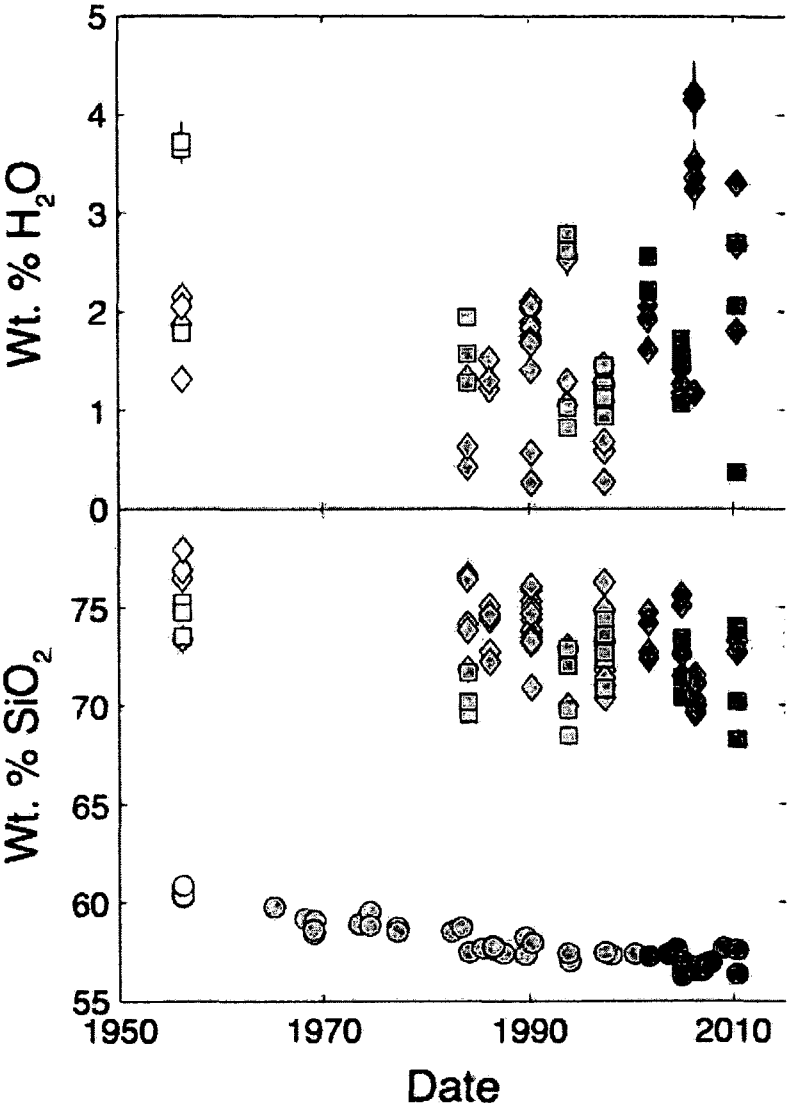

Figure 4-5: Variations in SiO_2 and H_2O with Eruption Date. Bulk-rock SiO_2 are shown, as well as variations in melt inclusion SiO_2 and H_2O concentration. Symbols and error bars as Fig. 4-4. Bulk compositions of Bezymianny eruptive products from Izbekov (2009), Izbekov et al. (2010) and Turner et al. (*in review*).

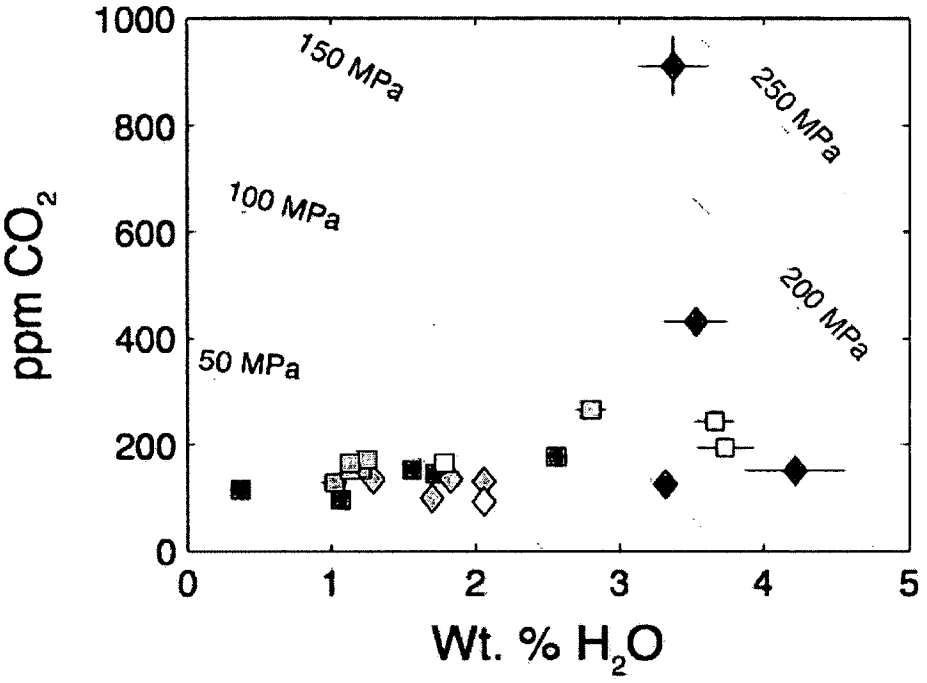

Figure 4-6: Melt Inclusion H_2O and CO_2 Concentrations. Concentrations of H_2O and CO_2 in Bezymianny melt inclusions measured by SHRIMP ion probe. Isobars calculated using the H_2O-CO_2 solubility model VolatileCalc (Newman and Lowenstern, 2002). Symbols and error bars as in Fig. 4-4.

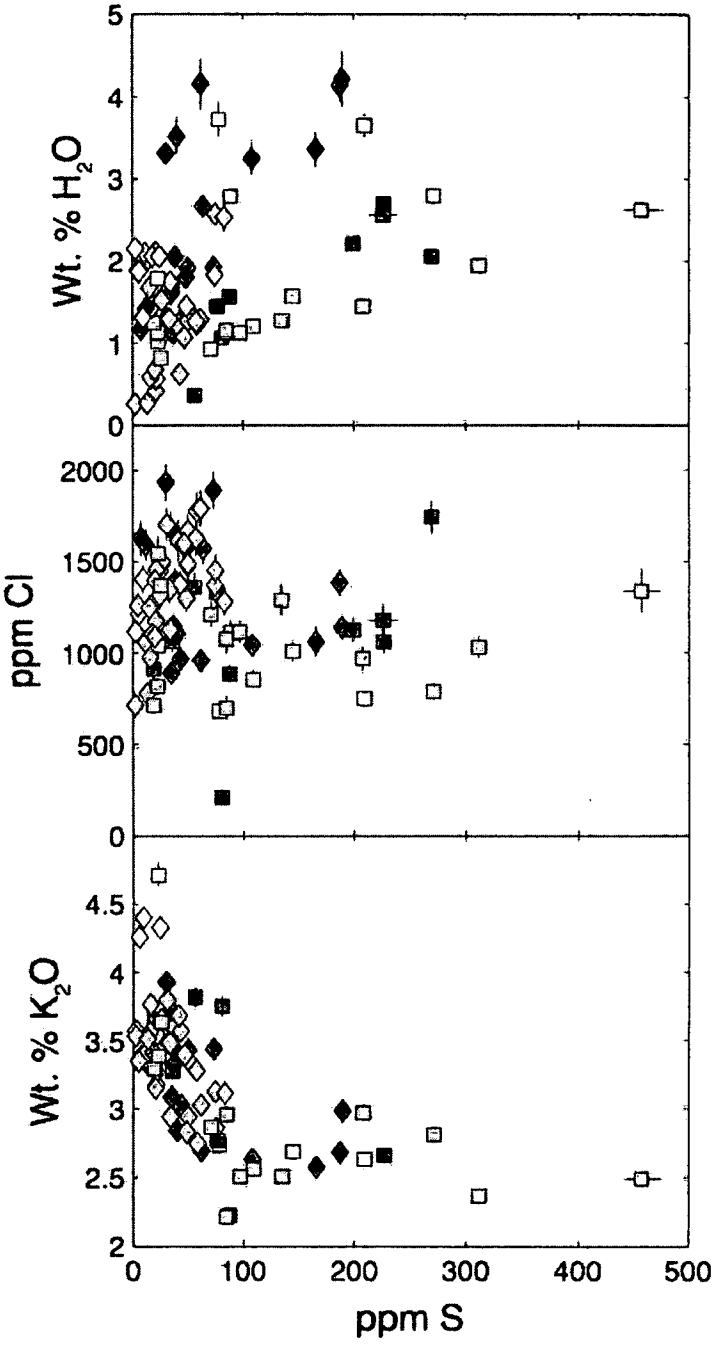

Figure 4-7: Variations in H_2O, Cl and K_2O Concentrations with S Concentration. All components analyzed by SHRIMP except K_2O. Symbols and error bars as in Fig. 4-4.

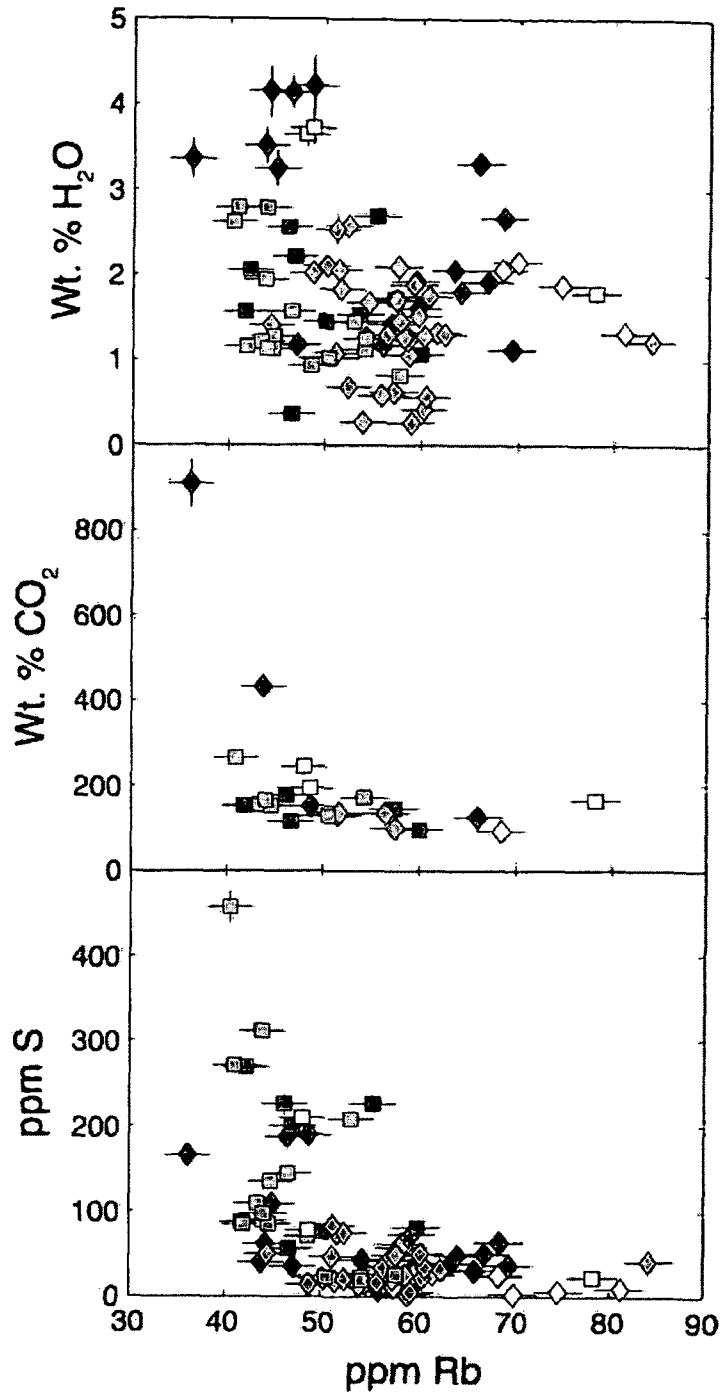

Figure 4-8: Variations in H_2O, CO_2 and S with Rb Concentration. All components analyzed by SHRIMP. Symbols and error bars as in Fig. 4-4.

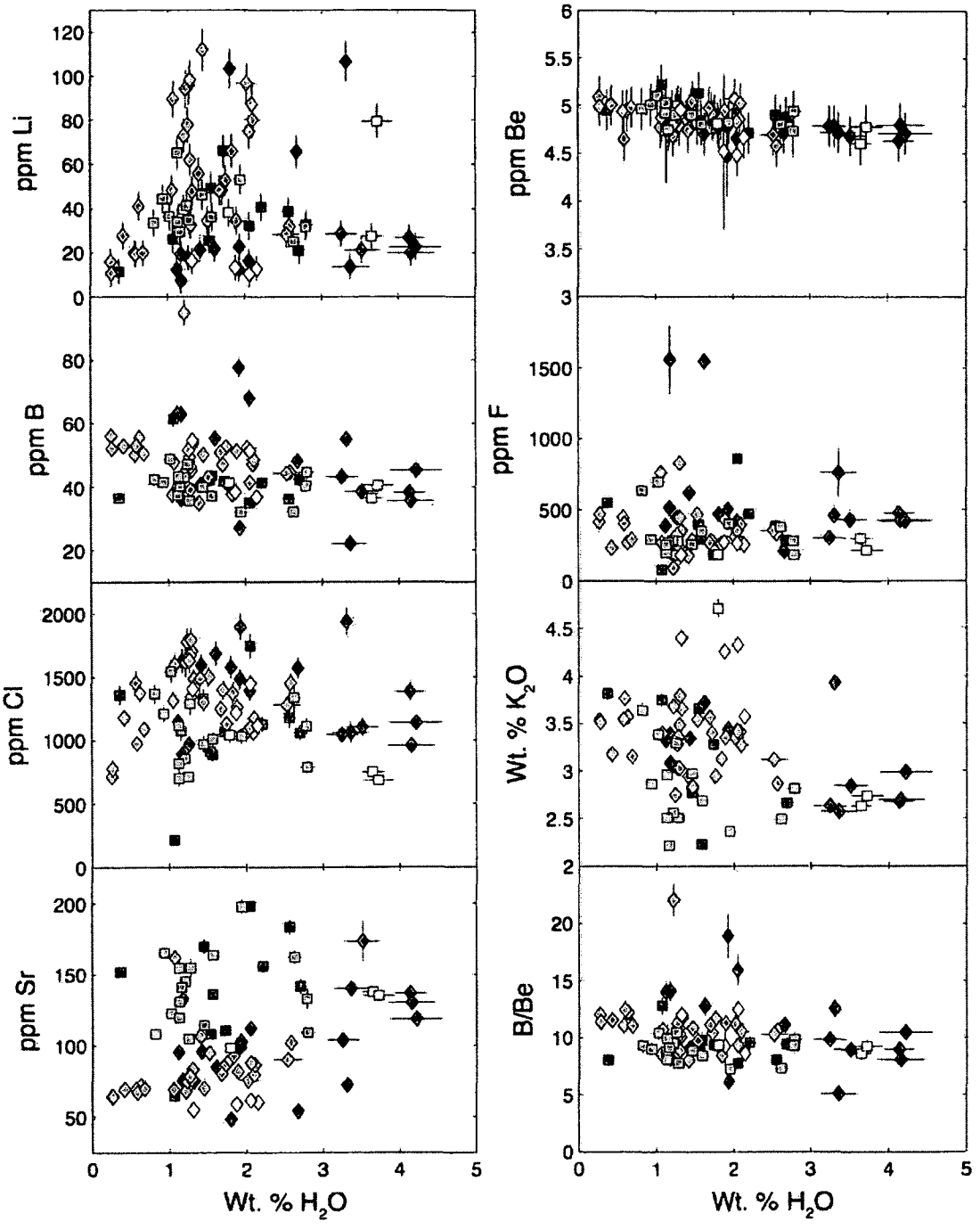

Figure 4-9: Variations in Light Trace Elements, Halogens, K_2O and Sr with H_2O Concentration. All components analyzed by SHRIMP except K_2O. Symbols and error bars as in Fig. 4-4.

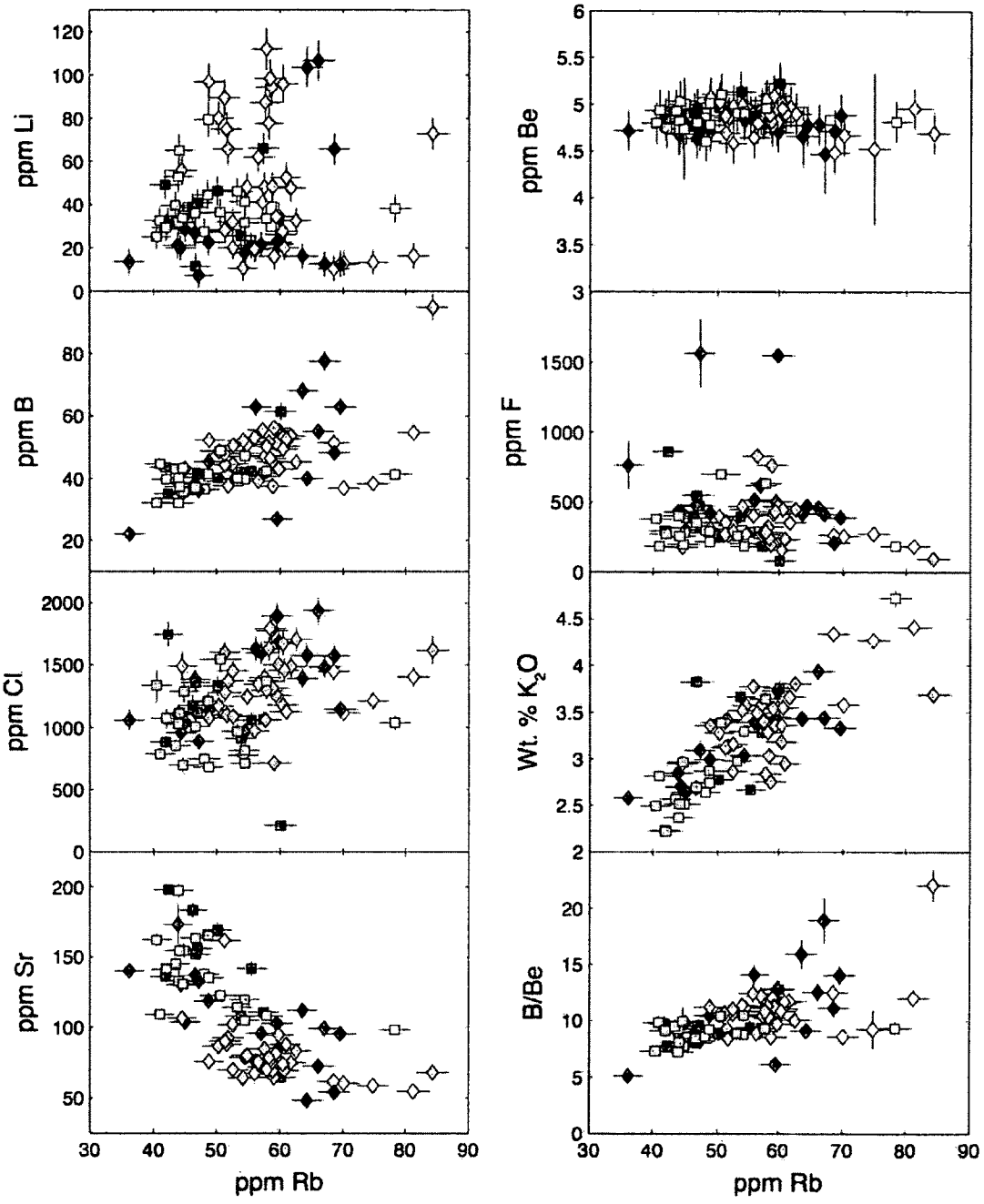

Figure 4-10: Variations in Light Trace Elements, Halogens, K_2O and Sr with Rb Concentration. All components analyzed by SHRIMP except K_2O. Symbols and error bars as in Fig. 4-4.

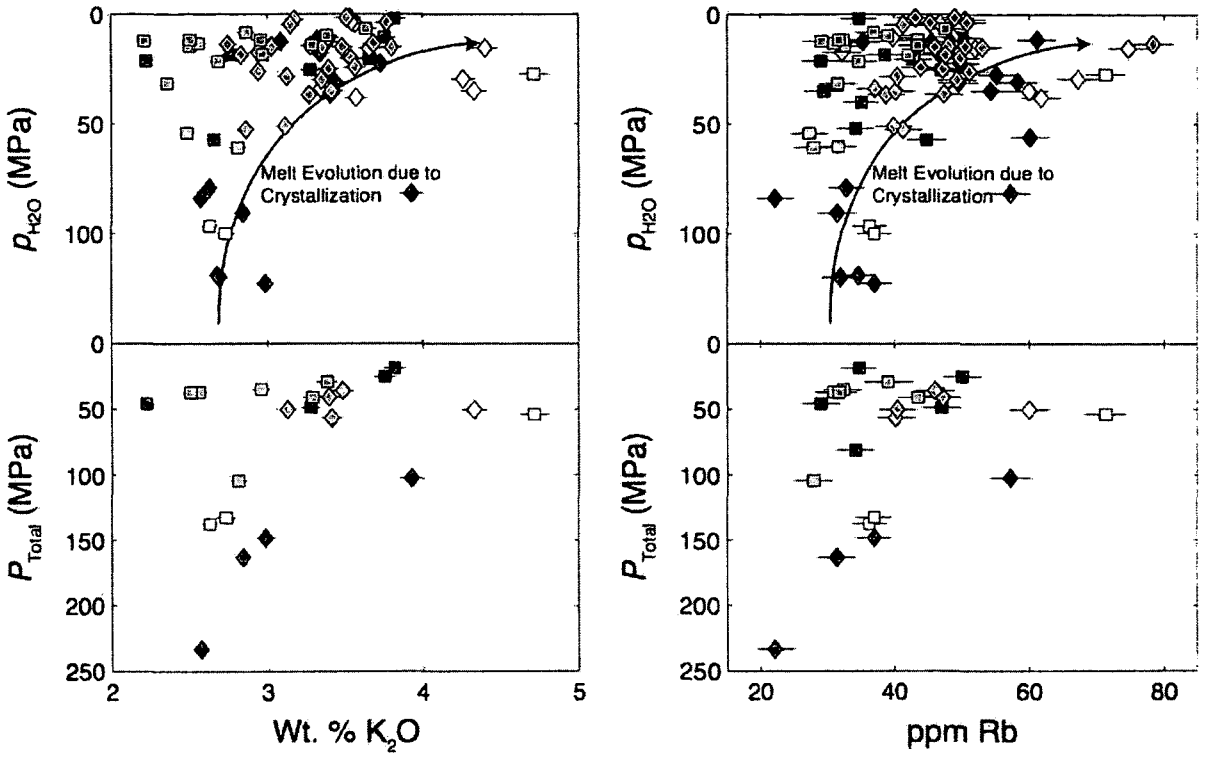

Figure 4-11: Variations in K_2O and Rb with Entrapment Pressure. Melt inclusion entrapment pressures represented as total pressure (P_{Total}) and partial pressure of H_2O (p_{H2O}). Black arrows represent schematic pressure-composition relationships likely for syn-eruptive degassing during rapid ascent and crystallization during slower ascent/shallow magmatic storage (see text), drawn after Blundy and Cashman (2005). All components analyzed by SHRIMP except K_2O. Symbols and error bars as in Fig. 4-4.

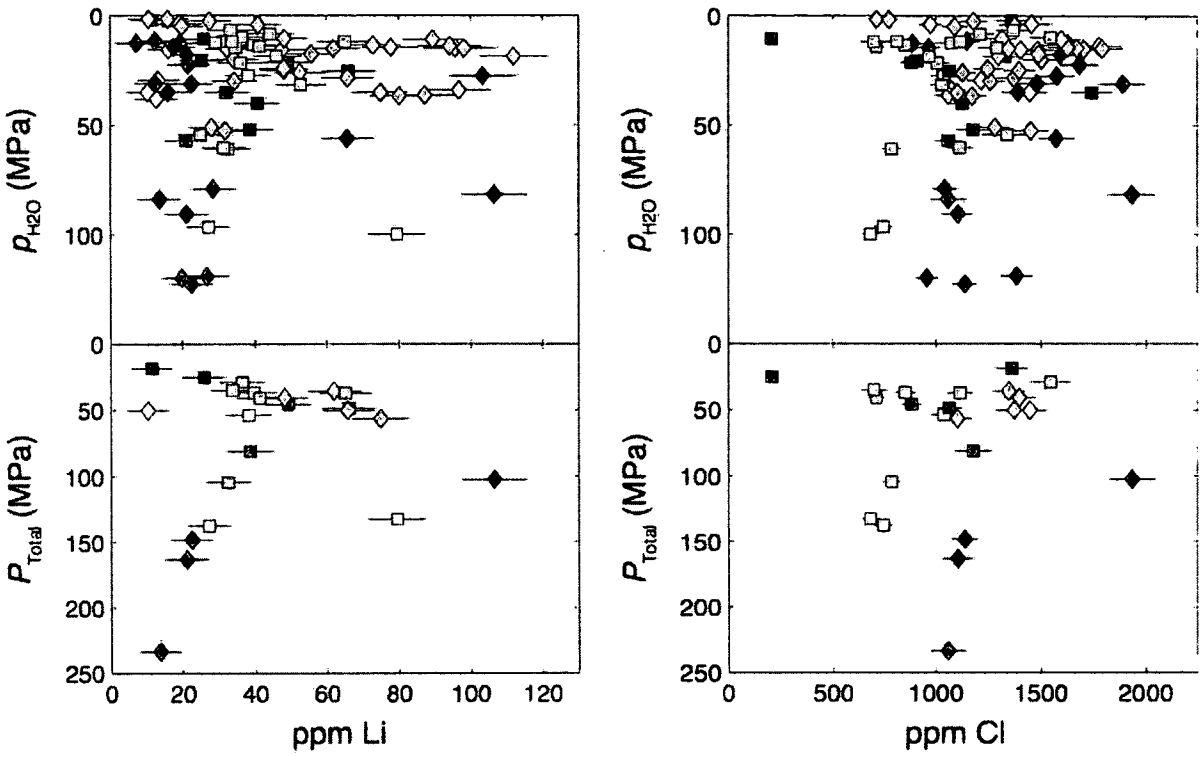

Figure 4-12: Variations in Li and Cl with Entrapment Pressure. Melt inclusion entrapment pressures represented as total pressure (P_{Total}) and partial pressure of H_2O (p_{H2O}). All components analyzed by SHRIMP. Symbols and error bars as in Fig. 4-4.

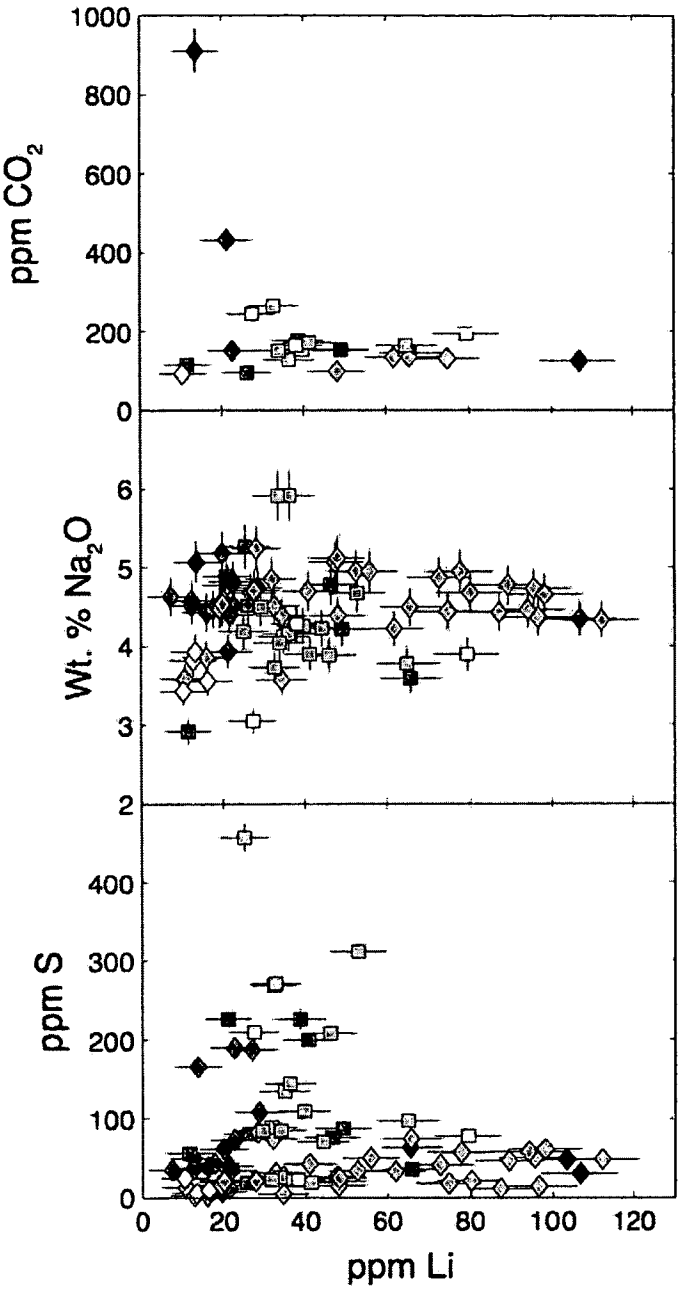

Figure 4-13: Variations in Melt Inclusion CO_2, S, and Na_2O with Li Concentration. All components analyzed by SHRIMP except Na_2O. Symbols and error bars as in Fig. 4-4.

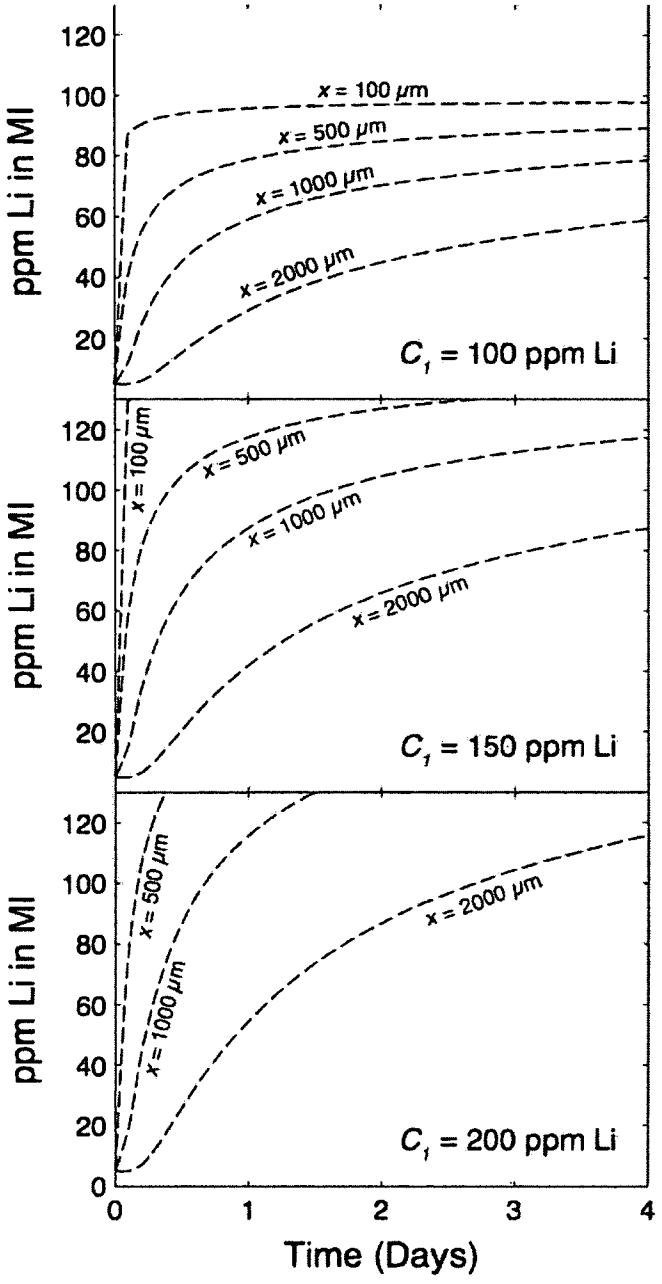

Figure 4-14: Timescales of Li Diffusion Through Plagioclase. Modeled changes in concentrations of Li in plagioclase-hosted melt inclusions due to diffusion of Li through plagioclase. Concentrations are modeled as a function of time allowed for diffusion using Fick's Second Law (see text) for inclusions of different distances (x) from the crystal rim, assuming different initial Li concentrations in the surrounding melt and initial melt inclusion Li concentrations of 5 ppm.

4.9: References

Albino, F., Pinel, V. and Sigmundsson, F., 2010. Influence of surface load variations on eruption likelihood: application to two Icelandic subglacial volcanoes, Grímsvötn and Katla. Geophys J Int, 181(3): 1510-1524. doi: 10.1111/j.1365-246X.2010.04603.x

Al'meev, R.R., Ariskin, A.A., Ozerov, A.Y. and Kononkova, N.N., 2002. Problems of the stoichiometry and thermobarometry of magmatic amphiboles: An example of hornblende from the andesites of Bezymyannyi volcano, eastern Kamchatka. Geochem Int, 40(8): 723-738.

Auer, S., Bindeman, I., Wallace, P., Ponomareva, V. and Portnyagin, M., 2009. The origin of hydrous, high-$\delta^{18}O$ voluminous volcanism: diverse oxygen isotope values and high magmatic water contents within the volcanic record of Klyuchevskoy volcano, Kamchatka, Russia. Contrib Mineral Petr, 157(2): 209-230. doi: 10.1007/s00410-008-0330-0

Bacon, C.R. and Druitt, T.H., 1988. Compositional evolution of the zoned calcalkaline magma chamber of Mount Mazama, Crater Lake, Oregon. Contrib Mineral Petr, 98(2): 224-256.

Belousov, A., 1996. Deposits of the 30 March 1956 directed blast at Bezymianny volcano, Kamchatka, Russia. B Volcanol, 57(8): 649-662.

Belousov, A.B. and Bogoyavlenskaya, G.E., 1988. Debris avalanche of the 1956 Bezymianny eruption, Kagoshima International Conference on Volcanoes, Kagoshima, Japan, pp. 565-568.

Belousov, A., Voight, B. and Belousova, M., 2007. Directed blasts and blast-generated pyroclastic density currents: a comparison of the Bezymianny 1956, Mount St Helens 1980, and Soufriere Hills, Montserrat 1997 eruptions and deposits. B Volcanol, 69(7): 701-740. doi: DOI 10.1007/s00445-006-0109-y

Berlo, K., Blundy, J., Turner, S., Cashman, K., Hawkesworth, C. and Black, S., 2004. Geochemical precursors to volcanic activity at Mount St. Helens, USA. Science, 306(5699): 1167-1169. doi: 10.1126/science.1103869

Berlo, K., Turner, S., Blundy, J., Black, S. and Hawkesworth, C., 2006. Tracing pre-eruptive magma degassing using ($^{210}Pb/^{226}Ra$) disequilibria in the volcanic deposits of the 1980-1986 eruption of Mount St. Helens. Earth Planet Sc Lett, 249(3-4): 337-349. doi: 10.1016/j.epsl.2006.07.018

Blundy, J. and Cashman, K., 2001. Ascent-driven crystallisation of dacite magmas at Mount St Helens, 1980-1986. Contrib Mineral Petr, 140(6): 631-650.

Blundy, J., Berlo, K. and Cashman, K., 2005. Lithium transport by a magmatic volatile phase beneath Mount St. Helens volcano. Geochim Cosmochim Acta, 69(10): A151-A151.

Blundy, J. and Cashman, K., 2005. Rapid decompression-driven crystallization recorded by melt inclusions from Mount St. Helens volcano. Geology, 33(10): 793-796. doi: 10.1130/G21668.1

Blundy, J., Cashman, K.V. and Berlo, K., 2008. Evolving magma storage conditions beneath Mount St. Helens inferred from chemical variations in melt inclusions from the 1980–1986 and current (2004–2006) eruptions. In: D.R. Sherrod, W.E. Scott and P.H. Stauffer (Editors), A Volcano Rekindled: The Renewed Eruption of Mount St. Helens, 2004-2006. U.S. Geol Surv Prof Pap 1750, pp. 775-790.

Bogoyavlenskaya, G.E., Braitseva, O.A., Melekestsev, I.V., Kiriyanov, V.Y. and Miller, C.D., 1985. Catastrophic eruptions of the directed-blast type at Mount St-Helens, Bezymianny and Shiveluch Volcanos. J Geodyn, 3(3-4): 189-218.

Bogoyavlenskaya, G.E., Braitseva, O.A., Melekestsev, I.V., Maksimov, A.P. and Ivanov, B.V., 1991. Bezymianny Volcano. In: S.A. Fedotov and Y.P. Masurenkov (Editors), Active Volcanoes of Kamchatka. Nauka, Moscow, pp. 168-197.

Braitseva, O., Melekestsev, I., Bogoyavlenskaya, G. and Maximov, A., 1991. Bezymianny: eruptive history and dynamics. Volcanol Seismol, 12: 165-195.

Brugger, C.R., Johnston, A.D. and Cashman, K.V., 2003. Phase relations in silicic systems at one-atmosphere pressure. Contrib Mineral Petr, 146(3): 356-369. doi: DOI 10.1007/s00410-003-0503-9

Clift, P.D., Layne, G.D., Najman, Y.M.R., Kopf, A., Shimizu, N. and Hunt, J., 2003. Temporal evolution of boron flux in the NE Japan and Izu arcs measured by ion microprobe from the forearc tephra record. J Petrol, 44(7): 1211-1236. doi: 10.1093/petrology/44.7.1211

Danyushevsky, L.V., Sokolov, S. and Falloon, T.J., 2002. Melt inclusions in olivine phenocrysts: Using diffusive re-equilibration to determine the cooling history of a crystal, with implications for the origin of olivine-phyric volcanic rocks. J Petrol, 43(9): 1651-1671.

Dolejš, D. and Baker, D.R., 2006. Fluorite solubility in hydrous haplogranitic melts at 100 MPa. Chem Geol, 225(1-2): 40-60. doi:10.1016/J.Chemgeo.2005.08.007

Donovan, J.J., Kremser, D. and Fournelle, J.H., 2007. Probe for Windows User's Guide and Reference, Enterprise Edition. Probe Software Inc., Eugene, OR.

Edmonds, M., 2008. New geochemical insights into volcanic degassing. Philos Transact A Math Phys Eng Sci, 366(1885): 4559-4579. doi: 10.1098/rsta.2008.0185

Fedotov, S., Zharinov, N. and Gontovaya, L., 2010. The magmatic system of the Klyuchevskaya group of volcanoes inferred from data on its eruptions, earthquakes, deformation, and deep structure. J Volcanol Seismol, 4(1): 1-33. doi: 10.1134/s074204631001001x

Fedotov, S.A., Zharinov, N.A., Sharoglazova, G.A. and Demianchuk, Y.V., 1992. Deformations of the Earth's surface in the Klyuchi geodynamic polygon,

Kamchatka, 1978-1987. Tectonophysics, 202(2-4): 151-156. doi: 10.1016/0040-1951(92)90095-n

Gauthier, P.J. and Condomines, M., 1999. Pb-210-Ra-226 radioactive disequilibria in recent lavas and radon degassing: inferences on the magma chamber dynamics at Stromboli and Merapi volcanoes. Earth Planet Sc Lett, 172(1-2): 111-126.

Gauthier, P.J., Le Cloarec, M.F. and Condomines, M., 2000. Degassing processes at Stromboli volcano inferred from short-lived disequilibria (^{210}Pb-^{210}Bi-^{210}Po) in volcanic gases. J Volcanol Geoth Res, 102(1-2): 1-19.

Geschwind, C.H. and Rutherford, M.J., 1995. Crystallization of microlites during magma ascent - the fluid-mechanics of 1980-1986 eruptions at Mount-St-Helens. B Volcanol, 57(5): 356-370.

Giletti, B.J. and Shanahan, T.M., 1997. Alkali diffusion in plagioclase feldspar. Chem Geol, 139(1-4): 3-20.

Girina, O.A., *in review*. Chronology of bezymianny volcano activity in 1956-2010. J Volcanol Geoth Res.

Gorshkov, G.S., 1959. Gigantic eruption of the Bezymianny volcano. B Volcanol, 20: 77-109.

Gorshkov, G.S., 1963. Directed volcanic blasts. B Volcanol, 26: 83-88.

Gorshkov, G.S. and Bogoyavlenskaya, G.E., 1965. Bezymyannyi volcano and peculiarities of its last eruption (1955–1963). Nauka, Moscow.

Grapenthin, R., Freymueller, J.T. and Serovetnikov, S.S., *in review*. Surface deformation of Bezymianny Volcano, Kamchatka, recorded by GPS: the eruptions from 2005-2010 and long-term, long-wavelength subsidence. J Volcanol Geoth Res.

Hammer, J.E. and Rutherford, M.J., 2002. An experimental study of the kinetics of decompression-induced crystallization in silicic melt. J Geophys Res-Sol Ea, 107(B1). doi: 10.1029/2001jb000281

Hooper, A., Ofeigsson, B., Sigmundsson, F., Lund, B., Einarsson, P., Geirsson, H. and Sturkell, E., 2011. Increased capture of magma in the crust promoted by ice-cap retreat in Iceland. Nature Geosci, 4(11): 783-786.

Humphreys, M.C.S., Kearns, S.L. and Blundy, J.D., 2006. SIMS investigation of electron-beam damage to hydrous, rhyolitic glasses: Implications for melt inclusion analysis. Am Mineral, 91(4): 667-679. doi: 10.2138/Am.2006.1936

Humphreys, M.C.S., Blundy, J.D. and Sparks, R.S.J., 2008. Shallow-level decompression crystallisation and deep magma supply at Shiveluch Volcano. Contrib Mineral Petr, 155(1): 45-61. doi: 10.1007/s00410-007-0223-7

Izbekov, P., 2009. Compositional trends At Bezymianny Volcano, 6th Bienniel Workshop on Japan-Kamchatka-Alaska Subduction Processes (JKASP-2009), Fairbanks, AK, pp. 218.

Izbekov, P.E., Neill, O.K., Shipman, J.S., Turner, S., Shcherbakov, V.D. and Plechov, P.Y., 2010. Silicic enclaves in products of 2009-2010 eruptions of Bezymianny Volcano, Kamchatka: Implications for magma processes. AGU Fall Meet 2010, Abs. #V33D-01, San Francisco, CA.

Jull, M. and McKenzie, D., 1996. The effect of deglaciation on mantle melting beneath Iceland. J. Geophys. Res., 101(B10): 21815-21828. doi: 10.1029/96jb01308

Kadik, A.A., Maksimov, A.P. and Ivanov, B.V. (Editors), 1986. Physico-chemical conditions for crystallization of andesites, Moscow, 158 pp.

Kayzar, T.M., 2012. The complexity of arc magmatism: A geochemical investigation of crustal processes beneath a highly productive volcanic center, Kamchatka, Russia. University of Washington, Ph.D. Dissertation, 188 pp.

Kayzar, T.M., Cooper, K.M., Reagan, M.K. and Kent, A.J.R., 2009. Gas transport model for the magmatic system at Mount Pinatubo, Philippines: Insights from (^{210}Pb)/(^{226}Ra). J Volcanol Geoth Res, 181(1-2): 124-140. doi: 10.1016/J.Jvolgeores.2009.01.006

Kent, A.J.R., Blundy, J., Cashman, K.V., Cooper, K.M., Donnelly, C., Pallister, J.S., Reagan, M., Rowe, M.C. and Thornber, C.R., 2007. Vapor transfer prior to the October 2004 eruption of Mount St. Helens, Washington. Geology, 35(3): 231-234. doi: 10.1130/G22809a.1

Kent, A.J.R., 2008. Melt inclusions in basaltic and related volcanic rocks. Rev Mineral Geochem, 69: 273-331. doi: 10.2138/rmg.2008.69.8

Liu, Y., Anderson, A.T., Wilson, C.J.N., Davis, A.M. and Steele, I.M., 2006. Mixing and differentiation in the Oruanui rhyolitic magma, Taupo, New Zealand: evidence from volatiles and trace elements in melt inclusions. Contrib Mineral Petr, 151(1): 71-87. doi: 10.1007/s00410-005-0046-3

Lopez, T., Ushakov, S.V., Izbekov, P.E., Tassi, F., Cahill, C.F., Neill, O.K. and Werner, C.A., *in review*. Constraints on magma processes, subsurface conditions, and total volatile flux at Bezymianny Volcano in 2007 – 2010 from direct and remote volcanic gas measurements. J Volcanol Geoth Res.

Lowenstern, J.B., 1995. Applications of silicate melt inclusions to the study of magmatic volatiles. In: J.F.H. Thompson (ed.), Magmas, Fluids, and Ore Deposits. Mineralogical Association of Canada Short Course 23, 71-99.

Ludwig, K.R., 2009. SQUID2: A User's Manual (v. 2.50). Berkeley Geochronology Center Special Publication, 5, 104 pp.

MacDonald, R., Smith. R.L. and Thomas, J.E., 1992. Chemistry of the subalkalic silicic obsidians. US Geol. Surv. Prof. Pap. 1523.

Mahon, K.I., 1996. The New "York" regression: Application of an improved statistical method to geochemistry. Int. Geol. Rev., 38, 293-303.

Mangan, M. and Sisson, T., 2000. Delayed, disequilibrium degassing in rhyolite magma: decompression experiments and implications for explosive volcanism. Earth Planet Sc Lett, 183(3-4): 441-455. doi: 10.1016/s0012-821x(00)00299-5

Metrich, N. and Rutherford, M.J., 1992. Experimental study of chlorine behavior in hydrous silicic melts. Geochim Cosmochim Acta, 56(2): 607-616.

Metrich, N. and Wallace, P.J., 2008. Volatile abundances in basaltic magmas and their degassing paths tracked by melt inclusions. Rev Mineral Geochem, 69: 363-402. doi: Doi 10.2138/Rmg.2008.69.10

Morris, J.D., Leeman, W.P. and Tera, F., 1990. The subducted component in island arc lavas: constraints from Be isotopes and B-Be systematics. Nature, 344(6261): 31-36.

Newman, S. and Lowenstern, J.B., 2002. VOLATILECALC: a silicate melt-H_2O-CO_2 solution model written in Visual Basic for Excel. Comp Geosci, 28(5): 597-604. doi: Pii S0098-3004(01)00081-4

Nielsen, C.H. and Sigurdsson, H., 1981. Quantitative methods for electron micro-probe analysis of sodium in natural and synthetic glasses. Am Mineral, 66(5-6): 547-552.

Ozerov, A.Y., Ariskin, A.A., Kyle, P., Bogoyavlenskaya, G.E. and Karpenko, S.F., 1997. Petrological-geochemical model for genetic relationships between basaltic and

andesitic magmatism of Klyuchevskoi and Bezymyannyi volcanoes, Kamchatka. Petrology, 5(6): 550-569.

Pearce, N.J.G., Perkins, W.T., Westgate, J.A., Gorton, M.P., Jackson, S.E., Neal, C.R. and Chenery, S.P., 1997. A compilation of new and published major and trace element data for NIST SRM 610 and NIST SRM 612 glass reference materials. Geostandard Newslett, 21(1): 115-144.

Pichavant, M., Kontak, D.J., Briqueu, L., Herrera, J.V. and Clark, A.H., 1988. The Miocene-Pliocene Macusani Volcanics, Se Peru .2. Geochemistry and origin of a felsic peraluminous magma. Contrib Mineral Petr, 100(3): 325-338.

Reagan, M.K., Tepley, F.J., Gill, J.B., Wortel, M. and Garrison, J., 2006. Timescales of degassing and crystallization implied by ^{210}Po-^{210}Pb-^{226}Ra disequilibria for andesitic lavas erupted from Arenal volcano. J Volcanol Geoth Res, 157(1-3): 135-146. doi: 10.1016/J.Jvolgeorges.2006.03.044

Ryan, J.G. and Langmuir, C.H., 1988. Beryllium systematics in young volcanic rocks: Implications for ^{10}Be. Geochim Cosmochim Acta, 52(1): 237-244. doi: 10.1016/0016-7037(88)90073-7

Ryan, J.G. and Langmuir, C.H., 1993. The systematics of boron abundances in young volcanic rocks. Geochim Cosmochim Acta, 57(7): 1489-1498. doi: 10.1016/0016-7037(93)90008-k

Shcherbakov, V.D., Neill, O.K., Izbekov, P.E., and Plechov, P.Yu (*in press*) Phase equilibria constraints on pre-eruptive magmatic conditions prior to the 30 March 1956 eruption of Bezymianny volcano, Kamchatka, Russia. J Volcanol Geoth Res, doi: 10.1016/j.jvolgeores.2013.02.010

Shcherbakov, V.D., Plechov, P.Y., Izbekov, P.E. and Shipman, J.S., 2011. Plagioclase zoning as an indicator of magma processes at Bezymianny Volcano, Kamchatka. Contrib Mineral Petr, 162(1): 83-99. doi: 10.1007/s00410-010-0584-1

Shinohara, H., Iiyama, J.T. and Matsuo, S., 1989. Partition of chlorine compounds between silicate melt and hydrothermal solutions (1) Partition of NaCl-KCl. Geochim Cosmochim Acta, 53(10): 2617-2630.

Sigmundsson, F., Pinel, V., Lund, B.r., Albino, F., Pagli, C., Geirsson, H.r. and Sturkell, E., 2010. Climate effects on volcanism: influence on magmatic systems of loading and unloading from ice mass variations, with examples from Iceland. Phil Trans Royal Soc A: Math Phys Eng, 368(1919): 2519-2534. doi: 10.1098/rsta.2010.0042

Signorelli, S. and Carroll, M.R., 2001. Experimental constraints on the origin of chlorine emissions at the Soufriere Hills volcano, Montserrat. B Volcanol, 62(6-7): 431-440.

Sigvaldason, G.E., Annertz, K. and Nilsson, M., 1992. Effect of glacier loading/deloading on volcanism: postglacial volcanic production rate of the

Dyngjufjöll area, central Iceland. B Volcanol, 54(5): 385-392. doi: 10.1007/bf00312320

Stix, J., Layne, G.D. and Spell, T.L., 1995. The behavior of light lithophile and halogen elements in felsic magma: geochemistry of the post-caldera Valles Rhyolites, Jemez Mountains Volcanic Field, New Mexico. J Volcanol Geoth Res, 67(1,Äi3): 61-77. doi: 10.1016/0377-0273(94)00098-2

Stix, J. and Layne, G.D., 1996. Gas saturation and evolution of volatile and light lithophile elements in the Bandelier magma chamber between two caldera-forming eruptions. J Geophys Res, 101(B11): 25181-25196. doi: 10.1029/96jb00815

Straub, S.M. and Layne, G.D., 2002. The systematics of boron isotopes in Izu arc front volcanic rocks. Earth Planet Sc Lett, 198(1-2): 25-39. doi: 10.1016/s0012-821x(02)00517-4

Straub, S.M., Layne, G.D., Schmidt, A. and Langmuir, C.H., 2004. Volcanic glasses at the Izu arc volcanic front: New perspectives on fluid and sediment melt recycling in subduction zones. Geochem Geophys Geosyst, 5(1): Q01007. doi: 10.1029/2002gc000408

Thelen, W., West, M. and Senyukoy, S., 2010. Seismic characterization of the fall 2007 eruptive sequence at Bezymianny Volcano, Russia. J Volcanol Geoth Res, 194(4): 201-213. doi: 10.1016/J.Jvolgeores.2010.05.010

Tolstykh, M.L., Naumov, V.B., Babanskii, A.D., Khubunaya, S.A. and Kononkova, N.N., 1998. Melt composition and andesite crystallization conditions of Sheveluch volcana (Kamchatka) based on the data of studies of inclusions in minerals. Doklady Akademii Nauk, 359(5): 676-679.

Tolstykh, M.L., Naumov, V.B., Bogoyavlenskaya, G.E. and Kononkova, N.N., 1999. The role of andesitic-rhyolitic-dacitic melts in the crystallization of phenocrysts in andesite of Bezymyannyi Volcano, Kamchatka. Geokhimiya(1): 14-24.

Tolstykh, M.L., Naumov, V.B., Babansky, A.D., Bogoyavlenskaya, G.E. and Khubunaya, S.A., 2003. Chemical composition, volatile components, and trace elements in andesitic magmas of the Kurile-Kamchatka region. Petrology, 11(5): 407-425.

Tuffen, H., 2010. How will melting of ice affect volcanic hazards in the twenty-first century? Phil Trans Royal Soc A: Math Phys Eng,, 368(1919): 2535-2558. doi: 10.1098/rsta.2010.0063

Turner, S., Black, S. and Berlo, K., 2004. ^{210}Pb-^{226}Ra and ^{228}Ra-^{232}Th systematics in young arc lavas: implications for magma degassing and ascent rates. Earth Planet Sc Lett, 227(1-2): 1-16. doi: Doi 10.1016/J.Epsl.2004.08.017

Turner, S., Sims, K.W.W., Reagan, M. and Cook, C., 2007. A ^{210}Pb–^{226}Ra–^{230}Th–^{238}U study of Klyuchevskoy and Bezymianny volcanoes, Kamchatka. Geochim Cosmochim Acta, 71(19): 4771-4785. doi: 10.1016/j.gca.2007.08.006

Turner, S.J., Izbekov, P.E. and Langmuir, C.H., *in review.* The magma plumbing system of Bezymianny Volcano: Insights from a 54 year time series of trace element whole-rock geochemistry and amphibole compositions. J Volcanol Geoth Res.

Wallace, P.J., Anderson, A.T. and Davis, A.M., 1999. Gradients in H_2O, CO_2, and exsolved gas in a large-volume silicic magma system: Interpreting the record preserved in melt inclusions from the Bishop Tuff. J Geophys Res-Sol Ea, 104(B9): 20097-20122.

Webster, J.D., 1997. Chloride solubility in felsic melts and the role of chloride in magmatic degassing. J Petrol, 38(12): 1793-1807. doi: 10.1093/petroj/38.12.1793

Webster, J.D., 2004. The exsolution of magmatic hydrosaline chloride liquids. Chem Geol, 210(1,Äì4): 33-48. doi: 10.1016/j.chemgeo.2004.06.003

Webster, J.D., Holloway, J.R. and Hervig, R.L., 1989. Partitioning of lithophile trace elements between H_2O and H_2O+CO_2 fluids and topaz rhyolite melt. Econ Geol, 84(1): 116-134. doi: 10.2113/gsecongeo.84.1.116

Webster, J.D., Tappen, C.M. and Mandeville, C.W., 2009. Partitioning behavior of chlorine and fluorine in the system apatite-melt-fluid. II: Felsic silicate systems at 2000 MPa. Geochim Cosmochim Acta, 73(3): 559-581. doi: 10.1016/j.gca.2008.10.034

Williams-Jones, A.E. and Heinrich, C.A., 2005. 100th Anniversary Special Paper: vapor transport of metals and the formation of magmatic-hydrothermal ore deposits. Econ Geol, 100(7): 1287-1312. doi: 10.2113/gsecongeo.100.7.1287

Wright, H., Bacon, C., Vazquez, J. and Sisson, T., 2012. Sixty thousand years of magmatic volatile history before the caldera-forming eruption of Mount Mazama, Crater Lake, Oregon. Contrib Mineral Petr: 1-26. doi: 10.1007/s00410-012-0787-8

York, D., 1969. Least squares fitting of a straight line with correlated errors. Earth Planet Sci Lett, 5:3 20–324.

Chapter 5: Concluding Remarks

«Ходит дурачок по лесу, ищет дурачок глупее себя».

Гражданская Оборона, «Про дурачка»,
Прыг-скок, ГрОб Records, 1990

In this dissertation, geochemical tracers of magma movement, mixing, crystallization and degassing were employed to better understand the magmatic systems of two different arc volcanoes. The purpose of the first study (Chapter 2) was to characterize the petrology and geochemistry of the eruptive products of the 2008 eruption of Kasatochi Island volcano in the central Aleutian Islands and determine the mechanisms by which the different lithologies produced during the eruption came to coexist and ascend together to the surface. The 2008 eruption produced white, pumiceous medium-K, slightly calc-alkaline andesite, as well as denser, grey-brown, medium-K, tholeiitic basaltic andesite. Both lithologies vary in bulk composition, with basaltic andesite clasts containing ~52-56 wt. % SiO_2 and andesite clasts falling between ~58-62 wt. % SiO_2; the compositions of banded samples span the full range of compositions. Some limited pre-eruptive homogenization must have taken place between the andesite and basaltic andesite, but pre-eruptive physical and chemical interactions between the two lithologies were very limited overall. As europium anomalies are absent, and the linear trends seen in element-element variation diagrams are not congruent throughout all components, any direct genetic link between the andesite and basaltic

andesite lithologies through fractional crystallization or simple two-component mixing is highly improbable. The basaltic andesite and andesite must have resided in spatially and chemically distinct storage areas until just prior to eruption, with any mixing between the two magmas limited to a brief period prior to eruption.

The second study (Chapter 3) focused on the plagioclase phenocryst populations and the anomalously high calcium concentrations of plagioclase microlites in the basaltic andesite from the 2008 Kasatochi eruption. The basaltic andesite also contains two plagioclase phenocryst populations. Group 1 phenocrysts have rim compositions of An_{55-65} and display osciallatory zonation with an overall normal compositional trend, while Group 2 phenocrysts are highly calcic (An_{85-95}) and texturally homogeneous. In contrast to standard models of plagioclase microlite formation, which suggest that these microlites should to have the similar or lower calcium concentrations to the phenocryst rim compositions, the 2008 basaltic andesite contains microlites with anomalously high calcium concentrations (up to ~An_{90}). Compositional heterogeneity in the 2008 Kasatochi basaltic andesite result from pre-eruptive magma mixing (see Chapter 2) between mafic and silicic compositional end members, compositionally similar to the most mafic and most silicic basaltic andesite whole-rock compositions. As the Group 2 plagioclase phenocrysts and the high-An microlites are out of equilibrium with the basaltic andesite groundmass glass, the microlites and Group 2 phenocrysts likely crystallized mostly in the mafic mixing end member at higher temperatures (900-1000 °C) than the Group 1 phenocrysts, which crystallized in the cooler (800-950 °C) felsic mixing end member. Mixing between the cooler, silicic end member and the hotter, mafic

end member imposed an undercooling on the mafic magma, triggering plagioclase microlite nucleation in the more calcic liquids of the mafic end member.

The purpose of the final study (Chapter 4) was to investigate the evolution of the magma system of Bezymianny Volcano in Kamchatka, Russia through analyses of the major, trace and volatile compositions of melt inclusions. Inclusions dominantly record pressures of inclusion entrapment (based on H_2O - CO_2 solubility) <50-100 MPa, with a maximum pressure of ~230 MPa, indicating a zone of magmatic storage 1-2 km below the surface. Magma degassing and crystallization during ascent to and storage in this shallow storage zone produces significant negative correlations between concentrations of incompatible lithophile (K_2O, Rb) and volatile (H_2O, CO_2, S) elements. Also, Li enrichment from the ascent of a fluid phase from deep in the Bezymianny magma system leads to enrichment of shallowly-stored magma in lithium. This fluid enrichment of the shallowly stored Bezymianny magma likely occurs on timescales of hours to days directly prior to eruption.